EUROPEAN ASSOCIATION OF NUCLEAR MEDICINE

PET TRACERS BEYOND [^{18}F]FDG

A TECHNOLOGISTS' GUIDE

Produced with the kind support of

SIEMENS Healthineers

Table of contents

Foreword

Multidimensional and interdisciplinary education and training is the leading pillar of the rapidly evolving discipline of nuclear medicine (NM). Among all the professions that make up this highly relevant field of medicine, the Technologist's profile has become an intersection between education, clinical practice and science. NM Technologists (NMTs) hold the key to efficient collaboration with the patient and can be considered a link between all the professions due to their complex and numerous competencies and the roles they are able to perform in their daily practice. Nevertheless, even such a broad profession cannot stand alone. Underlining the vital importance of the interdisciplinary team, the Technologists' Committee (EANM-TC) of the European Association of Nuclear Medicine presents **PET tracers beyond [^{18}F]FDG,** created by a heterogeneous group of experienced NM professionals who are passionate about the field and its complexity.

PET TRACERS BEYOND [^{18}F]FDG

The annual publication envisioned and edited by the EANM-TC members provides readers with the most relevant information on the state of the art in a variety of NM procedures, applications, and best practices. Though primarily aimed at NMTs, it includes reports presented by many specialists and can thus serve as a useful reference in the daily clinical routine of all NM professionals, both inside and outside Europe. Among the specialist contributors are our counterparts from the Society of Nuclear Medicine and Molecular Imaging (SNMMI), who have supported this educational and scientific journey since its incredible beginning.

This publication is an interdisciplinary effort involving all professional groups contributing to NM development, working together to achieve one of the most significant objectives within any medical domain: staying informed, constantly evolving and being aware of novel findings and developments in the field. As there is no NM diagnosis or therapy without the appropriate choice of radiopharmaceutical, **PET tracers beyond [^{18}F]FDG** seemed the best response to current NM considerations, drug development having become the most evident sign of the NM evolutionary process.

I would like to take this unique opportunity to thank our friends and collaborators: editors and authors whose work has ensured the outstanding quality of this book. I am very much indebted to the EANM-TC editorial team for their incredible dedication and extensive efforts in contributing to so many aspects of this educational and scientific project. I would also like to express my deepest gratitude to the EANM Board, EANM Guidelines and Publications Council & EANM Executive Office for their constant support, to the representatives of the various EANM Committees, to the language review team, and, most of all, to the authors for the time, experience and expertise they were willing to share with our readers.

Thank you for taking the time to familiarise yourself with the latest edition of the EANM-TC Technologists' Guide – I sincerely hope you will find it enriching for your professional awareness.

Agata Karolina Pietrzak
Chair, EANM Technologists' Committee

Introduction

Ever since its inception, Nuclear Medicine has been known as a constantly evolving field. Radiopharmaceutical research over the years has proven productive and has become increasingly recognised for its diagnostic and therapeutic value for a range of clinical indications and patient pathways. Consequently, it is upon the workforce to keep abreast of the latest developments, actively studying and remaining knowledgeable, and ultimately contributing to a smooth translation of theoretical research concepts into real everyday practice. In this respect, we also recognise that the use of some radiopharmaceuticals may be established in certain countries for a number of years, and yet simultaneously still feel new to others.

It is fundamental that the technologist understands the radiopharmaceutical journey from production to imaging acquisition, at the same time cultivating an understanding of imaging interpretation. This guide focuses on each element of that journey, based on a consistent structure introducing and explaining the basics and practicalities of each radiopharmaceutical. It embraces a wide spectrum of clinical applications, and while none is yet very commonly performed at the time of this first edition, all hold great promise for future patient care. Developments in more targeted PET radiopharmaceuticals, in particular, are taking on a pre-eminent role as staging and restaging tools, as well as in predicting and monitoring response.

The chapters are a useful mix of methodical literature review, input based on the authors' vast experience and critical thinking, with the goal of providing a summary of well-designed protocols and available techniques whilst acknowledging the dynamic nature of these new radiopharmaceuticals and how their use is still being optimised.

We hope it will serve as a reference toolkit, and that it spurs interest within multidisciplinary teams and encourages them to embrace novel procedures.

The editorial team appreciate the authors' efforts, commitment and their willingness to collaborate, and extend their thanks to the members of the Neuroimaging Committee who kindly reviewed the chapters relating to their respective spheres of expertise.

We sincerely hope that this booklet will be valuable, both as a guide for those learning how to perform these procedures and as a vehicle for dissemination of best practice in our ever more interesting specialty.

Luísa Roldão Pereira, Paolo Turco and Christopher Bruneby
The Editorial Team

1

FAP-TARGETING RADIOPHARMA-CEUTICALS

by Kim M. Pabst
Marta de Almeida Coelho
Pedro Fragoso Costa
Michael Nader

Department of Nuclear Medicine, University Hospital Essen, Germany

FAP-TARGETING RADIOPHARMACEUTICALS

Since 2018, fibroblast activation protein alpha (FAPα) has emerged as a promising target structure in the field of nuclear medicine. There is already speculation about whether it will become the next billion-dollar theranostics target [1].

The following chapter will provide detailed information on the new radioligand with regard to its background, radiopharmaceutical aspects, and clinical applications, with a focus on potential challenges and limitations.

BACKGROUND

In recent years, there has been a notable shift in the importance attributed to the tumour microenvironment (TME) in the field of molecular imaging and targeted therapies. The evidence that not only the tumour cells themselves, but also components of the surrounding stroma play a key role in tumour growth, migration, progression, and malignant cells' survival has led to a renewed interest in studying stromal structures [2,3]. In tumours with desmoplastic reaction, such as pancreatic ductal adenocarcinoma, colon and breast cancer, the stroma may represent

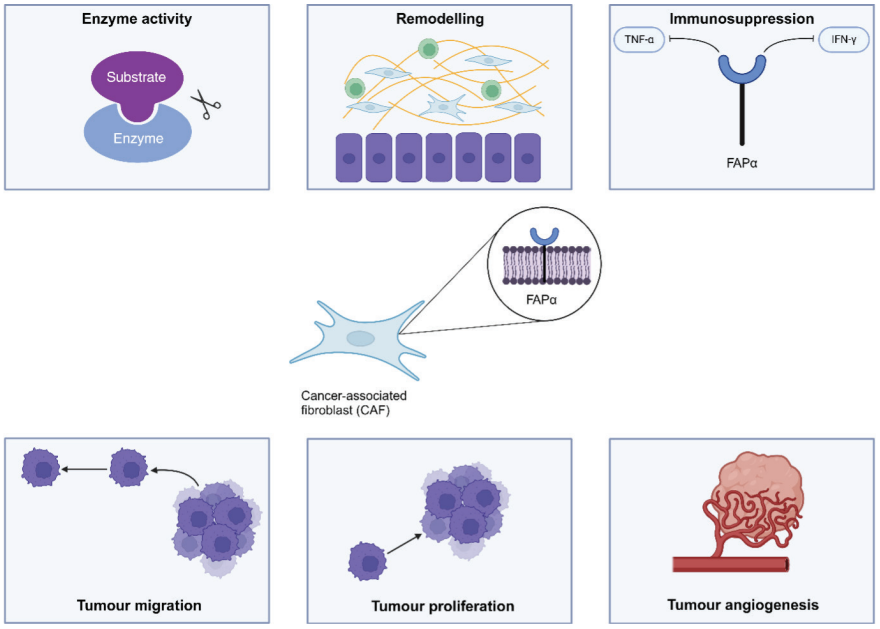

Figure 1. Summary of the fibroblast activation protein α (FAPα) role in tumours. TNF-α: Tumour necrosis factor-α. IFN-γ: Interferon-γ. Created with BioRender.com.

over 90% of the tumour mass. In particular, the heterogeneous subpopulation of fibroblast-like cells known as cancer-associated fibroblasts (CAFs) are among the critical cells of the tumour stroma [4].

CAFs overexpress FAPα, a type II transmembrane serine protease of the dipeptidyl peptidase subfamily and the oligopeptidase family, sharing 52% of the amino acid sequences with dipeptidyl peptidase 4 [5,6]. In addition to its proline-selective serine protease activity, FAPα also possesses an endopeptidase function. Consequently, FAPα is involved in remodelling of the TME by cleaving the structural proteins collagen I and III, and through other factors such as chemokines, cytokines and growth factors [7,8]. Thus, FAPα is involved in growth, proliferation and invasion of tumour cells [9]. Furthermore, FAPα is capable of suppressing the activity of interferon-γ and tumour necrosis factor-α, resulting in immunosuppression and the promotion of angiogenesis [9,10]. The proangiogenic potential is reinforced by the natural substrate of FAPα neuropeptide Y and the cleavage product [11]. The aforementioned mechanisms, summarised in Figure 1, indicate that FAPα plays a pivotal role in the resistance of tumours to various therapeutic modalities, including chemotherapy and targeted therapies [12]. Consequently, it can be concluded that FAPα expression is associated with an unfavourable prognosis, which has been investigated in particular in ovarian [13], pancreatic [14], hepatocellular [15] and colon carcinoma [16].

The major advantages of FAPα include its overexpression in more than 90% of epithelial tumours and the presence of a large extracellular domain, with the catalytic site also located extracellularly [17]. It can therefore be used as a pan-cancer target in molecular imaging [18]. In addition, FAPα is rarely found in healthy adult tissue [6]. However, FAP overexpression can also be observed in benign diseases that are predominantly based on fibrotic processes: examples include rheumatoid arthritis, wound healing and cardiovascular diseases [19].

CHEMISTRY AND PROPERTIES

Previously developed FAP inhibitors were structurally based on a quinoline amide core coupled to a 2-cyanopyrrolidine moiety; these showed a nanomolar affinity and selectivity for FAP with only a low affinity to other interfering dipeptidyl peptidases. Recently, the development of PET ligands was successfully achieved by the introduction of a dodecane tetra-acetic acid (DOTA) chelator coupled to an alkyl-piperazine spacer linked to the quinoline core and labelled with ^{68}Ga [20]. A ^{68}Ga–labelled FAPI tracer demonstrated high tumour-to-organ ratios and fast elimination in preclinical experiments. Moreover, first-in-human PET studies with [^{68}Ga]Ga-FAPI-04 revealed the excellent visualisation of a

broad range of tumours, with high tumour-to-noise ratios and the successful imaging of tumour metastases, since healthy fibroblasts, in contrast to tumour fibroblasts, express no or only very little FAP [17]. In view of the universal DOTA chelator and the low expression in normal organs, a theranostic application was a compelling approach. In 2018, a first therapeutic application of [^{90}Y]-FAPI-04 was published in a patient with advanced breast cancer [17]. [^{90}Y] has a high branching ratio for β-emission (99.99%) with an end-point energy of 2.280 MeV, which allows high dose deposition within defined tumour lesions. Its relatively short half-life of 64.1 h makes it appropriate for therapeutic combinations in which the biochemical vector exhibits short target retention time. A significant improvement in symptoms was achieved with a single administration and no toxicities were observed [17]. Further improvement of the FAPI core structure led to the theranostic pair [^{90}Y]Y-/[^{68}Ga]Y/Ga-FAPI-46, which demonstrated an increased tumour uptake and improved pharmacokinetic properties. In consequence, depending on the tumour type, tumour accumulation could be significantly prolonged [21,22].

LABELLING / PRODUCTION

Sterile [^{90}Y]yttrium chloride solution and a pharmaceutical grade ^{68}Ge/^{68}Ga generator were applied for the labelling of FAPI-46 using the cassette-based synthesis module Trasis EASYONE (Figure 2). All chemicals were GMP-grade or excipients with marketing authorisation. The quality control included test procedures according to Ph. Eur. Fully automated synthesis of the theranostic pair was achieved on the Trasis EASYONE synthesiser with a radiochemical yield of 56±5 % ([^{68}Ga]Ga-FAPI-46) and 88±7% ([^{90}Y]Y -FAPI-46) with a radiochemical purity of > 99%. Stability experiments showed a durability for [^{68}Ga] Ga-FAPI-46 within 4 h and for [^{90}Y]Y-FAPI-46 within 24 h. All obtained specifications and validations were compliant with the European Pharmacopoeia and regulatory guidelines. Both products were successfully applied in cancer patients (Figure 2) [22].

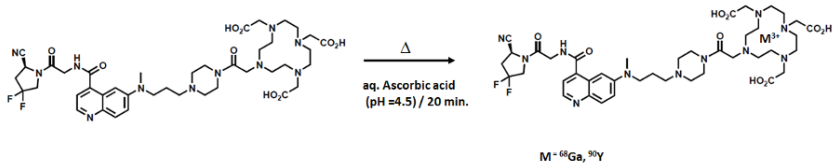

Figure 2. Scheme: Synthesis of [^{90}Y]Y-FAPI-46 and [^{68}Ga]Ga-FAPI-46

QUALITY CONTROL

The chemical and radiochemical purity were determined using a Chromolith Performance RP18e column (100 × 3 mm; 10 µm; Merck, Germany) eluted with solvent A, water containing 0.1% trifluoroacetic acid (TFA), and solvent B, acetonitrile containing 0.1% TFA. The conditions were as follows: linear gradient from 0–15% B over 5 min; flow rate of 1.1 mL min−1. In addition, for the determination of [^{68}Ga]GaCl3 and [^{68}Ga]Ga-FAPI-46, as well as the percentage of activity around the corresponding peaks, 0.1 M NH4OAc solution/MeOH (1:1) was used. [^{68}Ga]Ga-colloid was determined with trisodium citrate 1M solution (pH 5) as eluent system. For the determination of residual solvents GC analyses were performed using a Shimazu GC-2010 system including a Shimazu mass spectrometer GCMS-QP2010S and an AOC-20i auto-injector, which were controlled by LabSolution software (Shimadzu, Germany). A GC capillary column FS-INNOPEG-2000 (15 m×0.36 mm; CS-Chromatographie Service, Germany) was used as the stationary phase. The injector was set to 250°C at a split ratio of 48.5 and an injection volume of 0.8 µl. The column was operated at a constant helium carrier gas flow on the column of 0.92 ml/min. Sterility, pH and endotoxin testing were performed according to pharmacopoeial methods [22].

PHYSIOLOGICAL BIODISTRIBUTION

Since 2018, ^{68}Ga- or ^{18}F-labelled quinoline-based FAP inhibitors (FAPIs) have been utilised as radioligands for PET imaging, with continuous improvement in recent years [17,21].

Regarding the physiological bio-distribution of FAP-directed radioligands, it can be stated that the uptake by normal tissue is low, and the radioactivity is rapidly removed from the bloodstream and excreted primarily through the kidneys, resulting in high-contrast images [17]. Over time, the radioligands used have been continuously improved. The first radioligands, [^{68}Ga]Ga-FAPI-02 and [^{68}Ga]Ga-FAPI-04, demonstrated rapid achievement of a stable physiological distribution. The tumour uptake of [^{68}Ga] Ga-FAPI-02 showed an average wash-out of 75% between 1 hour and 3 hours, while [^{68}Ga]Ga-FAPI-04 already demonstrated an average wash-out of only 25%, resulting in a longer tumour retention. However, only minimal changes were observed in normal tissue between 10 minutes and 3 hours in both radioligands. The highest SUV_{mean} was found in the tumour lesions, followed by the kidneys, the blood pool, the parotid gland, and the oral mucosa [23]. In comparison to 2-[^{18}F]FDG, SUV_{max} demonstrated higher values in the following organs: the parotid gland, the blood pool and the kidneys, as well as the muscles and fat tissue [23].

Among various tumour entities, sarcoma, oesophageal, breast, lung, and cholangiocarcinoma demonstrated the highest mean SUV_{max} values (>12), followed by hepatocellular, colorectal, head and neck, ovarian, pancreatic, and prostate cancer (SUV_{max} 6-12). The lowest mean SUV_{max} values (<6) were observed in pheochromocytomas, renal cell, differentiated thyroid, adenoid cystic, and gastric carcinomas [18].

Based on FAPI-04, further derivatives with modifications of the linker region between the quinoline moiety and the chelator were developed. These derivatives demonstrated improved pharmacokinetic properties and a higher tumour uptake. [^{68}Ga]Ga-FAPI-46, in particular, exhibited an improved tumour-to-background ratio and a significantly longer accumulation, depending on the tumour entity investigated [21].

The ligands mentioned are all coupled with ^{68}Gallium. These compounds come with certain limitations, including the relatively short half-life of ^{68}Gallium (68 minutes) and the typical small batch size of 2–4 GBq for ^{68}Ge/^{68}Ga generators. To address these limitations, initial data on 18F-labelled FAP-directed ligands ([^{18}F] AlF-FAPI-74) with comparable properties were published in 2021 and are currently being used in prospective studies [24] (NCT05641896).

In conclusion, FAPα represents a promising pan-cancer target structure within the TME for further diagnostic and potentially therapeutic applications in various tumour entities. However, further large-scale prospective trials are pending for final decisions.

PATIENT PREPARATION AND AFTERCARE

Regarding patient preparation for [^{68}Ga]Ga-FAPI PET/CT and [^{18}F]FAPI PET/CT, there is no significant difference from other PET-CT examinations utilising the same isotope. In order to enhance the image quality of the examination and to minimise radiation exposure, patients should drink water before the examination, during the uptake period and following the procedure [25]. Prior to the examination, patients should void their bladder, which will reduce the background noise as well as the radiation dose to the kidneys and bladder.

There is no need for patients to fast before injection and no specific preparation is required for these examinations [26-28].

The physician or the technologist should provide the patient with a detailed explanation and information about the procedure.

Regarding precautions, we include pregnancy and breastfeeding. In the case of a diagnostic procedure in a patient who is or may be pregnant, a clinical decision is necessary to consider the benefits versus the possible harm of carrying out any procedure. It is recommended that breastfeeding be interrupted and restarted after the elapse of seven physical half-lives of radionuclide in a radiopharmaceutical [29].

IMAGING PROTOCOLS

In general, patients undergoing PET/CT examinations should positioned with the arms elevated and supported above the head to prevent beam-hardening artefacts and artefacts resulting from truncation of the measured field of view (FOV) [25]. Should the patient be unable to maintain the required position, one or both arms can be positioned alongside the body. Regarding the acquisition of scans for [^{68}Ga]Ga-FAPI PET/CT and [^{18}F]FAPI PET/CT, it can be ascertained from published articles that a whole-body acquisition (from the top of the head or base of the skull to the upper thigh) can be performed and obtained in a craniocaudal direction [26,30].

The CT image can be acquired in a low-dose protocol [26,31,32] or a full-dose protocol [30,33]. CT acquisition parameters including tube current, voltage, slice thickness, rotation time and pitch should be selected in accordance with the objective of the CT examination [25]. CT protocols must adhere to the international guidelines of the European Association of Nuclear Medicine [25].

Clinical PET/CT examinations with [^{68}Ga]Ga-FAPI PET/CT can be obtained at an early stage (approximately 10 minutes) [26,30-32] or at a late stage (approximately 60 minutes) [28,32,34] after intravenous injection. Regarding the injected activity, based on published articles it is possible to inject 80–200 MBq [26,28,30-32,34].

In a study by Ferdinandus et al., the authors compared the biodistribution and detection rate between early (approximately 10 minutes post-injection) and late (approximately 60 minutes post-injection) acquisition for [^{68}Ga]Ga-FAPI-46 PET/CT in patients with various types of cancer. In this study, it was found that intraindividual early versus late acquisition resulted in equivalent detection rates, with a slight, clinically non-relevant early-to-late increase in tumour-to-background ratios [28].

Clinical PET/CT examination with [^{18}F]FAPI can be obtained at an early stage (approximately 20 minutes) [27] or at a late stage (approximately 60–90 minutes) [27,33,35,36] after intravenous injection. Regarding the injected activity, it can be concluded from published articles that 3.7–4.44 MBq/kg can be injected [33].

In a study by Mu et al., the biodistribution, tracer retention, lesion detection, and uptake of early and late [^{18}F]AlF-FAPI-42 PET were compared. Both time points demonstrated equal lesion detection, but the early time point exhibited less tracer retention in the biliary system and significantly higher uptake of normal organs and lesions. However, this did not have a relevant impact on lesion detection or staging due to the higher tumour-to-background ratio for late acquisition [27].

PET scans are typically performed immediately after CT scan and obtained in three-dimensional mode. In terms of reconstruction, it is important to follow the relevant guidelines [25,29] for the radionuclide used. It is recommended that image reconstruction be performed using an iterative reconstruction algorithm (e.g. ordered subset expectation maximisation algorithm or equivalent) using the system's implementation and settings. It is also recommended that data be acquired and reconstructed with time-of-flight information (if available), with PSF (or equivalent) and also with Gaussian filter, which can be used for post-reconstruction filtering. It should be noted that all reconstruction methods depend on the system capabilities. Furthermore, it is recommended that reconstructions be performed including all regular corrections, such as normalisation, (CT-based) attenuation correction, dead time, decay correction, and, where possible, model-based scatter correction [29].

CLINICAL INDICATIONS, RESULTS AND INTERPRETATION

FAPα-directed radioligands represent a novel diagnostic imaging tool for PET/CT, applicable to a broad spectrum of tumour entities and various benign diseases. However, as with all PET/CT radioligands, there are potential pitfalls that must be considered when interpreting imaging results.

CLINICAL INDICATIONS - MALIGNANT DISEASES

In particular, FAPI-PET/CT is currently used for initial staging and restaging of various tumour diseases. Certain tumour entities appear to be particularly well-suited for this imaging modality and are presented in more detail below.

Sarcoma

Sarcomas represent a heterogeneous group of rare malignant, mesenchymal tumours with an unfavourable prognosis due to limited therapeutic options in the advanced/metastatic setting. However, a special feature of sarcomas is their frequent overexpression of FAPα, not only in the stroma, but also in the tumour cells themselves, rendering them a promising target for FAPα-directed imaging [37]. Retrospective analyses have demonstrated improved detection rates and accuracy in favour of [^{68}Ga]Ga-FAPI PET/CT for sarcomas compared to 2-[^{18}F]FDG PET/CT [30]. This is particularly evident in low-grade and potentially malignant intermediate or unpredictable sarcomas without a World Health Organization grade [38]. The subgroups with the highest tumour uptake include solitary fibrous tumours, undifferentiated pleomorphic sarcomas and leiomyosarcomas [38]. The additional use of [^{68}Ga]Ga-FAPI-PET/CT has led to an upstaging in 19% of patients and a change in clinical management in approximately one third of patients [30].

Cancers of the liver, biliary tract and pancreas

The incidence of hepatocellular carcinoma has increased in recent years. Combined with an unfavourable prognosis, this means that the malignancy is of great interest [39]. Staging is typically performed using MRI of the abdomen and CT of the thorax. 2-[^{18}F]FDG PET/CT is rarely used, as tumour uptake can be observed in less than 40% of cases and is negative in most well-differentiated hepatocellular carcinomas [40]. In several retrospective studies, FAPI-PET/CT demonstrated advantages over 2-[^{18}F]FDG PET/CT in the detection of tumour lesions due to a higher tumour-to-background ratio [41,42]. However, it should be noted that the main risk factor for hepatocellular carcinoma is liver cirrhosis, which shows an increased intrahepatic uptake on FAPI-PET/CT and makes it challenging to differentiate between benign and malignant lesions. Nevertheless, the uptake of tumour lesions appears to be higher than that of benign lesions, thus distinction is still feasible [19,43].

Cholangiocarcinomas originate from intra- and extrahepatic sites of the bile ducts. Following hepatocellular carcinoma, they are the second most common malignancies of the liver, with an increasing incidence [44,45]. They are often diagnosed late, frequently leading to a fatal outcome [46]. The treatment of cholangiocarcinoma is therefore critically dependent on accurate staging. Imaging with [^{68}Ga]Ga-FAPI demonstrated promising results. In particular, intrahepatic tumours benefit from the significantly higher tumoral uptake compared to 2-[^{18}F]FDG and high tumour-to-background ratios, leading to better delineation (Figure 3) [26]. Furthermore, the potential to improve decisions is evident. As with hepatocellular carcinoma, limitations arise from intrahepatic fibrotic/cirrhotic processes and inflammation of the bile ducts.

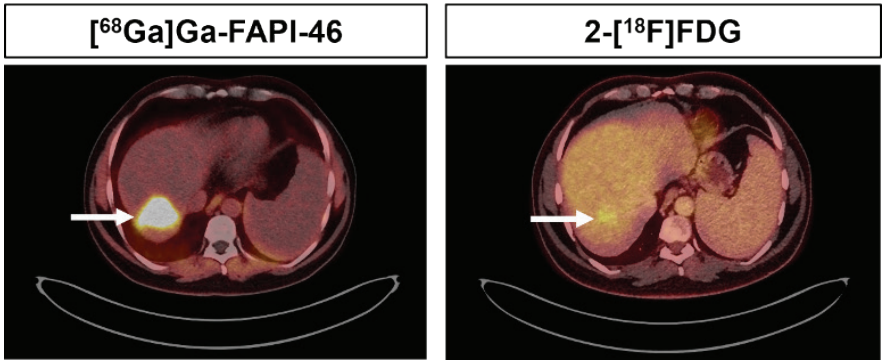

Figure 3. 43-year-old patient diagnosed with intrahepatic cholangiocarcinoma (white arrow).

However, differences in uptake were mentioned between malignant and benign diseases [47].

Pancreatic ductal adenocarcinoma (PDAC) is often diagnosed at an advanced/metastatic stage due to unspecific symptoms, resulting in a poor prognosis [48]. The use of [^{68}Ga]Ga-FAPI PET/CT also demonstrated a detection advantage in this indication, particularly for primary tumours, peritoneal and liver metastasis. In contrast, the detection rate for lung metastases was higher for 2-[^{18}F]FDG PET/CT and contrast-enhanced CT. Inter-reader agreement was limited for primary tumours, among others. This observation may be explained by false-positive uptake due to (obstructive) pancreatitis and scarring [49]. However, obstructive pancreatitis is associated with reduced overall survival in patients with PDAC, suggesting that an uptake of the entire pancreas may be helpful in prognostic stratification [50]. Furthermore, uptake was significantly higher in PDAC compared to pancreatitis, although there may be an overlap. Additional information can be provided by dynamic time-activity curves, which are characteristic for both diseases, PDAC and pancreatitis. This emphasises the additional value of dynamic [^{68}Ga]Ga-FAPI PET/CT imaging for differentiation between pancreatic malignant and inflammatory diseases [51].

Lung Cancer

The potential advantages of FAPα-directed PET/CT over 2-[^{18}F]FDG PET/CT in lung cancer have been the subject of several studies. It has been demonstrated that immunohistochemical FAP expression levels may reach up to 100% in non-small-cell lung cancer, while they are up to 67% in small-cell lung cancer and large-cell neuroendocrine carcinoma [52]. In malignant lung lesions, the SUV_{max} of FAPI-PET/CT compared to 2-[^{18}F]FDG PET/CT was only superior in individual studies [53], but more often comparable or inferior [54,55], not affecting the overall diagnostic accuracy [54]. A significant disadvantage of 2-[^{18}F]FDG PET/CT is the partially increased reactive/inflammatory uptake in mediastinal lymph nodes, which may result in a challenging differentiation from lymph node metastases [56]. Further treatment may be affected, particularly in the context of pre-operative staging. It has been demonstrated that [^{68}Ga]Ga-FAPI-46 PET/CT allows for more precise differentiation and has the potential to reduce false-positive results [57,58]. Nevertheless, the additional benefit is currently still controversial.

Gastrointestinal Tract Cancer

Oesophageal carcinomas, among other tumours, demonstrate the highest uptake of [^{68}Ga]Ga-FAPI-46 PET/CT [18]. In addition to a high uptake, there are also high tumour-to- background ratios, enabling precise differentiation [59]. Furthermore, first indications can be derived of significant differences in SUV_{mean} tumour-to-background ratio (blood) and (muscle) between patients responding to chemotherapy and non-responders [60]. A higher tumour-to-background ratio (blood) was associated with a poorer prognosis, suggesting that a response prediction may be feasible [60]. The impact of FAPI PET/CT on radiotherapeutic management in patients with oesophageal carcinoma has also been determined: the combination of [^{68}Ga]Ga-FAPI-46 and 2-[^{18}F]FDG PET/CT resulted in an increase in the irradiation field in 16% of patients, and in an adjustment of the treatment regime in 9% [59,61]. The advantages of mediastinal nodal staging mentioned for lung cancer could also be seen in this indication [57,58].

The use of 2-[^{18}F]FDG PET/CT in gastric cancer comes with several limitations, resulting in a pronounced and unsatisfactory variance in diagnostic sensitivity (17–95%) [62,63]. These limitations include physiological uptake of the stomach wall and false-positive uptake in the presence of gastritis [64]. Furthermore, some non-intestinal subtypes such as signet ring cell carcinoma and mucinous adenocarcinomas only show limited 2-[^{18}F]FDG uptake, leading to low sensitivity [65]. In contrast, a meta-analysis by Ruan et al. demonstrated a significantly higher sensitivity of FAPI-PET/CT for initial diagnosis/local recurrence of gastric cancer, lymph node and distant metastases compared to 2-[^{18}F]FDG PET/CT. This can be attributed to the high uptake and the low background activity [66]. However, the sensitivity crucially depends on the size of the primary tumour [67]. Regarding distant metastases, peritoneal carcinomatosis should be emphasised in particular. In bone metastases, the advantages are not clearly proven: FAPI-PET/CT displays a sensitivity that is either increased or comparable to that of 2-[^{18}F]FDG PET/CT. However, false-positive findings including osteophytes or other benign lesions may reduce the specificity [66,68]. Signet ring cell carcinomas frequently exhibit a high proportion of stroma with FAP overexpression, which is reflected in increased [^{68}Ga]Ga-FAPI uptake [69]. Mucinous adenocarcinomas also demonstrate relevant imaging FAP expression [70]. Limitations of FAPI-PET/CT include an increased uptake due to inflammation, radiotherapy or surgery-induced fibrosis [66].

FAPI-PET/CT also appears to be beneficial for colorectal cancer. Compared to other tumour entities, the SUV_{max} value of colorectal cancer can be classified as intermediate, and is reported to be equivalent to or even higher than that observed with 2-[^{18}F]FDG PET/CT [18,71]. One of the key advantages of FAPI-PET/CT over 2-[^{18}F]FDG PET/CT in colorectal cancer is the lower background uptake in relevant

anatomical regions, including the liver and intestine, improving the delineation of tumour lesions [72,73]. Moreover, several studies have demonstrated the potential impact of [^{68}Ga]Ga-FAPI-04 PET/CT on tumour treatment [72]. Furthermore, a positive correlation was identified between FAPI uptake and the consensus molecular subtype 4, which is associated with a poorer prognosis and treatment resistance [74].

Gynaecological Malignancies

In the context of gynaecological tumour entities, the current focus of FAPα-directed imaging is on breast cancer: breast cancer has so far shown an increased FAPI uptake compared to 2-[^{18}F]FDG PET/CT in primary tumours, lymph node, lung and bone metastases. However, liver metastases demonstrated no significant difference [75,76]. Tumour-to-background ratios of FAPI-PET/CT are also favourable compared to 2-[^{18}F]FDG PET/CT, leading to a higher

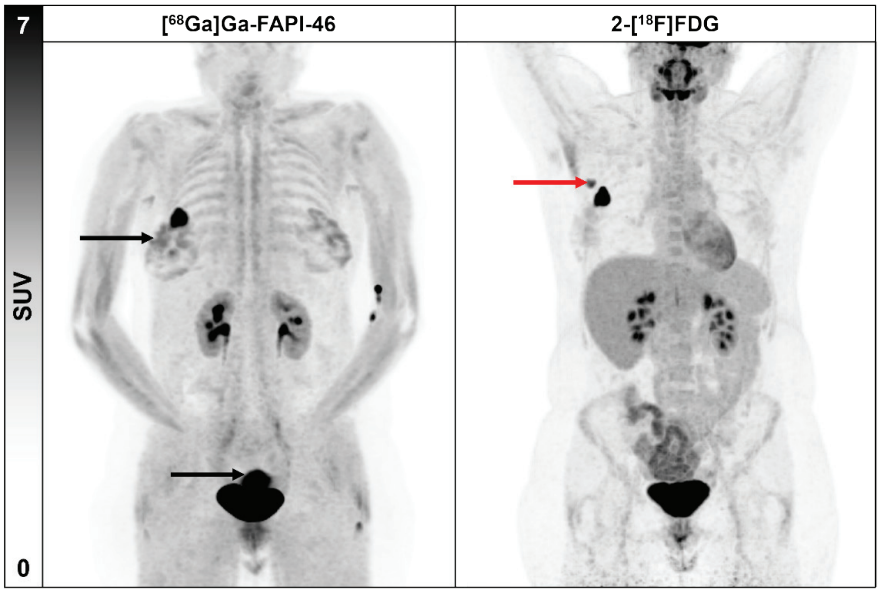

Figure 4. 40-year-old female patient with initial diagnosis of triple-negative breast cancer and a false-positive lymph node on 2-[^{18}F]FDG PET/CT (red arrow). Symmetrical physiological uptake of breast tissue and uterus on [^{68}Ga]Ga-FAPI-46 PET/CT (black arrows).

accuracy [76-78]. In dual application, the additional use of FAPI-PET/CT may help to detect false- positive lymph nodes on 2-[^{18}F]FDG PET/CT [58], which is particularly important in initial staging (Figure 4). It should be noted, however, that menstrual cycle-dependent uptake of the healthy breast tissue may represent a limitation [76].

The data on FAPI-PET/CT in ovarian cancer is currently limited. The efficacy of [^{68}Ga]Ga-FAPI-04 PET/CT in detecting lymph node metastases and peritoneal carcinomatosis has been demonstrated to be superior compared to 2-[^{18}F]FDG PET/CT [77,79]. A significantly increased tumour uptake was also detected in these regions [79]. Liu et al. reported that the uptake in recurrent lesions shows no significant difference on [^{68}Ga]Ga-FAPI-04 PET/CT compared to 2-[^{18}F]FDG PET/CT, but demonstrates a difference in tumour-to-background ratios [80]. In patients with treatment-naïve ovarian cancer, [^{68}Ga]Ga-FAPI-04 PET/CT resulted in upstaging in 14.3%, with tumour recurrence in 33.3%. The treatment regime was modified in 10.7% and 33.3% of patients, respectively [79].

CLINICAL INDICATIONS – BENIGN DISEASES

At present, two benign disease groups in particular have been increasingly investigated using FAPI-PET/CT, namely rheumatoid arthritis and cardiovascular diseases. The majority of other benign diseases have been described as pitfalls and are explained in more detail under this topic.

Rheumatoid Arthritis

Rheumatoid arthritis is an autoimmune-mediated inflammatory disease of the synovial joints. Fibroblast-like synoviocytes are involved in the pathogenesis of rheumatoid arthritis by contributing to the formation of pannus and the destruction of articular cartilage and bone. These cells express FAP and have therefore already been analysed in several studies using [^{68}Ga]Ga-FAPI PET/CT [81]. The SUV_{max} was found to be significantly higher compared to 2-[^{18}F]FDG PET/CT scans, and a correlation was identified between the number of affected joints on PET/CT/the degree of uptake and clinical/laboratory parameters [81]. Furthermore, the monitoring and prediction of therapeutic response using [^{68}Ga]Ga/[^{18}F]-FAPI PET/CT in rheumatoid arthritis appears to be feasible, as shown by the results of small prospective cohorts [82,83]. However, further studies are needed to confirm the clinical benefit.

Cardiovascular Diseases

FAPα-directed imaging also received attention due to the detection of inflammatory processes in the heart. These processes with subsequent fibroblast activation are followed by reparative processes and differentiation into myofibroblasts, which leads to the deposition of extracellular matrix and apoptosis of

granulation tissue [84]. The physiological balance between inflammatory and repair processes is critical for proper healing. Dysregulation is important in almost all myocardial diseases and may lead to increased tissue damage [85]. Studies of FAPI-PET/CT in cardiovascular diseases are still scarce and focus mainly on imaging after acute myocardial infarction. Pre-clinical studies have shown that FAP expression follows a dynamic time course [86]. In subsequent clinical studies, FAPI uptake after acute myocardial infarction was confirmed [87]. FAPI uptake was found in the infarct zone, which interestingly extended beyond the perfusion defect visualised by cardiac MRI and nuclear perfusion imaging [87]. FAPI PET/CT was also used to identify early signs of ventricular remodelling after diagnosed acute myocardial infarction, where FAPI uptake appeared to correlate well with signs of myocardial damage and provided predictive value for late remodelling of the left ventricular myocardium after 12 months [88]. Further studies providing a deeper insight into imaging with FAPI in patients with cardiovascular diseases, especially after acute myocardial infarction, are still pending.

PITFALLS IN THE INTERPRETATION OF FAPI-PET/CT

In the clinical application of FAPI-PET/CT, a number of pitfalls and common findings have emerged over time, which are summarised in Table 1.

Organ/Region	Pitfall
Intracranial	• Sinus thrombosis (Neuro-Behçet's disease) [88] • Progressive leukoencephalopathy [90]
Head and Neck	• Nasal mucosa [32] • Salivary glands [32] • Dental [32] • Mastoiditis [32] • (Hashimoto's) Thyroiditis [91] • Grave's disease including Graves ophthalmopathy [91,92]
Heart and blood vessels	• Pulmonary arterial hypertension [93] • Thermal damage after pulmonary vein isolation [94] • Myocarditis [84] • (Coronary) atherosclerotic plaques [19] • Takayasu arteritis [95]
Lung and Pleura	• Pneumonia [96] • Pulmonary tuberculosis [95] • Pulmonary fibrosis / interstitial lung diseases [97] • Silicosis nodules [95] • Pleuritis [95]
Thorax, other	• Oesophagitis [98]
Hepatopancreatico-biliary tract	• Liver fibrosis/cirrhosis [19] • Liver haemangioma [95] • Pancreatitis [49] • Sclerosing cholangitis and bile ducts (IgG4-related diseases) [99] • Cholecystitis [100]
Abdomen, other	• Renal fibrosis [101] • Haemorrhoid [95] • Crohn's disease [19] • Chronic colitis [19] • Idiopathic retroperitoneal fibrosis [102] • Schwannoma [103]
Primary/secondary sexual organs	• Breast uptake depending on menstrual cycle [76] • Endometrial/uterine uptake depending on menstrual cycle [32,76] • Uterine myoma [95] • Pre-menopausal uptake of the ovaries [76] • Prostatitis (IgG4-related) [95]
Bones and Joints	• Arthritis [32,103] • Exostosis [95] • Fractures [103] • Osteofibrous dysplasia [104] • Degenerative bone and joint lesions [19,32] • Brown tumour [105] • Inflammatory/trauma-related lesions [104] • Synovitis [95]
Muscles and Skin	• Unspecific muscle uptake, especially in larger muscle groups [32] • Enthesopathy [95] • Dermatomyositis [103] • Myelofibrosis [103] • Tendinopathy [95] • Cutaneous fibroma [95] • Post-surgery/wound healing [32] • Post-surgery inflammation [95] • Scarring [32]

Table 1. Summary of pitfalls and common findings on FAPI-PET/CT.
No claim to completeness.

In addition to the previously described malignant diseases, inflammatory and, in this context, fibrotic processes in particular demonstrate evidence of FAPα expression on imaging.

An interesting pitfall concerns, for example, Hashimoto's thyroiditis, Graves' disease and immune checkpoint inhibitor-induced thyroiditis (Figure 5) [91,92].

[^{68}Ga]Ga-FAPI-46

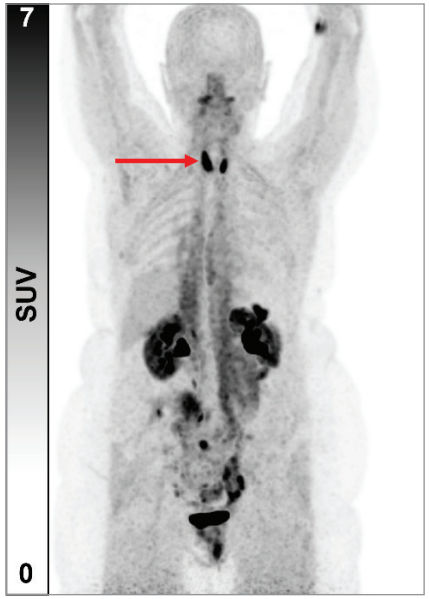

Figure 5. 71-year-old female patient for restaging of a solitary fibrous tumour with known Hashimoto's thyroiditis, taking levothyroxine (red arrow).

Processes such as liver fibrosis/cirrhosis can negate the advantage of low hepatic background activity on FAPI-PET/CT, making it more difficult to detect intrahepatic primary tumours, such as cholangiocarcinoma and hepatocellular carcinoma, and distant metastases (Figure 6) [19]. This also applies to pancreatitis, which can be mistaken for a PDAC, but can also misrepresent the extent of a known PDAC (Figure 7) [49]. Similar issues also arise in the context of gallbladder carcinoma and cholecystitis.

In addition to the aforementioned pathological FAPα expression in various malignant and non-malignant diseases, it can also be found in several physiological processes: the presence or absence of the menstrual cycle appears to correlate with FAPα expression in healthy breast tissue, the endometrium/uterus and the ovaries (Figure 4) [32,76,77].

Furthermore, an elevated FAPα expression can be observed in the musculature. Here, it mediates essential physiological functions, and its depletion leads to an atrophic muscle response [106]. Sites with predilection for this phenomenon are larger muscle groups, including the quadriceps femoris muscle, the latissimus dorsi muscle, the autochthonous back muscles, and the triceps muscle [32].

It is important to be aware that scarring and wound healing, particularly in patients with oncological diseases, may result in false-positive findings on FAPI-PET/CT [32]. The pitfalls summarised in Table 1 are intended to help recognise and correctly interpret false-positive findings, as well as to understand the limitations of FAPI-PET/CT.

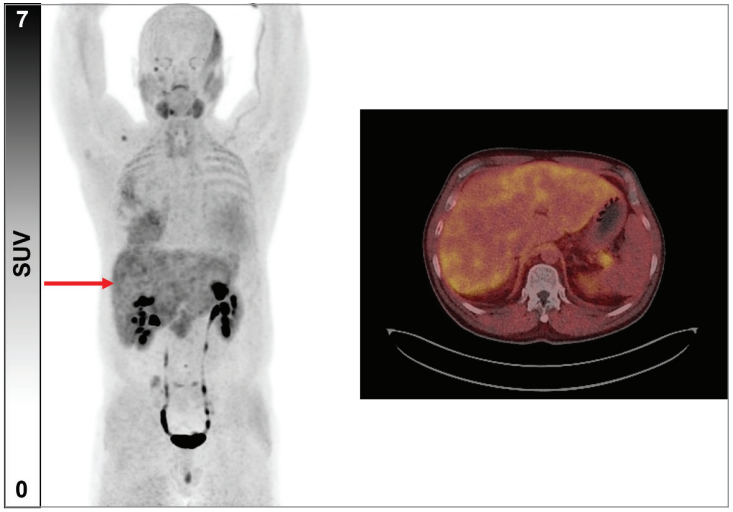

Figure 6. 46-year-old male patient with suspected pleural mesothelioma and known liver fibrosis (red arrow).

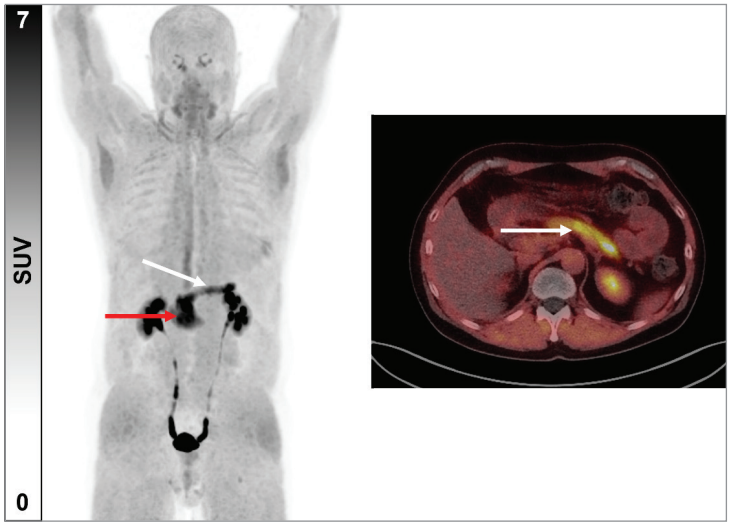

Figure 7. 59-year-old male patient with initial staging of pancreatic ductal adenocarcinoma (red arrow) and concomitant pancreatitis (white arrow).

DOSIMETRY AND THERANOSTICS POTENTIAL

Due to the favourable signal-to-background ratio in a number of carcinomas and sarcoma, FAPI-PET/CT emerges as a solid alternative to detect primary and metastatic disease [18, 107-110]. These facts combined with a fast clearance by the kidneys [111] formed the first body of evidence that motivated a theranostic approach and the development of therapeutic FAPI ligands.

Figure 8 depicts the principle by which the identification of tumoral regions and their FAP expression serves as a basis for enrolling patients in FAP-based radioligand therapy (RLT). RLT aims at delivering a lethal radiation dose to pathogenic regions, while avoiding toxicity to healthy organs.

As mentioned before, ^{68}Ga is the predominant radionuclide for diagnostic evaluation of FAP expression. Currently, the workflow of patient selection for FAPI-RLT consists of 1) FAP positivity of tumour lesions — in some cases defined as SUV_{max} > 3 [112] or SUV_{max} > 10 [113,114], 2) adequate bone marrow function and 3) maintenance of urinary tract function. Reported radionuclides for FAPI-RLT are ^{90}Y, ^{153}Sm and ^{177}Lu [112,114,115]. In terms of ligands, FAPI-04 [116], FAPI-46 [114], FAP-2286 [117], DOTA.SA.FAPI and the dimer DOTAGA.(SA.FAPI)2 [112] are among the most used.

Dosimetry Protocols

For those radionuclides with concomitant gamma emissions (notably ^{177}Lu), planar and SPECT data is acquired at 4, 24, 48, and 96 or 144 hours to capture the maximum uptake peak and characterise the late decay (exponential tail component). Ideally, a medium-energy collimator should be used, with acquisition and reconstruction parameters following the current guidelines for Lu-177 image-based dosimetry [118].

For ^{90}Y-based FAPI-RLT, the use of Si-PM PET/CT systems is recommended due to the very low internal positron-electron pair conversion rate (0.00326% pairs per decay) [119]. Specifically, for [^{90}Y]Y-FAPI-46, due to the rapid metabolisation, image data should be acquired in the first 24 h after administration (1, 4 and 20 hours).

According to the reported dosimetry results for the different ligand and radionuclide combinations available, it is notable that the organs at risk are the bone marrow and kidneys. For lesion and kidney dosimetry, planar and tomographic imaging is required. Since FAPI has no specific uptake in the bone marrow, the blood method should be performed to assess bone marrow absorbed doses [120].

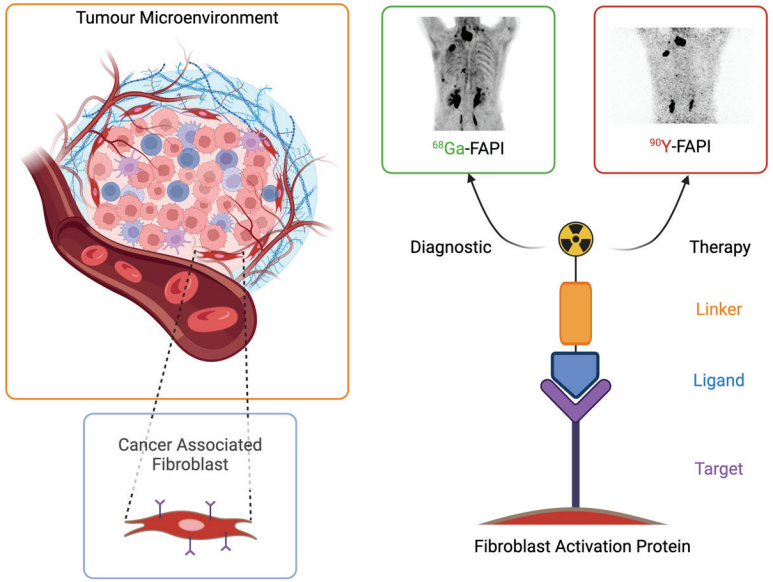

Figure 8. Theranostic principle for FAP ligands. A [^{68}Ga]Ga-FAPI-46 MIP (left) of a patient with a solitary fibrous tumour is presented for RLT selection with [^{90}Y]Y-FAPI-46 (right MIP) [120]

Drug	Total GBq	Tumour	Tumour dosimetry (Gy/GBq)	Tumour Effective Half- Life (h)	Bone marrow dosimetry (Gy/GBq)	Kidney dosimetry (Gy/GBq	Reference
[^{177}Lu] Lu-FAPI-04	0.27	Breast, thymus, thyroid, and ovarium	0.62	N/A	0.002	0.25	[116]
[^{90}Y]Y-FA-PI-46	3.7–7.4	Sarcoma, pancreas, prostate, gastric	2.81	8.7	0.040	0.53	[113,114]
[^{177}Lu]Lu-FAP-2286	5.8	Pancreas, breast, rectum, and ovarium	3.00	NA	0.050	1.00	[117]
[^{177}Lu] Lu-DOTA. SA.FAPI	2.96	Breast	0.60	14.0	0.001	0.62	[112]
[^{177}Lu] Lu-DOT-AGA.(SA. FAPI)2	1.48	Thyroid, breast, and paragan-glioma	6.70	86.6	0.020	0.37	[112]

Table 2. Dosimetry features of selected FAP-RLT publications. An extensive review of the current FAP-RLT is given in [121].

The current dosimetry findings on FAPI-RLT show that all procedures are safe, with organ-at- risk doses comparable to other RLT (such as [^{177}Lu]Lu-DOTATOC and [^{177}Lu]Lu-PSMA). The rapid washout of target lesions is one of the main causes for the reported low tumoral absorbed doses.

To overcome the rapid washout of radioligands from tumours, new generations of FAP inhibitors have been developed for better tumour retention and effective cytotoxic dose delivery. Strategies to enhance intratumoral retention of radiolabelled FAPI in cancer theranostics include conjugating ligands to albumin binders, ligand dimerisation, and substituting small molecular ligands with larger peptides.

REFERENCES

1. Calais J. FAP: The Next Billion Dollar Nuclear Theranostics Target? J Nucl Med. 2020;61:163-165.
2. Loktev A, Lindner T, Mier W, Debus J, Altmann A, Jager D, et al. A Tumor-Imaging Method Targeting Cancer-Associated Fibroblasts. J Nucl Med 2018;59:1423-1429.
3. Zhang Y & Weinberg RA. Epithelial-to-mesenchymal transition in cancer: complexity and opportunities. Front Med 2018; 361-373.
4. Zi F, He J, He D, Li Y, Yang L, Cai Z. Fibroblast activation protein α in tumor microenvironment: recent progression and implications. Mol Med Rep 2015;11:3203-3211.
5. Hamson EJ, Keane FM, Tholen S, Schilling O, Gorrell MD. Understanding fibroblast activation protein (FAP): substrates, activities, expression and targeting for cancer therapy. Proteomics Clin Appl 2014; 8:454-463.
6. Shahvali S, Rahiman N, Jaafari MR, Arabi L. Targeting fibroblast activation protein (FAP): advances in CAR-T cell, antibody, and vaccine in cancer immunotherapy. Drug Deliv. and Transl. Res 2023;13:2041-2056.
7. Kelly T. Fibroblast activation protein-alpha and dipeptidyl peptidase IV (CD26): cell-surface proteases that activate cell signaling and are potential targets for cancer therapy. Drug Resist Updat: Reviews and Commentaries in Antimicrobial and Anticancer Chemotherapy 2005;8:51-58.
8. Lo A, Wang L-CS, Scholler J, Monslow J, Avery D, Newick K, et al. Tumor-promoting desmoplasia is disrupted by depleting FAP-expressing stromal cells. Cancer Res 2015;75:2800-2810.
9. Chen WT, Kelly T. Seprase complexes in cellular invasiveness. Cancer Metastasis Rev 2008; 22:259-269.
10. Kuzet S-E, Gaggiolo C. Fibroblast activation in cancer: when seed fertilizes soil. Cell Tissue Res 2016;365:607-619.
11. Keane FM, Nadvi NA, Yao TW, Gorrell MD. Neuropeptide Y, B-type natriuretic peptide, substance P and peptide YY are novel substrates of fibroblast activation protein-alpha. FEBS J 2011;278:1316-1332.
12. Feng B, Wu J, Shen B, Jiang F, Feng J. Cancer-associated fibroblasts and resistance to anticancer therapies: status, mechanisms, and countermeasures. Cancer Cell Int 2022;22:166.
13. Zhang Y, Tang H, Cai J, Zhang T, Guo J, Feng D, et al. Ovarian cancer-associated fibroblasts contribute to epithelial ovarian carcinoma metastasis by promoting angiogenesis, lymphangiogenesis and tumor cell invasion. Cancer Lett 2011;303:47-55.
14. Cohen SJ, Alpaugh RK, Palazzo I, Meropol NJ, Rogatko A, Xu Z, et al. Fibroblast activation protein and its relationship to clinical outcome in pancreatic adenocarcinoma. Pancreas 2008;37:154-158.
15. u MJ, Qiu SJ, Fan J, Xiao YS, Gao Q, Zhou J, et al. Peritumoral activated hepatic stellate cells predict poor clinical outcome in hepatocellular carcinoma after curative resection. Am J Clin Pathol 2009;131:498-510.
16. Henry LR, Lee HO, Lee JS, Klein-Szanto A, Watts P, Ross EA, et al. Clinical implications of fibroblast activation protein in patients with colon cancer. Clin Cancer Res 2007;13:1736-1741.
17. Lindner T, Loktev A, Altmann A, Giesel F, Kratochwil C, Debus J, et al. Development of Quinoline-Based Theranostic Ligands for The Targeting of Fibroblast Activation Protein. J Nucl Med 2018;59:1415-1422.
18. Kratochwil C, Flechsig P, Lindner T, Abderrahim L, Altmann A, Mier W, et al. 68Ga-FAPI PET/CT: Tracer Uptake in 28 Different Kinds of Cancer. J Nucl Med 2019;60:801-805.
19. Dendl K, Koerber SA, Kratochwil C, Cardinale J, Finck R, Dabir M, et al. FAP and FAPI-PET/CT in Malignant and Non-Malignant Diseases: A Perfect Symbiosis? Cancers (Basel) 2021;13:4946.
20. Loktev A, Lindner T, Mier W, Debus J, Altmann A, Jäger D, et al. A Tumor-Imaging Method Targeting Cancer-Associated Fibroblasts. J Nucl Med. 2018;59:1423-1429.
21. Loktev A, Lindner T, Burger E-M, Altmann A, Giesel F, Kratochwil C, et al. Development of Fibroblast Activation Protein-Targeted Radiotracers with Improved Tumor Retention. J Nucl Med. 2019;60:1421-1429.

22. Nader M, Valla DF, Vriamont C, Masset J, Pacelli A, Herrmann K, et al. [^{68}Ga]/[^{90}Y]FAPI-46: Automated production and analytical validation of a theranostic pari. Nucl Med Biol. 2022;epub.
23. Giesel FL, Kratochwil C, Lindner T, Marschalek MM, Loktev A, Lehnert W, et al. 68Ga-FAPI PET/CT: Biodistribution and Preliminary Dosimetry Estimate of 2 DOTA-Containing FAP-Targeting Agents in Patients with Various Cancers. J Nucl Med 2019;60:386-392.
24. Lindner T, Altmann A, Giesel F, Kratochwil C, Kleist C, Krämer S, et al. 18F-labeled tracers targeting fibroblast activation protein. EJNMMI Radiopharm Chem 2021;26.
25. Boellaard R, Delgado-Bolton R, Oyen WJ, Giammarile F, Tatsch K, Eschner W, et al. European Association of Nuclear Medicine (EANM). FDG PET/CT: EANM procedure guidelines for tumour imaging: version 2.0. Eur J Nucl Med Mol Imaging. 2015;42:328-354.
26. Pabst KM, Trajkovic-Arsic M, Cheung PFY, Ballke S, Steiger K, Bartel T, et al. Superior Tumor Detection for 68Ga-FAPI-46 Versus 18F-FDG PET/CT and Conventional CT in Patients with Cholangiocarcinoma. J Nucl Med. 2023; 64:1049-1055.
27. Mu X, Mo B, Qin J, Li Z, Chong W, Zeng Y, et al. Comparative analysis of two timepoints on [^{18}F]FAPI-42 PET/CT in various cancers. Eur J Hybrid Imaging. 2023;7:27.
28. Ferdinandus J, Kessler L, Hirmas N, Trajkovic-Arsic M, Hamacher R, Umutlu L, et al. Equivalent tumor detection for early and late FAPI-46 PET acquisition. Eur J Nucl Med Mol Imaging. 2021;48:3221-3227.
29. Bozkurt MF, Virgolini I, Balgova S, Beheshti M, Rubello D, Decristoforo C, et al. Guideline for PET/CT imaging of neuroendocrine neoplasms with 68Ga-DOTA-conjugated somatostatin receptor targeting peptides and 18F-DOPA. Eur J Nucl Med Mol Imaging. 2017;44:1588-1601.
30. Kessler L, Ferdinandus J, Hirmas N, Bauer S, Dirksen U, Zarrad F, et al. 68Ga-FAPI as a Diagnostic Tool in Sarcoma: Data from the 68Ga-FAPI PET Prospective Observational Trial. J Nucl Med. 2022;63:89-95.
31. Siebermair J, Köhler MI, Kupusovic J, Nekolla SG, Kessler L, Ferdinandus J, et al. Cardiac fibroblast activation detected by Ga-68 FAPI PET imaging as a potential novel biomarker of cardiac injury/remodeling. J Nucl Cardiol. 2021;812-821.
32. Kessler L, Ferdinandus J, Hirmas N, Zarrad F, Nader M, Kersting D, et al. Pitfalls and Common Finding in 68Ga-FAPI PET: A Pictorial Analysis. J Nucl Med. 2022;63:890-896.
33. Li X, Lu N, Lin L, Chen Y, Yang S, Wang H, et al. 18F-FAPI-04 Outperforms 18F-FDG PET/CT in Clinical Assessments of Patients with Pancreatic Adenocarcinoma. J Nucl Med. 2024;65:206-212.
34. Miao Y, Feng R, Guo R, Huang X, Hai W, Li J, et al. Utility of [^{68}Ga]FAPI-04 and [^{18}F]FDG dual-tracer PET/CT in the initial evaluation of gastric cancer. Eur Radiol. 2023;33:4355-4366.
35. Li Y, Gao J, Li Y, Duan X, Shen C. Non-specific uptake of 18F-FAPI-04 in the pancreas and its related factors: a post-hoc analysis of an ongoing prospective clinical trial. Sci Rep. 2024;14:11141.
36. Watabe T, Naka S, Tatsumi M, Kamiya T, Kimura T, Shintani Y, et al. Initial Evaluation of [^{18}F]FAPI-74 PET for Various Histopathologically Confirmed Cancers and Benign Lesions. J Nucl Med. 2023;64:1225-1231.
37. Hamacher R, Lanzafame H, Mavroeidi IA, Pabst KM, Kessler L, Cheung PF, et al. Fibroblast Activation Protein Inhibitor Theranostics: The Case for Use in Sarcoma. PET Clin. 2023;18:361-367.
38. Lanzafame H, Mavroeidi IA, Pabst KM, Desaulniers M, Ingenwerth M, Hirmas N, et al. 68Ga-Fibroblast Activation Protein Inhibitor PET/CT Improves Detection of Intermediate and Low-Grade Sarcomas and Identifies Candidates for Radiopharmaceutical Therapy. J Nucl Med 2024; Epub ahead of print.
39. Vogel A, Cervantes A, Chau I, Daniele B, Llovet JM, Meyer T, et al. Hepatocellular carcinoma: ESMO Clinical Practice Guidelines for diagnosis, treatment and follow-up. Ann Oncol. 2018;29(Suppl 4): iv238-iv255.
40. Castilla-Lievre MA, Franco D, Gervais P, Kuhnast B, Agostini H, Marthey L, et al. Diagnostic value of combining (1)(1)C-choline and (1)(8)F-FDG PET/CT in hepatocellular carcinoma. Eur J Nucl Med Mol Imaging 2016;43:852-859.
41. Zhang J, Jiang S, Li M, Xue H, Zhong X, Li S, et al. Head-to-head comparison of 18F-FAPI and 18F-FDG PET/CT in staging and therapeutic management of hepatocellular carcinoma. Cancer Imaging. 2023;23:106.
42. Wang H, Zhu W, Ren S, Kong Y, Huang Q, Zhao J, et al. 68Ga-FAPI-04 Versus 18F-FDG PET/CT in the Detection of Hepatocellular Carcinoma. Front Oncol. 2021;11:693640.
43. Zhao L, Gu J, Fu K, Lin Q, Chen H. 68Ga-FAPI PET/CT in Assessment of Liver Nodules in a Cirrhotic Patient. Clin Nucl Med. 2020;45:e430-e432.
44. Bergquist A, von Seth E. Epidemiology of cholangiocarcinoma. Baillieres Best Pract Res Clin Gastroenterol. 2015;29:221-232.
45. Shaib Y, El-Serag HB. The epidemiology of cholangiocarcinoma. Semin Liver Dis. 2004; 24:115-125.
46. Razumilava N, Gores GJ. Cholangiocarcinoma. Lancet. 2014;383:2168-2179.
47. Lan L, Zhan S, Xu T, Liu H, Wang W, Feng Y, et al. Prospective Comparison of 68Ga-FAPI versus 18F-FDG PET/CT for Tumor Staging in Biliary Tract Cancers. Radiology. 2022;304:648-657.
48. Park W, Chawla A, O'Reilly EM. Pancreatic cancer: a review. JAMA. 2021;326:851-862.
49. Kessler L, Hirmas N, Pabst KM, Hamacher R, Ferdinandus J, Schaarschmidt BM, et al. 68Ga-Labeled Fibroblast Activation Protein Inhibitor (68Ga-FAPI) PET for Pancreatic Adenocarcinoma: Data from the 68Ga-FAPI PET Observational Trial. J Nucl Med. 2023;64:1910-1917.
50. Ding J, Qui J, Hao Z, Huang H, Liu Q, Liu W, et al. Comparing the clinical value of baseline [^{68}Ga]Ga-FAPI-04 PET/CT and [^{18}F]F-FDG PET/CT in pancreatic ductal adenocarcinoma: additional prognostic value of the distal pancreatitis. Eur J Nucl Med Mol Imaging. 2023;50:4036-4050.
51. Röhrich M, Preussig M, Lang M, Schroeter C, Gutjahr E, Schreckenberger M, et al. Diagnostic potential of static and dynamic 68Ga-FAPI PET/CT for differentiation of mass forming pancreatitis and pancreatic ductal adenocarcinoma. Nuklearmedizin – NuclearMedicine. 2024;63:93-94.
52. Chen X, Liu X, Wang L, Zhou W, Zhang Y, Tian Y, et al. Expression of fibroblast activation protein in lung cancer and its correlation with tumor glucose metabolism and histopathology. Eur J Nucl Med Mol Imaging. 2022;49:2938-2948.
53. Wu J, Deng H, Zhong H, Wang T, Rao Z, Wang Y, et al. Comparison of 68Ga-FAPI and 18F-FDG PET/CT in the Evaluation of Patients With Newly Diagnosed Non-Small Cell Lung Cancer. Front Oncol. 2022;12:924223.
54. Can C, Kepenek F, Kömek H, Gündoğan C, Kaplan I, Taşdemir B, et al. Comparison of 18F-FDG PET/CT and 68Ga-FAPI-04 PET/CT in patients with non-small cell lung cancer. Nucl Med Commun. 2022;43:1084-1091.
55. Qiao K, Qin X, Fu S, Ren J, Jia J, Hu X, et al. Value of [^{18}F]AlF-NOTA-FAPI-04 PET/CT for differential diagnosis of malignant and various inflammatory lung lesions: comparison with [8F]FDG PET/CT. Eur Radiol. 2024;34:1948-1959.
56. Zeman MN, Green C, Akin EA. Spectrum of [^{18}F]FDG-PET/CT Findings in Benign Lymph Node Pathology. Mol Imaging Biol. 2021;23:469-480.
57. Kang Y-k, Na KJ, Park J, Kwak N, Lee Y-S, Choi H, et al. Preoperative evaluation of mediastinal lymph nodes in non-small cell lung cancer using [^{68}Ga]FAPI-46 PET/CT: a prospective pilot study. Eur J Nucl Med Mol Imaging. 2024. Published ahead of print.
58. Demmert TT, Pomykala KL, Lanzafame H, Pabst KM, Lueckerath K, Siveke J, et al. Oncologic Staging with 68Ga-FAPI PET/CT Demonstrates a Lower Rate of Nonspecific Lymph Node Findings Than 18F-FDG PET/CT. J Nucl Med. 2023;64:1906-1909.
59. Ristau J, Giesel FL, Haefner MF, Staudinger F, Lindner T, Merkel A, et al. Impact of Primary Staging with Fibroblast Activation Protein Specific Enzyme Inhibitor (FAPI)-PET/CT on Radio-Oncologic Treatment Planning of Patients with Esophageal Cancer. Mol Imaging Biol. 2020;22:1495-1500.
60. Hu X, Zhou T, Ren J, Duan J, Wu H, Liu X, et al. Response Prediction Using 18F-FAPI-04 PET/CT in Patients with Esophageal Squamous Cell Carcinoma Treated with Concurrent Chemoradiotherapy. J Nucl Med. 2023;64:625-631.
61. Wegen S, Claus K, Linde P, Rosenbrock J, Trommer M, Zander T, et al. Impact of FAPI-46/dual-tracer PET/CT imaging on radiotherapeutic management in esophageal cancer. Radiat. Oncol. 2024;19:44.
62. Mukai K, Ishida Y, Okajima K, Isozaki H, Morimoto T, Nishiyama S. Usefulness of preoperative FDG-PET for detection of gastric cancer. Gastric Cancer. 2006;9:192-196.
63. Kameyama R, Yamamoto Y, Izuishi K, Takebayashi R, Hagiike M, Murota M, et al. Detection of gastric cancer using 18F-FLT PET: comparison with 18F-FDG PET. Eur J Nucl Med Mol Imaging. 2009;36:382-388.

64. Takahashi H, Ukawa K, Ohkawa N, Kato K, Hayashi Y, Yoshimoto K, et al. Significance of (18)F-2-deoxy-2-fluoro-glucose accumulation in the stomach on positron emission tomography. Ann Nucl Med. 2009;23:391-397.
65. Stahl A, Ott K, Weber WA, Becker K, Link T, Siewert JR, et al. FDG PET imaging of locally advanced gastric carcinomas: correlation with endoscopic and histopathological findings. Eur J Nucl Med Mol Imaging. 2003;30:288-295.
66. Ruan D, Zhao L, Cai J, Xu W, Sun L, Li J, et al. Evaluation of FAPI PET imaging in gastric cancer: a systematic review and meta-analysis. Theranostics. 2023;13:4594-4710.
67. Jiang D, Chen X, You Z, Wang H, Zhang X, Li X, et al. Comparison of [(68)Ga]Ga-FAPI-04 and [(18)F]-FDG for the detection of primary and metastatic lesions in patients with gastric cancer: a bicentric retrospective study. Eur J Nucl Med Mol Imaging. 2022;49:732-742.
68. Liu H, Wang Y, Zhang W, Cai L, Chen Y. Elevated [(68)Ga]Ga-DOTA-FAPI-04 activity in degenerative osteophyte in a patient with lung cancer. Eur J Nucl Med Mol Imaging. 2021;48:1254-1255.
69. Chen H, Pang Y, Kang F, Xu W, Meng T, et al. Comparison of [(68)Ga]Ga-FAPI and [(^{18})F]FDG uptake in patients with gastric signet-ring-cell carcinoma: a multicenter retrospective study. Eur Radiol. 2023;33:1329-1341.
70. Gundogan C, Komek H, Can C, Yildirim OA Kaplan I, Erdur E, et al. Comparison of 18F-FDG PET/CT and 68Ga-FAPI-04 PET/CT in the staging and restaging of gastric adenocarcinoma. Nucl Med Commun. 2022;43:64-72.
71. Hirmas N, Hamacher R, Sraieb M, Kessler L, Pabst KM, Barbato F, et al. Diagnostic Accuracy of 68Ga-FAPI Versus 18F-FDG PET in Patients with Various Malignancies. J Nucl Med. 2024; epub ahead of print.
72. Lin X, Li Y, Wang S, Zhang Y, Chen X, Wei M, et al. Diagnostic value of [^{68}Ga]Ga-FAPI-04 in patients with colorectal cancer in comparison with [^{18}F]F-FDG PET/CT. Front Oncol. 2023; epub ahead of print.
73. Dong Y, Sun P, Wu H, Zhong J, Cao M, Tang G, et al. PET/CT imaging fibroblast activation protein in initial colorectal cancer: compared to 18F-FDG PET/CT. Nucl Med Commun. 2023;44:1011-1019.
74. Strating E, Wassenaar E, Verhagen M, Rauwerdink P van Schelven S, de Hingh I, et al. Fibroblast activation protein identifies Consensus Molecular Subtype 4 in colorectal cancer and allows its detection by 68Ga-FAPI-PET imaging. Br. J. Cancer. 2022:127;145-155.
75. Kömek H, Can C, Güzel Y, Oruç Z, Gündoğan C, Yildirim ÖA, et al. 68Ga-FAPI-04 PET/CT, a new step in breast cancer imaging: a comparative pilot study with the 18F-FDG PET/CT. Ann Nucl Med. 2021;35:744-752.
76. Dendl K, Koerber SA, Finck R, Mokoala KMG, Staudinger F, Schillings L, et al. 68Ga-FAPI-PET/CT in patients with various gynecological malignancies. Eur J Nucl Med Mol Imaging. 2021;48:4089-4100.
77. Dendl K, Koerber SA, Watabe T, Haberkorn U, Giesel FL. Current Status of Fibroblast Activation Protein Imaging in Gynecologic Malignancy and Breast Cancer. PET Clin. 2023;18:345-351.
78. Elboga U, Sahin E, Kus T, Cayirli YB, Aktas G, Uzun E, et al. Superiority of 68Ga-FAPI PET/CT scan in detecting additional lesions compared to 18FDG PET/CT scan in breast cancer. Ann Nucl Med. 2021;35:1321-1331.
79. Chen J, Xu K, Li C, Tian Y, Li L, Wen B, et al. [^{68}Ga]Ga-FAPI-04 PET/CT in the evaluation of epithelial ovarian cancer: comparison with [^{18}F]F-FDG PET/CT. Eur J Nucl Med Mol Imaging. 2023;50:4064-4076.
80. Liu S, Feng Z, Xu X, Ge H, Ju X, Wu X, et al. Head-to-head comparison of [^{18}F]-FDG and [^{68}Ga]-DOTA-FAPI-04 PET/CT for radiological evaluation of platinum-sensitive recurrent ovarian cancer. Eur J Nucl Med Mol Imaging. 2023;50:1521-1531.
81. Luo Y, Pan Q, Zhou Z, Li M, Wei Y, Jiang X, et al. 68Ga-FAPI PET/CT for Rheumatoid Arthritis: A prospective study. Radiology. 2023;307:e222052.
82. Zhang Q, Lin X, Wang W, Zhang X, Lü M, Shao Z, et al. Evaluation of 18F-FAPI-4 Imaging in Assessing the Therapeutic Response of Rheumatoid Arthritis. Mol Imaging Biol. 2023;25:630-637.
83. Pan Q, Yang H, Zhou Z, Li M, Jiang X, Li F, et al. [^{68}Ga]Ga-FAPI-04 PET/CT may be a predictor for early treatment response in rheumatoid arthritis. EJNMMI Res. 2024;14:2
84. Popescu CE, Ferro P, Gotuzzi I, Burger I, Rominger A, Caobelli F. 68Ga-FAPi: Pathways and Diagnosis in Cardiac Imaging. Curr Cardiovasc Imaging Rep. 2023;16:93-101.
85. Kain V, Prabhu SD, Halade GV. Inflammation revisited: inflammation versus resolution of inflammation following myocardial infarction. Basic Res Cardiol. 2014;109:444.
86. Varasteh Z, Mohante S, Robu S, Braeuer M, Li Y, Omidvari N, et al. Molecular imaging of fibroblast activity after myocardial infarction using 68Ga-labeled fibroblast activation protein inhibitor, FAPI-04. J Nucl Med. 2019;60:1743-1749.
87. Xie B, Wang J, Xi XY, Guo X, Chen BX, Li L, et al. Fibroblast activation protein imaging in reperfused ST-elevation myocardial infarction: comparison with cardiac magnetic resonance imaging. Eur J Nucl Med Mol Imaging. 2022;49:2786-2797.
88. Zhang M, Quan W, Zhu T, Feng S, Huang X, Meng H, et al. [^{68}Ga]Ga-DOTA-FAPI-04 PET/MR in patients with acute myocardial infarction: potential role of predicting left ventricular remodeling. Eur J Nucl Med Mol Imaging. 2023;50:839-848.
89. Lin M, Xue Q, You X, Yao S, Miao W. Cerebral Venous Thrombosis Caused by Neuro-Behçet Disease Accidentally Detected by 68Ga-FAPI. Clin Nucl Med. 2021;46:1028-1029.
90. Gong W, Fu M, Zhang Y, Yang X, Zhang C. Progressive Multifocal Leukoencephalopathy Mimicking Malignancy on 68Ga-FAPI PET/CT: Potential Advantages of FAPI. Clin Nucl Med. 2022;47:430-432.
91. Liu H, Yang X, Liu L, Lei L, Wang L, Chen Y. Clinical Significance of Diffusely Increased Uptake of 68Ga-FAPI in Thyroid Gland. Clin Nucl Med. 2021; 6:938-939.
92. Rao Z, Wu J, Zhang C. A Case of Papillary Thyroid Carcinoma with Graves Ophthalmopathy Evaluated by 68Ga-FAPI PET/CT. Endocrine. 2022;76:243-244.
93. Gong J-N, Chen B-X, Xing H-Q, Huo L, Yang Y-H, Yang M-F. Pulmonary artery imaging with 68Ga-FAPI-04 in patients with chronic thromboembolic pulmonary hypertension. J Nucl Cardiol. 2023;30:1166-1172.
94. Kupusovic J, Kessler L, Nekolla SG, Riesinger L, Weber MM, Ferdinandus J, et al. Visualization of thermal damage using 68Ga-FAPI-PET/CT after pulmonary vein isolation. Eur J Nucl Med Mol Imaging. 2022;49:1553-1559.
95. Bentestuen M, Al-Obaydi N & Zacho HD. FAPI-avid nonmalignant PET/CT findings: An expedited systematic review. Semin Nucl Med. 2023; 53:694-705.
96. Tang W, Wu J, Yang S, Wang Q, Chen Y. Organizing Pneumonia With Intense 68Ga-FAPI Uptake Mimicking Lung Cancer on 68Ga-FAPI PET/CT. Clin Nucl Med. 2022;47:223-225.
97. Röhrich M, Leitz D, Glatting FM, Wefers AK, Weinheimer O, Flechsig P, et al. Fibroblast Activation Protein-Specific PET/CT Imaging in Fibrotic Interstitial Lung Diseases and Lung Cancer: A Translational Exploratory Study. J Nucl Med. 2022;63:127-133.
98. Yang X, You Z, Mou C, Hu Z, Liu H. Esophagitis Mimicking Esophageal Cancer on 68Ga-FAPI PET/CT. Clin Nucl Med. 2022;47:279-280.
99. Qin C, Yang L, Ruan W, Shao F, Lan X. Immunoglobulin G4-Related Sclerosing Cholangitis Revealed by 68Ga-FAPI PET/MR. Clin Nucl Med. 2021;46:419-421.
100. Liu H, Chen Z, Yang X, Fu W, Chen Y. Increased 68Ga-FAPI Uptake in Chronic Cholecystitis and Degenerative Osteophyte. Clin Nucl Med. 2021;46:601-602.
101. Zhou Y, Yang X, Liu H, Luo W, Liu H, Lv T, et al. Value of [^{68}ga]Ga-FAPI-04 imaging in the diagnosis of renal fibrosis. Eur J Nucl Med Mol Imaging. 2021;48:3493-3501.
102. Pan Q, Luo Y, Zhang W. Idiopathic Retroperitoneal Fibrosis With Intense Uptake of 68Ga-Fibroblast Activation Protein Inhibitor and 18F-FDG. Clin Nucl Med. 2021;46:175-176.
103. Li Y, Deng L, Feng Y, Liu L, Lv F, Qiu L. Potential utility of [^{68}Ga]DOTA-FAPI-04 as a broad-spectrum benign disease imaging agent – comparison with [^{18}F]FDG and [99mTc]MDP. Eur Radiol. 2023;33:9378-9389.
104. Qin C, Song Y, Liu X, Gai Y, Liu Q, Ruan W, et al. Increased uptake of 68Ga-DOTA-FAPI-04 in bones and joints: metastases and beyond. Eur J Nucl Med Mol Imaging. 2022;49:709-720.
105. Pang Y, Shang Q, Meng T, Chen H. [^{68}Ga]Ga-FAPI PET/CT of brown tumors in a patient with primary hyperparathyroidism. Eur J Nucl Med Mol Imaging. 2022;49:1770-1771.
106. Roberts EW, Deonarine A, Jones JO, Denton AE, Feig C, Lyons SK, et al. Depletion of stromal cells expressing fibroblast activation protein-α from skeletal muscle and bone marrow results in cachexia and anemia. J Exp Med. 2013;210:1137-1151.
107. Chen H, Pang Y, Wu J, Zhao L, Hao B, Wu J, et al. Comparison of [(68)Ga]Ga-DOTA-FAPI-04 and [(18)

F] FDG PET/CT for the diagnosis of primary and metastatic lesions in patients with various types of cancer. Eur J Nucl Med Mol Imaging. 2020;47:1820-1832.
108. Giesel FL, Kratochwil C, Schlittenhardt J, Dendl K, Eiber M, Staudinger F, et al. Head-to-head intra-individual comparison of biodistribution and tumor uptake of (68)Ga-FAPI and (^{18})F-FDG PET/CT in cancer patients. Eur J Nucl Med Mol Imaging. 2021;48:4377-4385.
109. Cermic TF, Ergul N, Yilmaz B, Mercanoglu G. Tumor Imaging With 68Ga-DOTA-FAPI-04 PET/CT: Comparison With 18F-FDG PET/CT in 22 Different Cancer Types. Clin Nucl Med. 2022;47:e333-e339.
110. Hirmas N, Hamacher R, Sraieb M, Ingenwerth M, Kessler L, Pabst KM, et al. Fibroblast-Activation Protein PET and Histopathology in a Single-Center Database of 324 Patients and 21 Tumor Entities. J Nucl Med. 2023;64:711-716.
111. Meyer C, Dahlbom M, Lindner T, Vauclin S, Mona C, Slavik R, et al. Radiation Dosimetry and Biodistribution of (68)Ga-FAPI-46 PET Imaging in Cancer Patients. J Nucl Med. 2020;61:1171-1177.
112. Ballal S, Yadav MP, Moon ES, Kramer VS, Roesch F, Kumari S, et al. First-in-human results on the biodistribution, pharmacokinetics, and dosimetry of [^{177}Lu]Lu-DOTA.SA.FAPi and [^{177}Lu]Lu-DOTAGA.(SA.FAPi)2. Pharmaceuticals. 2021;14:1212.
113. Fendler WP, Pabst KM, Kessler L, Fragoso Costa P, Ferdinandus J, Weber M, et al. Safety and Efficacy of ^{90}Y-FAPI-46 Radioligand Therapy in Patients with Advanced Sarcoma and Other Cancer Entities. Clin Cancer Res. 2022;28:4346-4353.
114. Ferdinandus J, Costa PF, Kessler L, Weber M, Hirmas N, Kostbade K, et al. Initial Clinical Experience wit (^{90})Y-FAPI-46 Radioligand Therapy for Advanced-Stage Solid Tumors: A Case Series of 9 Patients. J Nucl Med. 2022;63:727-734.
115. Kratochwil C, Giesel FL, Rathke H, Fink R, Dendl K, Debus J, et al. [153 Sm] Samarium-labeled FAPI-46 radioligand therapy in a patient with lung metastases of a sarcoma. Eur J Nucl Med Mol Imaging. 2021;48:3011-3013.
116. Kuyumcu S, Kovan B, Sanli Y, Buyukkaya F, Simsek DH, Özkan ZG, et al. Safety of fibroblast activation protein-targeted radionuclide therapy by a low-dose dosimetric approach using ^{177}Lu-FAPI-04. Clin Nucl Med. 2021;46:641-646.
117. Baum RP, Schuchardt C, Singh A, Chantadisai M, Robiller FC, Zhang J, et al. Feasibility, biodistribution, and preliminary dosimetry in peptide-targeted radionuclide therapy of diverse adenocarcinomas using ^{177}Lu-FAP-2286: first-in-humans results. J Nucl Med. 2022;63:415-423.
118. Ljungberg M, Celler A, Konijnenberg MW, Eckerman KF, Dewaraja YK, Sjögreen-Gleisner K. MIRD pamphlet no. 26: joint EANM/MIRD guidelines for quantitative ^{177}Lu SPECT applied for dosimetry of radiopharmaceutical therapy. J Nucl Med. 2016;57:151-162.
119. Kersting D, Jentzen W, Jeromin D, Mavroeidi I-A, Conti M, Büther F, et al. Lesion Quantification Accuracy of Digital ^{90}Y PET Imaging in the Context of Dosimetry in Systemic Fibroblast Activation Protein Inhibitor Radionuclide Therapy. J Nucl Med. 2023;64:329-336.
120. Hindorf C, Glatting G, Chiesa C, Lindén O, Flux G. EANM Dosimetry Committee guidelines for bone marrow and whole-body dosimetry. Eur J Nucl Med Mol Imaging. 2010;37:1238-1250.
121. Privé BM, Boussihmad MA, Timmermans B, van Gemert WA, Peters SM, Derks YH, et al. Fibroblast activation protein-targeted radionuclide therapy: background, opportunities, and challenges of first (pre) clinical studies. Eur J Nucl Med Mol Imaging. 2023;50:1906-1918.

2

[^{18}F] FLUCICLOVINE

by Monica Casanova Martins[1]
Ellen Bowen[2]
Grace Bowen[2]
Danielle Simpson[2]
Neil G. Hartman[1]

[1]Nuclear Medicine Department, Singleton Hospital, Swansea Bay University Health Board, Swansea, United Kingdom

[2]PharmD candidates, Purdue University, Indiana, US

[18F]FLUCICLOVINE

Amino acids are vital small molecules that, when linked through peptide bonds, form the core units of proteins. They play essential roles in cellular processes such as protein synthesis, energy metabolism, cell signalling, serving as carbon sources for cell growth, and neurotransmission.[1,2] Of the 20 basic amino acids, 9 are essential and are typically obtained from the diet, while the other 11 can be synthesised via metabolic pathways. Amino acids are also precursors for many other biomolecules and are crucial to metabolic cycles.[2] Amino acids either enter the cell from the external cellular environment or are a result of intracellular protein recycling, and although all amino acids can diffuse into cells, their movement favourably occurs through carrier-mediated processes.[2] Transmembrane amino acid transporters are upregulated in cancer cells, providing nutrients for tumour cell growth when compared with normal tissues.[1–3] While some radiolabelled amino acids are incorporated into proteins or follow other metabolic routes, tumour uptake and imaging properties mainly reflect the rate and mechanism of amino acid transport.[2] Because this upregulation also occurs in prostate cancer cells, amino acid-based radiotracers can be used to localise prostate cancer.[3,4]

Consequently, prostate cancer may be imaged using radiolabelled natural and synthetic amino acids.[2,3] In many instances, non-natural, non-metabolised amino acid analogues have advantages over natural amino acids, including the ability to incorporate longer-lived radionuclides such as Fluorine-18, simplified radiosynthetic methods, and lack of radiolabelled metabolite formation, which simplifies kinetic analysis and avoids potentially confounding accumulation of activity in non-target tissues.[2,3]

Anti-1-amino-3-18F-fluorocyclobutane-1-carboxylic acid (FACBC or [18F]Fluciclovine) is a synthetic amino acid and an analogue of L-leucine. It is preferentially taken up by prostate cancer cells and gliomas through specialised amino acid transporters, specifically alanine-serine-cysteine transporter 2 (ASCT2) and L-type amino acid transporter LAT-1.[3,5–9] Transporters like ASCT2 are crucial in amino acid metabolism in prostate cancer cells. ASCT2 is an important transporter of glutamine, an essential tumour nutrient associated with cancer signalling pathways.[9–11] [18F]Fluciclovine is mainly transported by ASCT2 and functions similarly to glutamine.[9,12] However, unlike glutamine, [18F]Fluciclovine does not undergo additional intracellular metabolism, leading to its intracellular accumulation, particularly in prostate cancer cells and at major sites of amino acid metabolism such as the liver and pancreas.[9,13]

Positron emission tomography (PET) with [18F]Fluciclovine is indicated in men with suspected prostate cancer recurrence, as evidenced by rising blood levels of prostate-specific antigen (PSA) following prior treatment.[14–20] Although there is no absolute PSA threshold for recommending a [18F]Fluciclovine PET/CT, diagnostic performance is known to vary with PSA levels and kinetics. The positivity rate of [18F]Fluciclovine PET/CT increases with increasing PSA and with more rapid doubling times.[3,20–23] However, a post hoc analysis of the EMPIRE-1 cohort, stratified by protocol-specified criteria, comparing failure-free survival (FFS), concluded that incorporating [18F]Fluciclovine PET/CT into salvage radiotherapy (SRT) offers survival benefits for patients with a PSA of less than 2 ng/mL but not for patients with a PSA of 2 ng/mL or higher.[16] Like other emerging prostate cancer-specific PET tracers, [18F] Fluciclovine provides opportunities to localise prostate cancer recurrence at an earlier stage in the disease course when the PSA level is low, to inform medical decision-making and to study PET-directed local therapy.[9,24–28] [18F]Fluciclovine PET/CT scan should be considered before salvage therapy, to assist with accurate treatment planning.[3]

[18F]Fluciclovine Radiopharmaceutical Chemistry and Properties

[18F]Fluciclovine is a radioactive diagnostic agent (radiopharmaceutical) indicated for positron emission tomography (PET) imaging in men with suspected prostate cancer recurrence based on elevated blood levels of prostate-specific antigen (PSA) following prior treatment.[29] Axumin® ([18F]Fluciclovine) is a registered trademark of Blue Earth Diagnostics Ltd. and was approved by the FDA in May 2016.[29]

The chemical name of [18F]Fluciclovine is (1r, 3r)-1-amino-3[18F]fluorocyclobutane-1-carboxylic acid (FACBC).[29] As described by the name and illustrated in the chemical structure diagram below, [18F]Fluciclovine is a cyclobutane with an amino group and carboxyl group at position 1, and an F-18 fluoro group at position 3 in the 1r, 3r stereoisomer.[30] The structure of [18F]Fluciclovine reveals that it is an F-18-tagged synthetic analogue of the amino acid L-leucine, which enables the mode of action of the radiopharmaceutical.[30]

Figure 1. [18F]Fluciclovine molecule.(29)

The radiopharmaceutical [18F]Fluciclovine is a synthetic amino acid which is transported across mammalian cell membranes by amino acid transporters such as LAT-1 (L-type amino acid transporter that has repeatedly been found to be overexpressed in a vast variety of cancers)(31) and ASCT2 (alanine, serine, cysteine transporter 2).(29) These transporters are upregulated in prostate cancer cells, which leads to greater accumulation of [18F] Fluciclovine in these

Principal Radiation Produced from Decay of F-18				
	Energy (keV)	Abundance (%)	^{177}mLu (0.01 %)	160 days
Positron	249.8	96.7	^{227}Ac (0.004 %) ^{227}Th (0.5 %) (9)	21.8 years 18.7 days
Gamma	511.0	193.5	^{88}Y (< 0.01 %) ^{152}Eu (< 0.01 %) ^{154}Eu (< 0.01 %)	107 days 13.5 years 8.6 years

Table 1. Radiation produced from decay of ^{18}F [29]

cancer cells compared to the surrounding normal tissue.[29]

However, [^{18}F]Fluciclovine uptake is not specific to prostate cancer only but can also occur in other types of cancer and in benign prostatic hypertrophy in primary prostate cancer.[29] Therefore, histopathological evaluation of the suspected recurrence site is recommended to rule out or confirm the presence of recurrent prostate cancer.(29)

Fluorine-18 (F-18) is a cyclotron-produced radionuclide that decays by positron emission (β+ decay, 96.7%) and orbital electron capture (3.3%) to stable oxygen-18 (O-18) with a half-life of 109.7 minutes.[29] The positron can undergo annihilation with an electron to produce two gamma rays; the energy of each gamma ray is 511 keV.[29]

[^{18}F]FLUCICLOVINE RADIOPHARMACEUTICAL LABELLING

[^{18}F]Fluciclovine, also commonly known in the United States (currently main country of usage) by the brand name Axumin©, is used as a diagnostic radiopharmaceutical in nuclear medicine. It was approved in 2016 by the U.S Food and Drug Administration and indicated for use in adults with suspected prostate cancer recurrence. The detection of recurrence is based on elevated blood prostate-specific antigen (PSA) levels following the use of a specific treatment regimen.[32]

Cancer cells have an elevated need for amino acids to help make proteins for growth and metabolism. [^{18}F]Fluciclovine is a synthetic amino acid analogue(33), meaning that it has a chemically modified "R" group that makes it slightly different from the 20 naturally occurring amino acids

that make proteins.[34] However, cancer cells are not able to detect the difference and recognise [^{18}F]Fluciclovine as they would any other amino acid, making it a great target for cancer cell uptake. There are two amino acid transporters that [^{18}F] Fluciclovine specifically targets, ASCT2 and LAT1, which are overexpressed in prostate cancer cells.[35]

The active component of [^{18}F]Fluciclovine is anti-1-amino-3-flurocyclobutane-1-carboxylic acid, which is radiolabelled with fluorine-18.[36]

Overall synthesis time of [^{18}F]Fluciclovine

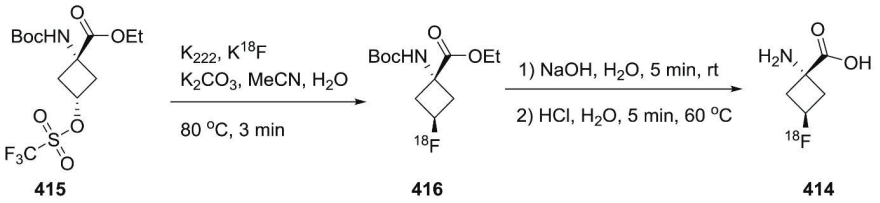

Figure 2. Synthesis of [^{18}F]Fluciclovine.(37)

is estimated to be approximately 72 minutes, with a radiochemical yield anywhere between 45–50%. Typical radiochemical concentration ranges between 2.18–3.64 GBq/mL, with an expiry time of 10 hours. [38] The actual production process for [^{18}F] Fluciclovine is as follows:

» The synthesis is based on nucleophilic displacement of the triflate group (trifluoromethanesulfonate) of the precursor by 18F-fluoride in the presence of Kryptofix 222 (4,7,13,16,21,24-Hexaoxa-1,10-diazabicyclo[8.8.8]hexacosane) and potassium carbonate.

» The triflate complex is named ethyl cis-1-(N-tert-butoxycarbonyl) amino-3-[(trifluromethyl)- sulfonyloxy] cyclobutane-carbo-xylate.

» This nucleophilic displacement of the triflate group process occurs for five minutes at 85 degrees Celsius, which turns the starting material into an intermediate.

» The intermediate is then diluted with H20 and passed through a C-18 Sep-Pak to trap the intermediate. The flow rate of the intermediate through the Sep-Pak is roughly 6 ml/min for ten minutes.

» Base hydrolysis is then done on the Sep-Pak with NaOH (sodium hydroxide) for five minutes at room temperature to cleave the acetyl group.

» The Sep-Pak is then eluted with water for injection followed by acid hydrolysis with HCl (hydrochloric acid) at 60 degrees Celsius. This is done to cleave the N-BOC group, which results in the desired product, which is passed through a final HLB Sep-Pak.

» The final product is delivered into a formulation vial containing citrate buffer, HCl and NaOH, followed by filter (end-product) sterilisation.[38]

[18F]FLUCICLOVINE RADIOPHARMACEUTICAL QUALITY CONTROL

Quality control tests are used to verify that the final radiopharmaceutical product meets the required standards for identity, purity, sterility, and other factors that ensure the product is safe and appropriate for patient administration. Since specifications for [18F] Fluciclovine quality control tests are yet to be determined in the pharmacopoeias, the final product should at least abide by the general F-18 radiopharmaceutical quality control test parameters.[39] F-18 radiopharmaceuticals, including [18F] Fluciclovine, require a variety of tests to be performed.

Appearance and pH

The appearance test requires visual inspection to verify that no colour change or particulate matter is found in the final product.[39]

A pH test uses either pH strips or a pH meter to validate that the product's pH falls into the acceptable physiological range of 4.5–8.5.[39]

Radionuclidic Identity and Purity

The radionuclidic identity test confirms that F-18 was the correct radionuclide actually produced during the manufacturing process.[39] This is performed by calculating the product's half-life and recording its gamma energy spectrum.[39] The half-life of F-18 is 109.7 minutes, and is expected to range from 105–115 minutes.[39] The half-life can be calculated by recording the activity of the product from a dose calibrator at two to three designated time intervals.[39] The product's gamma energy can be obtained using a gamma spectrometer, which should show a principal gamma photon peak at 511 keV, with or without a second sum peak at 1,022 keV.[39]

The radionuclidic purity test validates that no other radionuclides are present in the final product.[39] This test is completed by obtaining the gamma spectrum from a decayed product sample, since decreased levels of F-18 would reveal the presence of any radionuclidic impurities.[39] The European Pharmacopoeia (EP) and United States Pharmacopoeia (USP) recommend that the acceptance criteria for total radionuclidic impurities be no more than 0.1% and 0.5% of the total radioactivity, respectively.[39]

The radiochemical identity test is used to validate that the complete radiopharmaceutical [18F]Fluciclovine was actually produced.[39] This test is usually performed using either thin layer chromatography (TLC) or high-performance liquid chromatography (HPLC) to compare the product sample to a reference standard.[39] The relative retention factor or time when comparing the sample to the standard should be in the 0.9–1.1 range.[39]

The radiochemical purity test uses the TLC or HPLC radio-chromatogram to confirm that radiochemical impurity levels are below the accepted threshold.[39] Calculating the ratio between the peak corresponding to the product and the sum of all peaks detectable on the radio-chromatogram should result in a purity ≥ 90%.[39]

Chemical Purity

Gas chromatography evaluates the levels of residual solvents in the final product.[39] Limits for these residual solvents are found in ICH guideline Q3C (R6) on impurities: guideline for residual solvents.[39,40]

A Kryptofix or K222 test is performed either by TLC or HPLC to confirm that no residual K222 is left in the final product.[39] A spot test comparing the sample to a standard of the limit is a common and fast testing method.[39] Residual content of K222 should be less than 2.2 mg per volume (EP) or less than 50 µg/mL (USP).[39]

Microbiological Contamination

A bubble point test is used on the sterilising filter after use to confirm that the filter membrane maintained adequate integrity and filtration throughout the production process.[39] Acceptance criteria are defined by the manufacturer, but the formulation used for the product should be taken into consideration as this can affect the bubble point.[39]

A limulus amoebocyte lysate (LAL) test is used to determine the presence and quantity of bacterial endotoxin in the product.[39] The usual acceptance criterion is an endotoxin content less than 175 IU/injection.[39]

Sterility can be assessed either by direct inoculation or using membrane filtration methods, according to the relevant pharmacopoeial requirements.(39) This test is unique in that the results are obtained post-release to the customer due to the length of the test.[39]

A final product of [18F]Fluciclovine must pass all these quality control tests to ensure it is safe and appropriate for patient administration.

Physiological Biodistribution

[18F]Fluciclovine is a radiolabelled analogue of L-leucine for PET imaging, which was initially developed for the evaluation of cerebral gliomas.[3,41] Its normal biodistribution includes intense hepatic and pancreatic uptake and heterogeneous mild to moderate uptake in the salivary, adrenal and pituitary glands, bowel, bone marrow, lymphoid tissue, thyroid, breast parenchyma, oesophagus, stomach, and renal tissue.[3,4,20,42] Uptake is only minimal in the brain.

[18F]Fluciclovine has only minimal urinary excretion. The urinary bladder wall may have mild to moderate diffuse physiological activity, as does the peri-urethral tissue, but rapid cellular uptake.[3,4,20,42] Given the rapid cellular uptake, imaging can be performed before the tracer accumulates in the bladder, typically 3 minutes after administration. In addition, [18F]Fluciclovine increasingly accumulates in muscle tissue with time since L-leucine is metabolised in muscle cells.[4] Uptake of [18F]Fluciclovine in prostate cancer is not specific, however, and might also be observed in benign prostatic hyperplasia, inflammation, and benign tumours.[3,4] It is common for activity to be retained in the injected vessel, and this should also not be confused with pathology.[20]

[18F]Fluciclovine can accurately detect prostate cancer within the gland itself and in pelvic lymph node metastases.[2,43] An example of [18F]Fluciclovine PET/CT imaging in a patient with recurrent prostate cancer is shown in Figure 4. One advantage of [18F]Fluciclovine over other radiolabelled amino acids is that the relatively low levels of urinary excretion simplify imaging of the pelvis.[2]

[18F]Fluciclovine is predominantly transported via ASCT2 and LAT1, transporters that mediate both the influx and efflux of amino acids. Peak uptake in tumours occurs at 5 to 20 minutes after injection with variable washout.[3,41,44] This allows for early imaging acquisition with benefits for the clinical workflow.

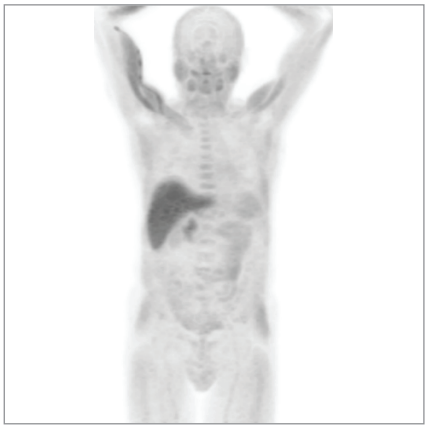

Figure 3. Normal physiological biodistribution of [18F]Fluciclovine. Physiological uptake of [18F]Fluciclovine includes activity in the pancreas, liver, bone marrow, and muscle, with negligible uptake in kidneys, bowel, and delayed urinary excretion.[3]

PATIENT PREPARATION

Patients must fast for at least 4 hours before the injection and should avoid strenuous exercise for at least 24 hours before PET imaging.[3,20,32,45–47] After intense exercise, there is an increase in the rate of protein synthesis and degradation and of amino acid transport, which may cause an increase in muscle uptake of [18F]Fluciclovine and lead to degradation of image quality.[20,32] At this stage, oral hydration is also generally discouraged, though small amounts are allowed, if necessary.[3,20,46,47] There are no known contraindicated medicines so patients can take their prescribed medication as usual with sips of water.[3,32]

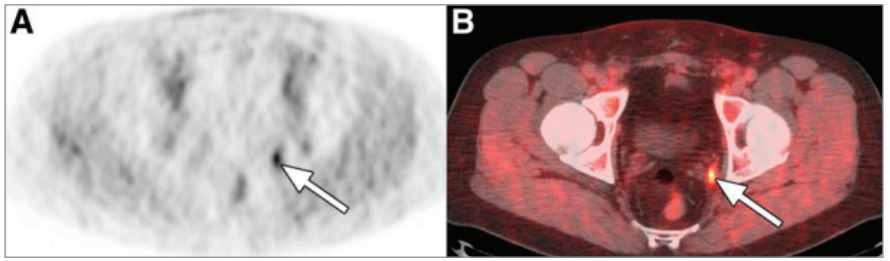

Figure 4. Prostate cancer imaging with [18F]Fluciclovine. [18F]Fluciclovine PET (A) and [18F]Fluciclovine PET/CT (B) images from a patient with suspected recurrence of prostate cancer demonstrate focal uptake in left pelvic lymph node metastasis that measures less than 1 cm in short-axis diameter (indicated with arrows). Biopsy demonstrated recurrent prostate cancer in this location.[2]

Patients' adherence to the preparation instructions should be assessed on the day of imaging by the clinical technologist.[32] Since amino acid transporters are also upregulated in inflamed cells, although to a lesser extent than in prostate cancer cells, it is advisable to schedule the [18F]Fluciclovine PET/CT scan at least 2 weeks after an intervention (e.g., biopsy). This allows time for any inflammation to resolve and helps maintain an optimal tumour-to-background ratio.[32] There is, however, no current official recommendation regarding optimal wait time between [18F]Fluciclovine PET/CT imaging and an intervention.[12,32]

It is recommended that patients are asked not to void for 30 to 60 min prior to the [18F]Fluciclovine injection.[20] For centres performing PET/CT imaging with an oral contrast agent, it is suggested that patients refrain from voiding for 1h after contrast administration until after the [18F]Fluciclovine has been injected and imaging completed.[32,46] Voiding just before the injection of [18F]Fluciclovine has been associated with increased likelihood of visualised bladder with intense activity (despite lower volume).[32,47] By contrast, refraining from voiding before the [18F]Fluciclovine injection and scan can significantly reduce bladder activity.[46,47] A relatively full bladder might help mitigate the effect of urinary radiotracer excretion into the bladder through different theoretical mechanisms.[46,47] One of the suggested mechanisms is that the resultant higher volume of urine in the bladder might result in a lower concentration of radioactivity in the bladder in men who do not void before [18F]Fluciclovine injection.[47–49] Alternatively, elevated pressure in the urinary collecting system as a result of a full bladder may result in slower urinary excretion of [18F]Fluciclovine. There are known effects of mechanical obstruction on renal function, such as reduced glomerular filtration rate, decreased renal plasma flow,

and profound changes in renal tubular cell function, that support this theory.[50] The reduction in scans with intense bladder activity simplifies image interpretation and enhances the evaluation of the prostate and prostate bed, as high [18F]Fluciclovine activity in the bladder can interfere with assessing local prostate cancer recurrence. For instance, [18F]Fluciclovine activity in the bladder or urethra may mimic or obscure activity in the prostate or prostate bed. [47] This is, therefore, an important aspect of patient preparation ahead of [18F] Fluciclovine PET/CT imaging. Nonetheless, patients' comfort on the PET/CT table should also be taken into consideration, as it is important to guarantee that they are able to remain still for the duration of the imaging procedure in order to avoid any movement artefacts.[20,32,46] In addition to assessing their voiding needs prior to imaging, it is also important for staff to know about any comorbidities that may affect the patient's ability to lie still and flat for approximately 30 min (or the duration of the imaging acquisition) prior to injection of [18F]Fluciclovine. The interpreting physician should be informed of any conditions that may pose challenges for imaging by preventing the patient from lying flat or still, together with any adjustments needed to accommodate for this inability. [32] This can be done via a patient questionnaire ahead of the imaging test.

Parameters such as PSA and Gleason score have been shown to have a positive correlation with the detection of prostate cancer recurrence, with a higher risk of having bone metastasis at PSA levels above 20 ng/mL.[23,32] PSA demonstrated a strong linear correlation with positive findings in [18F]Fluciclovine PET/CT imaging. [3,21–23,51] These parameters should therefore be recorded ahead of imaging in a [18F]Fluciclovine PET/CT patient questionnaire, including: Gleason score, current and prior lowest PSA values, use of hormonal therapy (current or past), prior therapy (e.g., prostatectomy, radiation therapy, chemotherapy or cryotherapy), known metastatic disease, availability of prior scans, claustrophobia, date and time of last consumed food and drink, last exercise undertaken, recent biopsies, history of epileptic seizures, presence of infections, recent injuries, previous surgery history and areas of pain and/or discomfort (what, type, when and laterality (if applicable); for example, total hip replacement, etc.). Collating such information can help prevent incidents where patients are unable to tolerate the scan after injection or where the quality of the acquired images is substandard. It can also provide the reporting physician with important information during final image interpretation, especially in equivocal cases.[32,46]

Aftercare

Patients should be advised to be well hydrated and void frequently during the first hours after [18F]Fluciclovine PET/CT to reduce radiation exposure to the bladder.[20]

IMAGING PROTOCOL

Administered Activity

The recommended activity for an adult patient is 370 MBq of [18F]Fluciclovine injected as an intravenous bolus.[18–20,29,52–55] The recommended maximum volume of injection of the undiluted product is 5 mL. It can, however, be diluted with sodium chloride 9 mg/mL (0.9%) solution by a factor of 8 (dilution 1+7).(20) Injection into the right upper extremity is suggested, with the arms down, to avoid misinterpretation caused by uptake in the supraclavicular vein.[3,20,32,45] This should be followed by administration of an intravenous flush of sterile sodium chloride injection, 9 mg/mL (0.9%), to ensure full delivery of the activity.[18–20,29,47,52,53] The patient's arms should be positioned above the head immediately after the injection.[20]

Uptake Time

[18F]Fluciclovine is preferably taken up by prostate cancer cells in comparison with normal surrounding tissues. Tumours exhibit quick uptake, with peak tumour-to-normal tissue ratio occurring between 4 and 10 min post-injection. After this, uptake in the tumour cells reaches a plateau that lasts for approximately 30 minutes. Primary tumour efflux of [18F]Fluciclovine begins within 15 min. A 61% reduction in mean tumour uptake is detected at 90 min. In lymph node metastases, uptake is also rapid but followed by a faster washout than in prostate tumour. Early image acquisition starting immediately after the initial injection is therefore recommended.[20,56,57]

Image Acquisition

Patients are positioned supine with arms above the head if possible. Prior to injection, a low- dose CT acquisition (140kV, average 50mAs) is acquired for attenuation correction and localisation. Half-body PET imaging acquisition should start within an acceptable range between 3–5 min after injection. A 4-min interval from the completion of the injection to the start of PET imaging acquisition, for uptake time, is considered ideal. Half-body acquisition should start at the proximal mid-thighs, including the inguinal lymph nodes and prostate bed, and proceed to the base of the skull.[3,20,29,47] For clinical reasons, the scan may need to be extended to the top of the skull and/or include the lower extremities. The interval between [18F]Fluciclovine injection and half-body imaging should be recorded. An initial dynamic scan (0–5 min) of the pelvic region is optional.[20] 5 min per bed position in the pelvis and 3 min per bed position in the remainder of the body are recommended. The use of a high-quality

diagnostic CT may be considered, especially for characterisation of small lesions seen on PET images. Both CT and PET acquisition parameters are scanner dependent.[3,20] Intravenous CT contrast is optional but seems to have a limited impact on image quality and interpretation.[20]

Multiple time points can be used for [18F] Fluciclovine PET/CT imaging. However, this methodology is considered not to be clinically practical. A retrospective analysis comparing single- and triple-time-point [18F] Fluciclovine PET/CT concluded that early imaging is feasible with marginal increased sensitivity and decreased specificity.[3] Early half-body single-time-point imaging has been used successfully.[58] As the efflux of [18F]Fluciclovine is generally represented by a down-sloping time-activity curve, early imaging within the first 30 minutes after injection is recommended.[3,59]

Image Reconstruction

For scanners with time-of-flight (TOF) technology, iterative reconstruction and/or a reconstruction algorithm using resolution recovery (point spread function (PSF) reconstruction) should be used, as this may help with the detection of small lesions.[3,20] If applicable, the Gaussian smoothing filter should not exceed 5 mm.[3] A bone CT reconstruction algorithm is recommended in addition to the standard CT reconstruction. PET data should be fused with both standard and bone CT reconstructions.[20]

[18F]FLUCICLOVINE PET/CT RESULTS AND INTERPRETATION

Diagnostic Criteria

Increased uptake in soft-tissue lesions is generally defined as uptake visually clearly above that of the bone marrow (L3 vertebrae is preferred) for lesions >1cm (longest dimension). Soft-tissue lesions which are <1 cm (longest dimension) are subject to partial volume effect, but in a typical location for metastases may still be interpreted as suspicious if uptake is visually equal to or approaches that of the marrow and is significantly greater than that of blood pool.[20]

In the prostate bed following prostatectomy:

Malignancy:

- Focal uptake (SUV_{max}) visually equal to or greater than that of bone marrow (SUV_{mean}), within the prostate bed, is suspicious for malignancy.[3,20]
- Asymmetric seminal vesicle uptake between blood pool and bone marrow may represent malignancy. Correlation with MRI is recommended.[20]

Suspicious:

- If a focus of uptake is small (<1 cm), it may be considered suspicious if the uptake is visually greater than that of blood pool and lesser than that of bone marrow. Correlation with MRI is recommended.[3,20]

Requiring close follow-up:

- If uptake is between that of blood pool and bone marrow, it does not meet criteria for malignancy but may still be reported as requiring close follow-up.[20]

Benign:

- If there is no increased uptake.
- In seminal vesicles, with or without a prostate, symmetric bilateral uptake similar to that of blood pool is likely physiological.[20]

In non-prostatectomy cases:

Malignancy:

- Moderate focal asymmetric uptake, visually equal to or greater than that of bone marrow, is suspicious for recurrence.[3]

Requiring close follow-up:

- If uptake is between that of blood pool and bone marrow, it does not meet criteria for malignancy but may still be reported as requiring close follow-up.[20]

Suspicious:

- If a focus of uptake is small (<1 cm) and in a site typical for recurrence, it may still be considered suspicious if the uptake is visually greater than that of blood pool.[3]

Uptake within lymph nodes at sites of typical prostate cancer dissemination is highly specific for neoplastic involvement with a low false-positive rate.[3,43,58,60,61] Uptake visually equal to or above that of lumbar marrow should be considered abnormal, although with nodes less than 1 cm, uptake may be suspicious if in a typical pattern of spread and greater than that of blood pool. However, if a node is small (<1 cm) and in a site typical for recurrence, it may still be considered suspicious if visually greater than that of blood pool.[3]

In atypical sites for recurrence (inguinal, distal external iliac, hilar, and axillary nodes), mild, symmetric uptake is typically considered physiological uptake, but if uptake is present within the context of other clear malignant disease, it may be considered suspicious for cancer recurrence.[3]

For bone lesions to be considered positive, focal uptake should be clearly seen on maximum intensity projection (MIP) or PET-only images. Densely sclerotic lesions may not be [18F]Fluciclovine avid. Unlike in [18F]FDG PET, degenerative uptake of [18F]Fluciclovine is not a common variant. Skeletal metastases resembling Schmorl's nodes but with [18F]Fluciclovine uptake have been described. [3,62] Uptake in lytic skeletal lesions is typically intense, moderate in mixed lesions, but may be absent in densely sclerotic lesions. If skeletal lesion is seen on CT (e.g., dense sclerosis without uptake), skeletal-specific imaging should be considered, as the absence of

[18F]Fluciclovine uptake does not exclude the presence of metastasis. Unlike in [18F]FDG, degenerative uptake in bone is not a common vari-ant in [18F]Fluciclovine and should be further evaluated for the presence of metastatic bone lesions.[3,62]

Differential Diagnosis

Prostate: cancer, inflammatory changes, benign prostatic hypertrophy.

Extra-prostate: typical locations for nodal dissemination of prostate cancer (metastatic prostate cancer). Uptake may occur in other cancers. Nodal inflammation, especially if mild and symmetric and in atypical locations for prostate cancer spread, such as inguinal or distal external iliac. Uptake may also occur from benign processes such as infection, and metabolically active benign bone lesions such as osteoid osteoma.[3,62]

Pearls, Pitfalls and Variants

[18F]Fluciclovine PET/CT performance is affected by PSA levels and is less likely to be positive with PSA <1 ng/mL, unless doubling time is rapid.[3] [18F]Fluciclovine PET can identify true positive prostate cancer foci even when conventional imaging, such as CT, MRI, and isotope bone scan, is negative. [3] Understanding the common patterns of [18F]Fluciclovine uptake in prostate cancer and being familiar with typical locations for prostate cancer dissemination (deep pelvic vs. peripheral inguinal or distal external iliac nodes) are essential in order to minimise false-positive and false-negative interpretation. It is also important to have a good knowledge of factors that may lead to typical false-positive and false-negative findings in [18F]Fluciclovine PET, especially as uptake of [18F]Fluciclovine may be present in benign conditions such as inflammation and infection and other metabolically active benign lesions such as meningioma and osteoid osteoma.[3,20,62]

Potential reasons for uptake in the prostate gland that may lead to false-positive results in patients who have undergone non-prostatectomy therapy include benign prostatic hyperplasia and post-radiation inflammation and fibrosis.[3,20,63,64] There is a higher false- positive rate within intact or treated prostate.[3]

Uptake in nodes may be due to acute and chronic inflammation and infection, especially if symmetric and in atypical locations for prostate cancer spread.[3,20] Mild benign symmetric uptake within the inguinal lymph nodes may demonstrate non-specific moderate symmetric inflammatory uptake and lead to false-positive results.[3]

[18F]Fluciclovine uptake can be observed in inflammatory skin lesions, inguinal nodes due to ringworm infection, and musculoskeletal inflammation.[20] Uptake may occur not only in prostate cancer but also in other malignancies with upregulated amino acid transport such as breast cancer, lung cancer, colon cancer, lymphoma, hepatocellular carcinoma, multiple myeloma, squamous cell carcinoma of the scalp, and primary and metastatic tumours in the brain, among others.[3,20,41,62,65–71] Uptake in renal masses should be further investigated as, similarly to [18F]FDG, any degree of [18F]Fluciclovine uptake in a renal mass might represent malignant aetiology.[20]

Benign bone lesions such as osteoid osteoma may have moderate uptake. Mild uptake may be seen in degenerative disc and facet disease, but this is less common and less intense than usually seen with [18F]FDG. Intense though benign activity within a joint or at a muscular insertion has occasionally been observed.[20]

Benign meningioma may have intense uptake.[20,72] Pituitary and adrenal adenomas can have focal uptake greater than that of the surrounding tissue.[20] In a small percentage of patients, [18F]Fluciclovine may demonstrate moderate early bladder activity, interfering with evaluation of the prostate bed.[3,62]

Theranostics Potential

It is unlikely that [18F]Fluciclovine can easily be modified to present a theranostic equivalent. Since the size of the fluciclovine molecule is rather small, any labelling with a large therapeutic radionuclide (for therapeutic purposes) will give the molecule a totally different pKa and presumably result in a concomitant change in pharmacokinetics/biodistribution.

Radiation Exposure

The effective dose from [18F]Fluciclovine is 22 µSv/MBq, and the organs receiving the highest equivalent doses are the pancreas, heart wall, and uterus.[29] Typical administered activity is 370 MBq per 70 kg body weight.

The mean absorbed dose per unit of administered activity varies significantly across different organs and tissues. The pancreas receives the highest absorbed dose, at 102 µGy/MBq. The heart wall absorbs 52 µGy/MBq, and the uterus receives 45 µGy/MBq. The lungs and liver absorb 34 µGy/MBq and 33 µGy/MBq, respectively.[29]

Overall, the total body mean absorbed dose is 13 µGy/MBq, with an effective dose of 22 µSv/MBq.[29]

The summary of product characteristics (SmPC, or 'package insert') from the FDA quotes the doses shown [29] in Table 2.

Organ/Tissue	Mean Absorbed Dose per Unit Administered Activity (µGy/MBq)
Adrenal glands	16
Brain	9
Breasts	14
Gallbladder wall	17
Lower large intestine wall	12
Small intestine wall	13
Stomach wall	14
Upper large intestine wall	13
Heart wall	52
Kidneys	14
Liver	33
Lungs	34
Muscle	11
Ovaries	13
Pancreas	102
Red bone marrow	25
Osteogenic cells	23
Skin	8
Spleen	24
Testes	17
Thymus gland	12
Thyroid	10
Urinary bladder wall	25
Uterus	45
Total body	13
Effective dose	22 (µSv/MBq)

Table 2. Estimated absorbed radiation doses in various organs/tissues in adults who received [18F]Fluciclovine.[29]

REFERENCES

1. Jager PL, Vaalburg W, Pruim J, Vries EGE De, Langen K josef, Piers DA. Radiolabeled Amino Acids: Basic Aspects and Clinical Applications in Oncology ; Contnuing Education. J Nucl Med. 2001; 42(3):432–45.
2. Huang C, McConathy J. Radiolabeled Amino Acids for Oncologic Imaging. J Nucl Med [Internet]. 2013 Jul [cited 2024 Jun 23];54(7):1007–10. Available from: http://jnm.snmjournals.org/lookup/doi/10.2967/jnumed.112.113100
3. Savir-Baruch B, Zanoni L, Schuster DM. Imaging of Prostate Cancer Using Fluciclovine. PET Clin [Internet]. 2017;12(2):145–57. Available from: http://dx.doi.org/10.1016/j.cpet.2016.11.005
4. Wibmer AG, Burger IA, Sala E, Hricak H, Weber WA, Vargas HA. Molecular imaging of prostate cancer. Radiographics [Internet]. 2016 [cited 2024 Jun 23];36(1):142–61. Available from: www.rsna.org/education/search/RG.
5. Oka S, Hattori R, Kurosaki F, Toyama M, Williams LA, Yu W, et al. A preliminary study of anti-1-amino-3-18f-fluorocyclobutyl-1- carboxylic acid for the detection of prostate cancer. J Nucl Med. 2007;48(1):46–55.
6. Sasajima T, Ono T, Shimada N, Doi Y, Oka S, Kanagawa M, et al. Trans-1-amino-3-18 F-fluorocyclobutanecarboxylic acid (anti-18 F-FACBC) is a feasible alternative to 11 C-methyl-L-methionine and magnetic resonance imaging for monitoring treatment response in gliomas. 2013 [cited 2024 Jun 23]; Available from: http://dx.doi.org/10.1016/j.nucmedbio.2013.04.007
7. Oka S, Okudaira H, Yoshida Y, Schuster DM, Goodman MM, Shirakami Y. Transport mechanisms of trans-1-amino-3-fluoro[1- 14C] cyclobutanecarboxylic acid in prostate cancer cells. Nucl Med Biol [Internet]. 2012;39(1):109–19. Available from: http://dx.doi.org/10.1016/j.nucmedbio.2011.06.008
8. Schuster DM, Nanni C, Fanti S. PET Tracers Beyond FDG in Prostate Cancer [Internet]. Vol. 46, Seminars in Nuclear Medicine. 2016 [cited 2024 Jun 23]. p. 507–21. Available from: https://linkinghub.elsevier.com/retrieve/pii/S0001299816300472
9. Evans JD, Jethwa KR, Ost P, Williams S, Kwon ED, Lowe VJ, et al. Prostate cancer–specific PET radiotracers: A review on the clinical utility in recurrent disease. Pract Radiat Oncol [Internet]. 2018;8(1):28–39. Available from: https://doi.org/10.1016/j.prro.2017.07.011
10. Nakanishi T, Tamai I. Solute Carrier Transporters as Targets for Drug Delivery and Pharmacological Intervention for Chemotherapy. J Pharm Sci. 2011 Sep 1;100(9):3731–50.
11. Ganapathy V, Thangaraju M, Prasad PD. Nutrient transporters in cancer: Relevance to Warburg hypothesis and beyond. Pharmacol Ther. 2009 Jan 1;121(1):29–40.
12. Oka S, Okudaira H, Ono M, Schuster DM, Goodman MM, Kawai K, et al. Differences in transport mechanisms of trans-1-amino-3-[18F] fluorocyclobutanecarboxylic acid in inflammation, prostate cancer, and glioma cells: Comparison with L-[methyl-11C]methionine and 2-deoxy-2-[18F] fluoro-D-glucose. Mol Imaging Biol [Internet]. 2014 Oct 18 [cited 2024 Jun 23];16(3):322–9. Available from: https://link.springer.com/article/10.1007/s11307-013-0693-0
13. Asano Y, Inoue Y, Ikeda Y, Kikuchi K, Hara T, Taguchi C, et al. Phase i clinical study of NMK36: A new PET tracer with the synthetic amino acid analogue anti-[18F]FACBC. Ann Nucl Med [Internet]. 2011 Jul 16 [cited 2024 Jun 23];25(6):414–8. Available from: https://link.springer.com/article/10.1007/s12149-011-0477-z
14. Abiodun-Ojo OA, Jani AB, Akintayo AA, Akin-Akintayo OO, Odewole OA, Tade FI, et al. Salvage Radiotherapy Management Decisions in Postprostatectomy Patients with Recurrent Prostate Cancer Based on 18F-Fluciclovine PET/CT Guidance. J Nucl Med [Internet]. 2021 Aug 1;62(8):1089–96. Available from: http://jnm.snmjournals.org/lookup/doi/10.2967/jnumed.120.256784
15. Schreibmann E, Schuster DM, Rossi PJ, Shelton J, Cooper S, Jani AB. Image Guided Planning for Prostate Carcinomas With Incorporation of Anti-3-[18F]FACBC (Fluciclovine) Positron Emission Tomography: Workflow and Initial Findings From a Randomized Trial. Int J Radiat Oncol Biol Phys. 2016;96(1):206–13.

16. Lawal IO, Jani AB, Adediran OA, Goyal S, Abiodun-Ojo OA, Dhere VR, et al. Differences in Failure-Free Survival After Salvage Radiotherapy Guided by Conventional Imaging Versus 18F-Fluciclovine PET/CT in Postprostatectomy Patients: A Post Hoc Substratification Analysis of the EMPIRE-1 Trial. J Nucl Med. 2023;64(4):586–91.
17. Blue Earth Diagnosis. Axumin SPC. 2016. p. 1–9.
18. Kalss S, Oppitz M, Torggler U, Winner M, editors. Annex I - SUMMARY OF PRODUCT CHARACTERISTICS [Internet]. European Medicines Agency. Edward Elgar Publishing; 2021 Dec. Available from: https://china.elgaronline.com/view/edcoll/9781800882232/9781800882232.00051.xml
19. Fda; Cder. HIGHLIGHTS OF PRESCRIBING. INFORMATION [Internet]. 2021 [cited 2024 Jun 22]. Available from: www.fda.gov/medwatch.
20. Nanni C, Zanoni L, Bach-Gansmo T, Minn H, Willoch F, Bogsrud TV, et al. [18F]Fluciclovine PET/CT: joint EANM and SNMMI procedure guideline for prostate cancer imaging - version 1.0. Eur J Nucl Med Mol Imaging. 2020;47(3):579–91.
21. Odewole OA, Tade FI, Nieh PT, Savir-Baruch B, Jani AB, Master VA, et al. Recurrent Prostate Cancer Detection with anti-3-[18F] FACBC PET-CT: Comparison with Computed Tomography HHS Public Access. Eur J Nucl Med Mol Imaging [Internet]. 2016;43(10):1773–83. Available from: https://www.ncbi.nlm.nih.gov/pmc/articles/PMC4970909/pdf/nihms779715.pdf
22. Jani AB, Schreibmann E, Goyal S, Halkar R, Hershatter B, Rossi PJ, et al. 18F-fluciclovine-PET/CT imaging versus conventional imaging alone to guide postprostatectomy salvage radiotherapy for prostate cancer (EMPIRE-1): a single centre, open-label, phase 2/3 randomised controlled trial. Lancet [Internet]. 2021 May;397(10288):1895–904. Available from: https://linkinghub.elsevier.com/retrieve/pii/S014067362100581X
23. Kairemo K, Rasulova N, Partanen K, Joensuu T. Preliminary clinical experience of trans-1-amino-3-(18)F- fluorocyclobutanecarboxylic acid (anti-(18)F-FACBC) PET/CT imaging in prostate cancer patients. Biomed Res Int. 2014;2014.
24. Evangelista L, Briganti A, Fanti S, Joniau S, Reske S, Schiavina R, et al. New Clinical Indications for 18F/11C-choline, New Tracers for Positron Emission Tomography and a Promising Hybrid Device for Prostate Cancer Staging: A Systematic Review of the Literature [Figure presented]. Eur Urol [Internet]. 2016 [cited 2024 Jun 23];70(1):161–75. Available from: http://dx.doi.org/10.1016/j.eururo.2016.01.029
25. Supiot S, Rio E, Pacteau V, Mauboussin MH, Campion L, Pein F. OLIGOPELVIS – GETUG P07: a multicentre phase II trial of combined salvage radiotherapy and hormone therapy in oligometastatic pelvic node relapses of prostate cancer. 2015 [cited 2024 Jun 23]; Available from: http://uroweb.org/individual-guidelines/oncology-guide-
26. Mohsen B, Giorgio T, Rasoul ZS, Werner L, Rad G, Ali M, et al. Application of 11 C-acetate positron-emission tomography (PET) imaging in prostate cancer : systematic review and meta-analysis of the literature. 2013;1062–72.
27. Perera M, Papa N, Christidis D, Wetherell D, Hofman MS, Murphy DG, et al. Sensitivity, Specificity, and Predictors of Positive 68 Ga–Prostate-specific Membrane Antigen Positron Emission Tomography in Advanced Prostate Cancer: A Systematic Review and Meta-analysis. Eur Urol [Internet]. 2016 Dec;70(6):926–37. Available from: http://dx.doi.org/10.1016/j.eururo.2016.06.021
28. Ost P, Bossi A, Decaestecker K, De Meerleer G, Giannarini G, Karnes RJ, et al. Metastasis-directed therapy of regional and distant recurrences after curative treatment of prostate cancer: A systematic review of the literature. Eur Urol [Internet]. 2015;67(5):852–63. Available from: http://dx.doi.org/10.1016/j.eururo.2014.09.004
29. Food and Drug Administration. Highlights of Prescribing Information: AXUMIN (fluciclovine F 18) injection. FDA website. 2016;1–8.
30. PubChem. National Library of Medicine. [cited 2024 Jun 28]. Fluciclovine (18F) | C5H8FNO2 | CID 450601 - PubChem. Available from: https://pubchem.ncbi.nlm.nih.gov/compound/Fluciclovine-_18F
31. Häfliger P, Charles RP. The l-type amino acid transporter LAT1—an emerging target in cancer. Int J Mol Sci. 2019;20(10):1–14.
32. Tade FI, Sajdak RA, Gabriel M, Wagner RH, Savir-Baruch B. Best practices for 18F-Fluciclovine PET/CT imaging of recurrent prostate cancer: A guide for technologists. J Nucl Med Technol. 2019;47(4):282–7.
33. Gusman M, Aminsharifi JA, Peacock JG, Anderson SB, Clemenshaw MN, Banks KP. Review of 18F-Fluciclovine PET for Detection of Recurrent Prostate Cancer. Radiographics [Internet]. 2019 May 1 [cited 2024 Jun 28];39(3):822–41. Available from: https://doi.org/10.1148/rg.2019180139
34. What is an amino acid analogue? - Quora [Internet]. [cited 2024 Jun 28]. Available from: https://www.quora.com/What-is-an-amino-acid-analogue
35. Lowentritt BH, Kipper MS. Understanding and Improving 18F-Fluciclovine PET/CT Reports: A Guide for Physicians Treating Patients with Biochemical Recurrence of Prostate Cancer. Prostate Cancer. 2020;2020:1–11.
36. National Cancer Institute. Definition of tesevatinib - NCI Drug Dictionary [Internet]. [cited 2024 Jun 28]. Available from: https://www.cancer.gov/publications/dictionaries/cancer-drug/def/fluciclovine-f18
37. Mei H, Han J, Klika KD, Izawa K, Sato T, Meanwell NA, et al. Applications of fluorine-containing amino acids for drug design. Eur J Med Chem. 2020 Jan 15;186:111826.
38. Haka M, Walsh J, Webster E. Production of Fluciclovine F18 (FACBC) on a Siemens< PETNET GN Platform. J Nucl Med [Internet]. 2017 May 1 [cited 2024 Jun 28];58(supplement 1):893–893. Available from: https://jnm.snmjournals.org/content/58/supplement_1/893
39. International Atomic Energy Agency. Production and Quality Control of Fluorine-18 Labelled Radiopharmaceuticals [Internet]. Iaea-Tecdoc-1968. 2021. 166 p. Available from: https://www-pub.iaea.org/MTCD/Publications/PDF/TE-1968web.pdf
40. ICH Expert Working Group. Ich Harmonised Guideline - Impurities: Guideline for Residual Solvents Q3C(R8). Int Counc Harmon Tech Requir Pharm Hum Use. 2021;(April):1–43.
41. Shoup TM, Olson J, Hoffman JM, Votaw J, Eshima D, Eshima L, et al. Synthesis and Evaluation of 1-carboxylic Acid to Image Brain Tumors. :331–8.
42. Nye JA, Schuster DM, Yu W, Camp VM, Goodman MM, Votaw JR. Biodistribution and radiation dosimetry of the synthetic nonmetabolized amino acid analogue anti- 18F-FACBC in humans. J Nucl Med. 2007;48(6):1017–20.
43. Schuster DM, Savir-Baruch B, Nieh PT, Master VA, Halkar RK, Rossi PJ, et al. Detection of recurrent prostate carcinoma with anti-1-amino-3-18F-fluorocyclobutane-1-carboxylic acid PET/CT and 111In-capromab pendetide SPECT/CT. Radiology. 2011;259(3):852–61.
44. Martarello L, McConathy J, Camp VM, Malveaux EJ, Simpson NE, Simpson CP, et al. Synthesis of syn- and anti-1-amino-3-[18 F]fluoromethyl-cyclobutane-1-carboxylic acid (FMACBC), potential PET ligands for tumor detection. J Med Chem [Internet]. 2002 May 23 [cited 2024 Jun 25];45(11):2250–9. Available from: https://pubs.acs.org/doi/abs/10.1021/jm010242p
45. Witney TH, Editors AJS. Positron Emission Tomography: Methods and Protocols [Internet]. Vol. 2729, Methods in Molecular Biology. 2023. Available from: http://www.springer.com/series/7651
46. Savir-Baruch B, Banks KP, McConathy JE, Molchanova-Cook OP, Parent EE, Takalkar A, et al. ACR-ACNM Practice Parameter for the Performance of Fluorine-18 Fluciclovine-PET/CT for Recurrent Prostate Cancer. Clin Nucl Med. 2018;43(12):909–17.
47. Lovrec P, Schuster DM, Wagner RH, Gabriel M, Savir-Baruch B. Characterizing and mitigating bladder radioactivity on 18F-fluciclovine PET/CT. J Nucl Med Technol. 2020;48(1):24–9.
48. Moran JK, Lee HB, Blaufox MD. Optimization of urinary FDG excretion during PET imaging. J Nucl Med [Internet]. 1999 [cited 2024 Jun 25];40(8):1352–7. Available from: https://pubmed.ncbi.nlm.nih.gov/10450688/
49. Diehl M, Manolopoulou M, Risse J, Kranert T, Menzel C, Döbert N, et al. Urinary fluorine-18 flourodeoxyglucose excretion with and without intravenous application of furosemide. Acta Med Austriaca [Internet]. 2004 [cited 2024 Jun 25];31(3):76–8. Available from: https://pubmed.ncbi.nlm.nih.gov/15515481/
50. Klahr S, Harris K, Purkerson ML. Effects of obstruction on renal functions. Pediatr Nephrol [Internet]. 1988 Mar [cited 2024 Jun 25];2(1):34–42. Available from: https://pubmed.ncbi.nlm.nih.gov/3152999/

51. Lovrec P, Solanki AA, Yonover PM, Gupta GN, Adams W, Wagner R, et al. Factors influencing the positivity rate of commercial 18F-Fluciclovine imaging in men with suspected recurrent prostate cancer. J Nucl Med [Internet]. 2018;59:4–5. Available from: https://www.embase.com/search/
53. Administration of Radioactive Substances Advisory Committee. Notes for guidance on the clinical administration of radiopharmaceuticals and use of sealed radioactive sources. Administration of Radioactive Substances Advisory Committee. Nucl Med Commun [Internet]. 2024 Jan;21 Suppl(March):S1-93. Available from: http://www.ncbi.nlm.nih.gov/pubmed/10732169
54. Bar-Shalom R, Yefremov N, Guralnik L, Gaitini D, Frenkel A, Kuten A, et al. Clinical performance of PET/CT in evaluation of cancer: additional value for diagnostic imaging and patient management. J Nuc Med [Internet]. 2003 Aug;44(8):1200–9. Available from: http://www.ncbi.nlm.nih.gov/pubmed/12902408
55. Joslyn SA. Racial differences in survival from breast cancer. Vol. 273, Jama The Journal Of The American Medical Association. 1995. p. 1000.
56. Sörensen J, Owenius R, Lax M, Johansson S. Regional distribution and kinetics of [18F]fluciclovine (anti-[18F]FACBC), a tracer of amino acid transport, in subjects with primary prostate cancer. Eur J Nucl Med Mol Imaging [Internet]. 2013 Feb 4 [cited 2024 Jun 29];40(3):394–402. Available from: https://link.springer.com/article/10.1007/s00259-012-2291-9
57. McParland BJ, Wall A, Johansson S, Sørensen J. The clinical safety, biodistribution and internal radiation dosimetry of [18F]fluciclovine in healthy adult volunteers. Eur J Nucl Med Mol Imaging [Internet]. 2013 Aug 24 [cited 2024 Jun 29];40(8):1256–64. Available from: https://link.springer.com/article/10.1007/s00259-013-2403-1
58. Nanni C, Zanoni L, Pultrone C, Schiavina R, Brunocilla E, Lodi F, et al. 18F-FACBC (anti1-amino-3-18F-fluorocyclobutane-1-carboxylic acid) versus 11C-choline PET/CT in prostate cancer relapse: results of a prospective trial. Eur J Nucl Med Mol Imaging [Internet]. 2016 Aug 10 [cited 2024 Jun 29];43(9):1601–10. Available from: https://link.springer.com/article/10.1007/s00259-016-3329-1
59. Fuchs BC, Bode BP. Amino acid transporters ASCT2 and LAT1 in cancer: Partners in crime? Semin Cancer Biol. 2005 Aug 1;15(4):254–66.
60. Schuster DM, Nieh PT, Jani AB, Amzat R, Bowman FD, Halkar RK, et al. Anti-3-[18F]FACBC positron emission tomography-computerized tomography and 111In-capromab pendetide single photon emission computerized tomography-computerized tomography for recurrent prostate carcinoma: Results of a prospective clinical trial. J Urol [Internet]. 2014;191(5):1446–53. Available from: http://dx.doi.org/10.1016/j.juro.2013.10.065
61. Nanni C, Schiavina R, Brunocilla E, Boschi S, Borghesi M, Zanoni L, et al. 18F-Fluciclovine PET/CT for the Detection of Prostate Cancer Relapse: A Comparison to 11C-Choline PET/CT. Clin Nucl Med. 2015;40(8):e386–91.
62. Schuster DM, Nanni C, Fanti S, Oka S, Okudaira H, Inoue Y, et al. Anti-1-amino-3-18F-fluorocyclobutane-1-carboxylic acid: Physiologic uptake patterns, incidental findings, and variants that may simulate disease. J Nucl Med. 2014;55(12):1986–92.
63. D.M. S, P.A. T, P.T. N, V.A. M, R. A, B. SB, et al. Characterization of primary prostate carcinoma by anti-1-amino-2-[18F] -fuorocyclobutane-1-carboxylic acid (anti-3-[18F] FACBC) uptake. Am J Nucl Med Mol Imaging [Internet]. 2013;3(1):85–96. Available from: http://www.embase.com/search/
64. Turkbey B, Mena E, Shih J, Pinto PA, Merino MJ, Lindenberg ML, et al. Localized prostate cancer detection with 18F FACBC PET/CT: Comparison with MR imaging and histopathologic analysis. Radiology. 2014;270(3):849–56.
65. Schuster DM, Nanni C, Fanti S, Oka S, Okudaira H, Inoue Y, et al. Anti-1-amino-3-18F-fluorocyclobutane-1-carboxylic acid: Physiologic uptake patterns, incidental findings, and variants that may simulate disease. J Nucl Med. 2014;55(12):1986–92.
66. Schuster DM, Votaw JR, Nieh PT, Yu W, Nye JA, Master V, et al. Initial experience with the radiotracer anti-1-amino-3-18F- fluorocyclobutane-1-carboxylic acid with PET/CT in prostate carcinoma. J Nucl Med [Internet]. 2007 [cited 2024 Jul 1];48(1):56–63. Available from: https://pubmed.ncbi.nlm.nih.gov/17204699/
67. Ulaner GA, Schuster DM. Amino Acid Metabolism as a Target for Breast Cancer Imaging. Vol. 13, PET Clinics. 2018. p. 437–44.
68. Parent EE, Benayoun M, Ibeanu I, Olson JJ, Hadjipanayis CG, Brat DJ, et al. [18F]Fluciclovine PET discrimination between high- and low-grade gliomas. EJNMMI Res. 2018;8.
69. Sannananja B, Shah HU, Behnia F. 18F-fluciclovine uptake by an incidentally detected hepatocellular carcinoma in a case of biochemically recurrent prostate cancer. Clin Nucl Med. 2018;43(9):692–3.
70. Amzat R, Taleghani P, Miller DL, Beitler JJ, Bellamy LM, Nye JA, et al. Pilot Study of the utility of the synthetic pet amino-acid radiotracer anti-1-amino-3-[18f]fluorocyclobutane-1-carboxylic acid for the noninvasive imaging of pulmonary lesions. Mol Imaging Biol [Internet]. 2013 Oct 18 [cited 2024 Jul 1];15(5):633–43. Available from: https://link.springer.com/article/10.1007/s11307-012-0606-7
71. Schuster DM, Nye JA, Nieh PT, Votaw JR, Halkar RK, Issa MM, et al. Initial experience with the radiotracer anti-1-amino-3-[18F] fluorocyclobutane-1-carboxylic acid (Anti-[18F]FACBC) with PET in renal carcinoma. Mol Imaging Biol [Internet]. 2009 [cited 2024 Jun 25];11(6):434–8. Available from: https://pubmed.ncbi.nlm.nih.gov/17204699/
72. Nguyen QBD, Amato R, Riascos R, Ballester L, Tandon N, Blanco A, et al. Fluciclovine, Anti-1-Amino-3-[18F]-Fluorocyclobutane-1-Carboxylic Acid: A Novel Radiotracer for Meningioma. World Neurosurg [Internet]. 2018;119:132–6. Available from: https://doi.org/10.1016/j.wneu.2018.07.231

CHAPTER 2

[18F]FLUCICLOVINE

3

[^{11}C] ACETATE

by Valentina Mautone[1]
Valentina Di Iorio[2]
Marco Marcolin[3]
Giacomo Foschi[2]

[1]U.O.s Diagnostic Medical Dept., Istituto Romagnolo per lo Studio dei Tumori "Dino Amadori" - IRST IRCCS, Meldola

[2]Radiopharmacy, Istituto Romagnolo per lo Studio dei Tumori "Dino Amadori" - IRST IRCCS

[3]Radiopharmacy, Istituto Oncologico Veneto IOV-IRCCS Castelfranco Veneto (TV) Italy

[11C]ACETATE

[1-11C]acetate, the salt of acetic acid radiolabelled in position 1 (carboxylic group) of the molecule (for simplification referred to as [11C]acetate for the rest of this chapter), was one of the first radiopharmaceuticals labelled with the radionuclide carbon-11 (11C) to be widely used in clinical settings, thanks also to the increasingly widespread use of self-shielded low-energy medical cyclotrons and the inclusion of a monograph on 1920 Sodium Acetatis ([1-11C]) in the European Pharmacopoeia (Ph. Eur.)

The most widely used nuclear reaction to produce 11C is 14N(p,α)11C, as it can be obtained at high yields using low energies with relatively short irradiation times. The precursor, nitrogen-14 gas, is very cheap and readily available. The synthesis of [11C]acetate has been achieved by various methods, as carbon-11 has significant advantages over other radionuclides. Unfortunately, the short half-life (T1/2 = 20.4 minutes) limits its production to centres equipped with on-site cyclotrons.

Initially used in cardiology to study myocardial metabolism, the radio-pharmaceutical [11C]acetate subsequently began to be used in oncology: in hepatocarcinomas, meningiomas, and later in prostate diseases and other urological malignancies such as renal cell carcinoma and bladder cancer [1]. [11C] acetate PET has also been used in the diagnosis of malignancies such as brain and lung tumours.

The advent of new radiopharmaceuticals such as those based on 18F or 68Ga for prostate diseases, which can also be used by centres not equipped with a cyclotron, have limited the clinical use of [11C]acetate over the years.

Nevertheless, [11C]acetate remains an important option in nuclear medical diagnostics. The short half-life allows it to be used only in centres equipped with a cyclotron and only in the presence of medical physicists, medical radiology technologists, radiochemists and/or radiopharmacists, nurses and nuclear medicine physicians who are trained to work in multidisciplinary environments such as nuclear medicine and radiopharmacy practice.

CHEMISTRY & PROPERTIES

The radionuclide 11C

In 1934, Lauritsen and Crane carried out the pioneering production of 11C and simultaneously identified its physical properties. These include the predominant type of decay (99.8% Beta+ and 0.2% EC) and a half-life of approximately 20 minutes [1,2].

Subsequently, in 1939, Barkas succeeded in producing 11C by bombarding 14N gas with high-energy cyclotron-produced protons [3]. The 14N(p,α)11C method remains the most common approach to producing 11C.

11C undergoes decay to stable 11B (boron-11). This decay primarily occurs (99.8%) through positron emission with a mean energy of 0.386 MeV. The versatility of 11C as a radiolabel for biological applications is evident due to the ubiquity of carbon in biomolecules. It allows the substitution of stable 12C, resulting in a radioactive analogue with chemical and physiological properties indistinguishable from those of the carbon-12 analogue. Authentic radiolabelling of substances occurring in physiological processes and experimental or established drugs thus becomes possible.

Human studies with 11C began in 1945, with Tobias et al. investigating [11C]CO uptake and bodily distribution following gas inhalation [4].

The advent of commercially available cyclotrons and PET scanners fuelled 11C radiochemistry research to meet the demand for new or improved tracers targeting an expanding range of biological entities. Short-lived positron-emitting 11C has since been extensively utilised to study the fate of labelled molecules in biological systems, particularly through the in-vivo medical imaging PET technique.

A final consideration must be mentioned regarding the specific or molar activity. While theoretical molar activities for PET radionuclides such as 11C (341.1 TBq/μmol) and Fluorine-18 (63.3 TBq/μmol) appear exceptionally high, the practical values obtained post-synthesis are typically 10–10,000 times lower. This drastic difference is mainly due to the broad presence of the non-radioactive isotope, commonly occurring during radionuclide production, manipulation, and radiotracer preparation [5].

Acetate

Acetate has several roles in cellular metabolism, such as energy production, lipid synthesis and protein acetylation. Acetate is actively transported into cells through mono-carboxylate transporters and is quickly converted to acetyl-CoA by acetyl kinase. Acetyl-CoA is a reactive unit that participates both in catabolic and anabolic metabolism. As an example, it can be utilised in the anabolic pathway to generate fatty acids and cholesterol, which forms the cell membrane; or it can be oxidized (catabolic manner) in the mitochondria via the tricarboxylic acid cycle (TCA), which produces CO2 and H_2O, which produces energy [6]. In this sense, acetate can be viewed as the shortest possible fatty acid.

Conversely, tumour cells, characterised by elevated fatty acid synthetase (FAS), channel acetate predominantly into fatty acid synthesis, incorporating them into vital membrane microdomains crucial for tumour development and metastasis. Under nutritional replete conditions, Acetyl-CoA is mainly derived from glucose. Otherwise, during hypoxia or nutritional challenges, acetate becomes the main source of Acetyl-CoA. This phenomenon is well studied in the tumour microenvironment, where there is a

symbiotic relationship between nutrient-rich tumour cells which have hyperactive metabolism (Warburg Effect) and release metabolic intermediates (e.g. acetate) for nutrient-poor tumour cells. Another way of producing acetate inside cells is via the ketoacid dehydrogenases and ROS, also called the *de novo* pathway. This *de novo* pathway can be useful in maintaining adequate levels of acetate when it is limited in the extracellular compartment [7].

LABELLING / PRODUCTION

Radioactive drugs are pharmaceuticals, and their preparation method and quality specifications must comply with the requirements defined by the European Pharmacopoeia (Pharm. Eur.).

Most radioactive drugs are intended for parenteral use, and must therefore be sterile and free of pyrogens. Sterility assurance is determined by various factors such as handling procedures under aseptic conditions, raw materials, equipment, personnel, and the facility in which these factors interact. For radiopharmaceuticals, having a system that consistently and effectively ensures the sterility of the finished product is even more crucial, considering that, due to the half-life, (1) no full sterilisation of the final product can be performed and (2) the sterility test is conducted post-release. Typically, the final product solution is passed through a sterile filter (0.22µm) under aseptic conditions (laminar air flow / grade A environment).

All radiochemical syntheses must be conducted utilising suitable equipment within a facility authorised for handling radioactive materials. It is imperative to wear personal protective equipment and adhere to all relevant local radiation safety regulations.

A quality assurance system must be implemented, and if national legislation mandates Good Manufacturing Practice (GMP), all information can be found in the current version including the relevant annexes. Also, EANM's GRPP (Good Radiopharmaceutical Practices) might be of special interest for the preparation of ^{11}C-labelled radiotracers in a non-commercial environment.

[^{11}C]CO2 preparation

The most prevalent approach for producing [^{11}C]CO2 involves irradiating a ^{14}N target, with a small addition of oxygen [^{16}O] (<2%), with protons through the reaction [^{14}N(p,α)^{11}C]. The presence of [^{16}O] oxygen (^{16}O2) in the target gas, besides triggering the desired in-target formation of carbon dioxide, also results in the undesired formation of [^{13}N]nitrogen during irradiation, predominantly in the form of nitrogen oxides (NOx). These undesired by-products must be eliminated before proceeding with further conversions.

The operation of separation and concentration of CO2 can be carried out in two ways: cryogenically, or using molecular sieves [8].

In the first case, after bombardment, the target content is passed through a loop immersed in liquid nitrogen (-196°C). The CO2, having a sublimation point of -78.6°C, solidifies, while the remaining gases pass through undisturbed. The subsequent release phase involves bringing the loop to room temperature and flowing an inert gas through it. However, a slight vacuum must be applied at the exit of the loop to prevent nitrogen and oxygen from being trapped.

The second process begins by selectively binding [^{11}C]CO2 onto the molecular sieve, which is preconditioned by heating to remove traces of CO2, O2 and H_2O. Subsequent purging with an inert carrier gas eliminates unwanted by-products. At elevated temperatures (>250°C), pure [^{11}C]CO2 is released and can either be used directly for synthesis (CO2 bypass in standard synthesizers) or converted to [^{11}C] methyl-iodide for subsequent methylation reactions.

[^{11}C]acetate synthesis

The description of the preparation of [^{11}C]acetate and [^{11}C]acetic acid was attributed to Kamen in 1947 [9]. The process involved obtaining [^{11}C]CO2 through proton bombardment of a ^{14}N target via the nuclear reaction ^{14}N(p,α)^{11}C. This [^{11}C]CO2 was then introduced into methylmagnesium iodide (Grignard reagent) to generate the carbon-11-labelled radiopharmaceutical.

These days, one common method for accessing ^{11}C-labelled radiopharmaceuticals involves the direct activation of [^{11}C]CO2 with organometallic reagents. Alternatively, [^{11}C]CO2 can be transformed into [^{11}C]CH3I [10,11] or [^{11}C]CH3OTf [12] and then utilised for radiolabelling. In both approaches, the radioactive building block is employed in gaseous form with an inert carrier gas, typically helium. The actual labelling process is carried out by introducing the gas mixture into a reactor, a reaction loop, or onto a solid matrix. Subsequent tracer-specific work-up is commonly achieved through solid-phase extraction (SPE) and cartridge purification, a widely accepted method. In general, SPE cartridges are pre-conditioned: PS–H+, PS–Ag+ with 10 mL of water, Maxiclean SAX was previously activated with 10 mL of ethanol 70%, 5 mL of NaCl 0.9%, and 10 mL of sterile water.

A potential automated synthesizer suitable for ^{11}C-labelling reactions is the TRACERlab FXc-pro (GE Healthcare), as previously reported [13,14]. [^{11}C]CO2 is produced after irradiation for 30 min at 40 mA to yield approximately 3 Ci, which is delivered directly to the Tracerlab FXC-Pro module, where it is bubbled through a solution containing 200 µL 0.5M methylmagnesium chloride in the reaction vessel for a duration of 4 minutes. Subsequently, the reaction is quenched with 1 mM acetic acid and further diluted into 5 mL of 1 mM acetic acid. The resulting solution undergoes a series of Sep-Paks to remove excess acid, magnesium, and halide ions. It then passes through a Maxiclean SAX anion exchange column, where the [^{11}C]acetate is captured on the cartridge. Following this, the SAX column is

rinsed with 10 mL sterile H_2O and the [11C] acetate is eluted off the column with 10 mL NaCl, 0.9% USP. In the final steps, the eluted product is passed through a sterile 0.22-µm filter into a sterile dose vial and the resulting solution is subjected to quality control testing. Typical yields of [11C]acetate prepared using this method are reported at 18%, based on starting [11C]CO2 non-decay-corrected, n = 3 [13] and 8.1% based upon starting [11C]CO2 non-decay-corrected, n = 5 [14].

In 2012, Lodi et al. published a monograph about [11C]acetate synthesis in "Radiochemical Syntheses, Volume 1: Radiopharmaceuticals for Positron Emission Tomography" that made small modifications to the aforementioned methods. The radiochemical yield of [11C]acetate was 63% EOB decay-corrected (n=3) [15].

In 2022, Wenz et al. published a new concept for producing ^{11}C-labelled radiotracers. They designed a setup by modifying TRACERlab FX FE Pro with disposable materials and pressure control as an innovative alternative to the conventional stepper-motor-controlled rotary valves,This novel concept proved successful in the synthesis of N-methyl-[11C]choline, L-S-methyl-[11C]methionine, and [11C]acetate. The radiochemical yield of [11C]acetate was 52% EOB decay-corrected (n=9) [16].

Also in 2022, Wenz et al. published a [11C] acetate synthesis on a modified TRACERLab FX C pro module. The final radiochemical yield of [11C]acetate was 56% EOB decay-corrected (n=10) [17].

The use of automatic modules (not only GETRACERLab, but also, for example, IBA) for the synthesis of positron-emitting radiopharmaceuticals has always been necessary, especially for compounds containing short-lived radionuclides. [11C], with a half-life of 20.4 minutes, requires high starting activities (typically more than 50GBq [11C]acetate) which must be processed sequentially and within a short time. The automation of syntheses using dedicated equipment known as "synthesis modules" (once called "black boxes") has evolved over the years, and now involves modules that use synthesis reagents pre-filled in dedicated KIT cassettes.

These synthesis modules allow control of the radioprotection aspects but also greater reliability in terms of the synthesis yields (EOS), allowing more regular planning of the clinical routine. The latest synthesis modules are equipped with GMP compliance software capable of controlling and recording all parameters and events of the synthesis process (audit trail) in order to facilitate analysis, traceability and optimisation. Delivery and set-up of these modules nowadays includes IQ (Installation Qualification), OQ (Operation Qualification) and PQ (Performance Qualification) certification in compliance with current legislation, in particular Annex 15 of the GMP guideline.

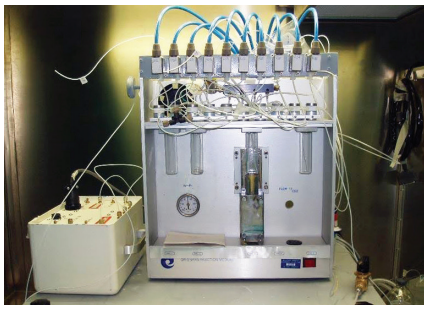

Figure 1. IBA acetate processing module setup (modified valves), used until 2008 at Castelfranco Veneto (TV) Nuclear Medicine PET Center, Italy. The module was controlled by a programmable Siemens Logic Controller PLC.

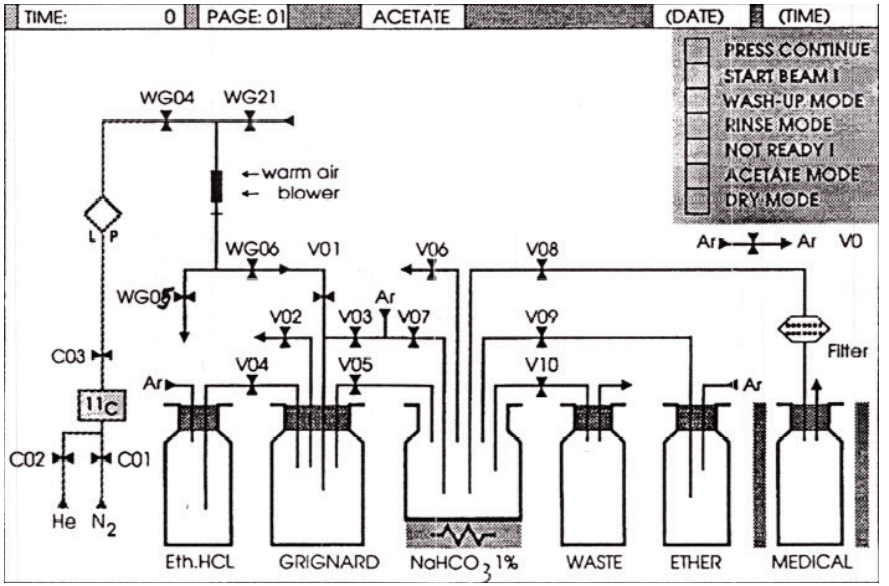

Figure 2. IBA acetate processing module based on a Grignard reaction, used at Castelfranco Veneto (TV) PET Center, Italy.

QUALITY CONTROL PROCEDURES

Generally speaking, if the radiopharmaceutical has a monograph in the European Pharmacopoeia and the described method is exactly followed, a method validation is not required. However, the laboratory is required to verify that the described method has been implemented and functions correctly. The laboratory must validate a method when it is not described in the Pharmacopoeia, following the guidelines outlined in the ICH Q2(R2) Guideline on validation of analytical procedures.

Quality control is based on European Pharmacopoeia Monograph SODIUM ACETATE ([1-11C]) INJECTION ed. 11.1 [18]

Pre-release tests

Visual Inspection/Appearance: Clear, colourless solution; no particles

Radiochemical Identity: Radiochemical identity is determined using the high-performance liquid chromatography (HPLC) method described in Pharma Eur. using a strong anion-exchange column (CarboPac PA10 column, 4 × 250 mm) with NaOH 0.1 M as mobile phase at a flow rate of 1 mL/min. Another HPLC method was described by Soloviev et al. [19] using a PLRPS 100A, 5 mm, 150 × 4.6 mm column with KH2PO40.4 M/acetonitrile 99.5/0.5 as mobile phase at a flow rate of 1 mL/min. HPLCs were equipped with radio and UV detectors (λ = 220 nm).

The retention time of [11C]acetate is compared to that of sodium acetate reference standard and must be ±10%.

Chromatogram examples are given in Figure 3.

Radiochemical Purity: Radiochemical purity was determined using the two HPLC methods described above. Radiochemical purity must be a minimum of 95%.

Chemical Purity: Chemical purity was assessed by means of the two HPLC methods described using a UV detector (λ = 220 nm). The area of acetate mass peak obtained by injecting the final solution of [11C]acetate must be lower than the corresponding area for a sodium acetate reference solution (20 mg per V).

Residual Solvents Analysis: Residual organic solvents were measured by gas chromatography on a capillary column. The limits for the residual solvents reported in the residual solvents monograph of the Pharma Eur. are 50 mg/V for acetone and ethanol (class 3) and 7.2 mg/V for tetrahydrofuran (class 2).

pH: The pH value of the injectable solution must be between 4.5 and 8.5.

Radionuclidic Identity: Radionuclidic identity can be determined using two techniques: gamma spectroscopy and half-life measurement. Regarding gamma spectroscopy, the principal gamma photons have an energy of 0.511 MeV (annihilation) and, depending on the measurement geometry, a sum peak of 1.022 MeV may be observed, as stated in the Sodium acetate ([1-11C]) injection monograph. The approximate half-life must be between 18.3 and 22.4 min, and its determination is mandatory for positron emitters which cannot be distinguished from one another using gamma spectroscopy.

Radionuclidic Purity: Radionuclidic purity is determined by gamma spectroscopy. Peaks in the gamma spectrum corresponding to photons with an energy different from 0.511 MeV or 1.022 MeV must not represent more than 1 per cent of the total radioactivity.

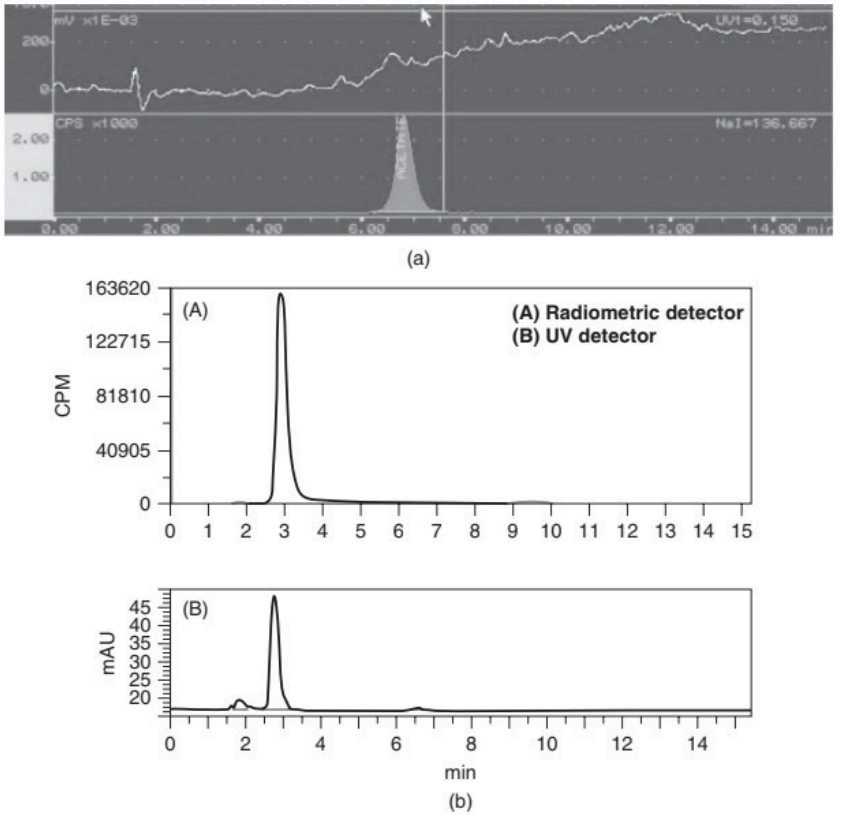

Figure 3. Analytical UV and radioactive HPLC traces for [11C]acetate: (a) method 1 (Eu. Ph. method), (b) method 2.

Post-release tests (parametric release)

Bacterial endotoxins: Radiopharmaceuticals for parenteral administration must comply with the test for bacterial endotoxins (Pharm Eur, chapter 2.6.14). Bacterial endotoxins must be less than 175/V IU/mL, V being the maximum recommended dose in millilitres. The injection may be released for use before completion of the test.

Sterility Testing: Radiopharmaceuticals must comply with the test for sterility prescribed in the monograph on Radiopharmaceutical preparations (Pharm Eur, monograph 0125). The injection may be released for use before completion of the test.

PHYSIOLOGICAL BIODISTRIBUTION

It is fascinating how [11C]acetate PET has diverse applications, from studying myocardial oxygen consumption to exploring various cancers such as prostate cancer, hepatocellular carcinoma (HCC), renal cell carcinoma (RCC), bladder carcinoma, and brain tumours. The discovery of incidental findings in rare conditions such as thymoma, cerebellopontine angle schwannoma, angiomyolipoma and encephalitis, and even attempts to study multiple myeloma with this tracer, underscore its versatility in medical imaging [21].

[11C]acetate plays a role in assessing myocardial perfusion and metabolism. In cardiac imaging, [11C]acetate is primarily utilised to evaluate myocardial oxygen consumption and cardiac efficiency. By visualising the distribution of [11C]acetate in the myocardium, clinicians can gain insights into the regional metabolic activity of the heart, aiding in the diagnosis and management of various cardiac conditions.

The first study in the field of oncology was performed by Shreve and co-workers (University of Michigan) for renal physiopathology [21]. In contrast to 2-[18F] FDG, [11C]acetate was able to discriminate between normal renal tissue, diseased non-neoplastic renal tissue, and renal cell carcinoma. Moreover, there is a significant disparity in the rate of tracer clearance from renal cell carcinoma tissue compared to normal and diseased non-neoplastic renal tissue. This discrepancy results in the ability to readily differentiate renal cell carcinoma from non-neoplastic renal tissue on images acquired beyond 10 minutes post-tracer administration [21]. Generally speaking, tumour retention of [11C]acetate is due to increased fatty acid metabolism. In fact, [11C]acetate is biologically incorporated into the membrane lipids in tumour cells through fatty acid synthase (FAS). The correlation between FAS activity and [11C] acetate accumulation in cancer cells was then confirmed by Vavere and co-workers [22].

In the realm of prostate cancer, [11C] acetate fails to reliably differentiate between benign prostatic hyperplasia and prostate cancer, exhibiting similar uptake in both conditions. Kato et al. [23] confirmed this by a systematic study involving 30 subjects without prostate cancer and 6 patients with prostate cancer, revealing that although primary prostate cancer was detectable in all patients, there were no statistically significant differences in [11C]acetate SUV between individuals aged 50 years and older with normal prostates or benign prostatic hyperplasia and those with prostate cancer [23].

On the flip side, other experiments indicated increased affinities for [11C] acetate in tumour cells compared to normal prostate tissue [25]. However, it is crucial to acknowledge that potential false-positive uptakes could be attributed to inflammatory effects within the cancer cells. In 2012, Schöder et al. reinforced these conclusions by noting a substantial number of false-positive lymph nodes in their study, attributed to chronic granulomatous disease (CGD) [26].

Finally, Jambor et al. conducted an assessment on 36 untreated, non-metastatic prostate cancer patients. Their lobe-based analysis revealed a high sensitivity of 88% but a low specificity of 41%. The observed low specificity could be attributed to benign prostatic hyperplasia, although uptake in inflammatory cells might also contribute to false-positive findings [27].

There is insufficient data regarding the use of [11C]acetate for detecting primary prostate cancer and staging lymph nodes. The four studies cited in the review by Spick C. et al published in 2016 show sparse values in terms of specificity and selectivity in detecting lymph node involvement with a Prostate Specific Antigen (PSA) level between 11.8 and 37 ng/mL [28].

Biochemical evidence indicating the recurrence of prostate cancer following radical prostatectomy or radiation treatment is typically identified by a serum PSA level equal to or greater than 0.2 ng/mL. This evidence often precedes the clinical manifestations. The early and accurate detection of the recurrence site is of utmost importance for effective patient management and therapy decision-making [28]. When assessing patients with PSA levels below 1 ng/mL, [11C]acetate identifies only around 50% of recurrence sites and fails in the case of reduced volume of tumour tissue. In contrast, endorectal MRI demonstrated superior performance in patients with low serum PSA levels [29].

The rates of detection rose as PSA levels and PSA velocity increased. In fact, a comprehensive retrospective analysis involving 120 patients revealed that positivity rates correlated with serum PSA levels and PSA velocity. Employing a PSA velocity threshold of 1.32 ng/mL/y yielded a sensitivity of 74% and specificity of 75%. Meanwhile, a serum PSA level of 1.24 ng/

mL was linked to a sensitivity of 87% and specificity of 66% [30].

Finally, utilising PET/MRI software fusion, the authors noted enhanced diagnostic information through image fusion, with MRI fusion revealing 9 malignant and 5 benign cases in 14 patients with equivocal PET findings. Notably, fusion with MR images proved more informative than fusion with CT images, indicating a crucial potential application for integrated clinical PET/MRI in patients with recurrent prostate cancer [31].

Spick et al. conducted a retrospective analysis comparing conventional bone scans with the findings from [11C]acetate PET in the detection of bone metastases among 90 patients experiencing elevated PSA levels following initial definitive therapy. The reference standard for assessment was established through clinical and imaging follow-up. Patient-based analysis revealed comparable results between conventional bone scans and [11C]acetate PET. This finding indicates that [11C]acetate PET imaging is a reliable method for comprehensive assessment of bone involvement throughout the entire body [32].

The focus on prostate-specific membrane antigen (PSMA) has grown due to its significant overexpression in prostate cancer (PCa) cells. PSMA's rapid internalisation and blood clearance make it an attractive target for PCa PET imaging. The extracellular domain of PSMA, with a binding site for urea, is suitable for radioligand labelling. Initial studies with [68Ga]Ga-PSMA-11 indicate its potential for detecting PCa recurrence with higher contrast than existing tracers.

A recent study compared performance of [11C]acetate versus [68Ga]Ga-PSMA-11 in detecting PCa recurrence after curative therapy in 30 patients. Overall, PSMA-PET performs better than acetate-PET in localising PCa biochemical relapse in lymph nodes and bone metastases. It is plausible that the observed phenomenon could be attributed to the existence of metabolically dormant metastases with elevated PSMA receptor expression. Paschalis et al. reported heightened heterogeneity in PSMA expression within individual prostate cancer patients, showing variability both among patients and within the same individual. Given the heterogeneity of PSMA expression, integrating PET with a tracer for anabolic metabolism could prove essential for making informed therapy decisions [33].

PATIENT PREPARATION & AFTERCARE

No particular patient preparation is required, except fasting for at least 4 hours and good hydration prior to the examination. Due to the very low half-life of this radionuclide, patients have to maintain a safety distance from babies and pregnant people for up to 4h after the examination.

IMAGING PROTOCOL

At present there is no standardised imaging protocol for [11C]acetate. There are a lot of studies that use protocols with [11C]acetate alone or with a double tracer without an overarching guideline.

Based on what has been said before, there are two types of acquisition protocols: dynamic or static.

Dynamic imaging

Dynamic acquisition is frequently used for evaluation of myocardial oxygen consumption [34], HCC and prostate cancer. There are a lot of studies where [11C]acetate is used with another tracer in double acquisition (for example with 2-[18F]FDG or [15O]water) [33].

The acquisition is performed directly on the disease sites.

After placing the patient on the PET/CT with arms above the head, the topogram is done. A low-dose CT scan of 120 kV is done prior to radiopharmaceutical administration. We also suggest using a Dose Care protocol.

PET acquisition is done directly after intravenous injection of about 4–5 MBq [11C] acetate per kg body weight and lasts about 30–40 minutes.

The modality acquisition mode is usually List Mode, which consists of a data format acquisition that uses data packets (RAW DATA and Sinogram) containing the information for the creation of subsequent images: static or dynamic.

The data are collected in frames with different timing.

Dynamic acquisition is usually reconstructed using an algorithm: OSEM, OSEM+TOF, True X or TrueX+TOF, depending on the different vendors.

Static Imaging

Static imaging is used for many types of tumours, in particular prostate cancer and HCC, renal cell carcinoma, bladder carcinoma and brain carcinoma [36,30,31].

The acquisition starts 10–20 minutes post intravenous injection of [11C]acetate.

After placing the patient on the PET/CT with the arm above the head, the topogram is done, usually from vertex to mid-thigh.

A low-dose CT scan of 120 kV is performed for the AC/CT, and we suggest using a Dose Care protocol to minimise the dose to the patient.

PET acquisition needs to achieve an adequate count rate: usually 1.5–3 mins/bed position or 0.7–1.2 mm/sec in Flow Motion.

Static acquisition is usually reconstructed using an algorithm: OSEM, OSEM+TOF, True X or TrueX+TOF, depending on the different PET/CT vendors.

Tables of PET/CT parameters

The following tables show some suggested parameters for image settings in static and dynamic imaging.

CT PARAMETERS

Eff mAs	Care dose 4D
kV	120 or Care kV
Slice	3.0 mm
Acq	16 × 1.2 mm
Pitch	1,2
Direction	Craniocaudal
Kernel	B30f medium smooth
FoV	780 mm with HDFoV
Increment	3.0 mm

Table 1. CT parameters

STATIC PET PARAMETERS

	CORRECTED	UNCORRECTED
Scan duration/bed	2–3 min or 0.7–1.2 mm/sec	
Recon meth	TrueX + TOF (UltraHD-PET)	TrueX + TOF (UltraHD-PET)
Iteration	3	2
Subset	21	21
Image size	200	200
Filter	Gaussian	Gaussian
Zoom	1.0	1.0
FWHM	5.0	2.0

Table 2. PET imaging parameters for static acquisitions

DYNAMIC PET PARAMETERS (LIST MODE ACQUISITION)

	CORRECTED	UNCORRECTED
Scan duration	30–40 mins	
Recon meth	TrueX + TOF (UltraHD-PET)	TrueX + TOF (UltraHD-PET)
Iteration	3	2
Subset	21	21
Image size	200	200
Filter	Gaussian	Gaussian
Zoom	1.0	1.0
FWHM	5.0	2.0

Table 3. PET imaging parameters for list mode acquisitions

RESULTS & INTERPRETATION (TYPICAL ABNORMAL FINDINGS/UPTAKE AND EXAMPLES)

[11C]acetate has a rapid accumulation of activity in the heart, liver, kidney, pancreas, stomach, spleen, bowel and bone marrow.

As Song and al. said in their work: *"The lack of information regarding normal physiologic uptake of [11C]acetate makes the interpretation of abnormal uptake difficult for inexperienced readers. However, a range of normal standard uptake values (SUV) has not been described. By defining normal SUV of [11C]Acetate in normal organs, abnormal focal or diffuse [11C]acetate activity can be more accurately assessed, thus improving the sensitivity and specificity of this emerging diagnostic radiopharmaceutical."* [35]

According to the review by Mohsen and Georgis [37]:

A small set of tumours like **glioblastomas** and **meningiomas** can convert the [11C]acetate into acid and amino acid metabolites, so it could be possible to see them. In particular, in meningiomas, [11C] acetate is used to evaluate the extent of disease and the post-therapy monitoring. Inflammatory cells, especially macrophages, in meningeal tuberculoma could increase the uptake of [11C]acetate.

Lung and parenchyma have faint tracer accumulation, but mediastinum has minimum uptake. Some lymph nodes not related to the primary tumour show enhanced [11C]acetate, but this could be considered reactive and/or inflammatory.

Bone marrow has a minimum uptake, in particular in the dorsal vertebrae; in the case of degenerative changes in the bone it shows an inhomogeneous moderate uptake.

In abdomen upper organs the highest uptake is found in **liver, pancreas and spleen.** Pancreas is clearly visualised after 2 minutes from intravenous administration and it remains well defined until 30 minutes. In particular the head, body and tail are well delineated after 10 minutes due to the high background ratio. The high tracer concentration within the pancreas is believed to be due to a high rate of lipid synthesis within the pancreatic acinar cell.

Bowel shows a minor uptake, but sometimes patients show high accumulation of tracer. In other cases, the accumulation is shown in **bladder and urethra.**

False-positive cases could be possible in proliferative **granulomatous cystitis,** and other false-positive cases may occur in **inflammation,** in particular in patients pre-treated with Bacillus Calmette-Guérin (BCG). This is in contrast to patients with non-BCG in transitional cell carcinoma, where [11C] acetate has a useful role in staging.

RADIATION EXPOSURE

The most important radiation exposure study in humans was performed by Selzer and Co. [38]. The critical organ is the pancreas, with an average injected activity of 0.017mGy/MBq (after intravenous administration of 525 MBq of [11C]acetate). The high tracer uptake in pancreas is believed to be due to the high rate of lipid synthesis in the pancreatic acinar cells. This is followed by bowel (0.011 mGy/MBq), kidneys (0.0092 mGy/MBq), spleen (0.0092 mGy/MBq), heart (0.0066 mGy/MBq), and liver (0.006 mGy/MBq). The effective dose is 0.0049 mSv/MBq.

[11C]acetate has minimal renal excretion, which may present a potential advantage for evaluating pelvic malignancies in PET/CT.

REFERENCES

1. Lauritsen CC, Crane HR, Harper WW. Artificial Production of Radioactive Substances. Science. 1934 Mar 9;79(2045):234–5.
2. Crane HR, Lauritsen CC. Radioactivity from Carbon and Boron Oxide Bombarded with Deutons and the Conversion of Positrons into Radiation. Physical Review. 1934 Mar 15;45(6):430–2.
3. Barkas WH. Some New Reactions in Light Nuclei with High Energy Protons. Physical Review. 1939 Aug 1;56(3):287–7.
4. Tobias CA, Lawrence JH, Roughton FJW, Root WS, Gregersen MI. THE ELIMINATION OF CARBON MONOXIDE FROM THE HUMAN BODY WITH REFERENCE TO THE POSSIBLE CONVERSION OF CO TO CO2. American Journal of Physiology-Legacy Content. 1945 Dec 1;145(2):253–63.
5. Gómez-Vallejo V, Vijay Gaja, Jacek Koziorowski, Jordi Llop. Specific Activity of 11C-Labelled Radiotracers: A Big Challenge for PET Chemists. InTech eBooks. 2012 Feb 8
6. Rodnick ME, Runkle AC, Littich R, et al. [11C] Acetate for Positron Emission Tomography Imaging. In: Sanders DA, ed. Acetate. Nova Science Publishers, Inc. 2013.
7. Bose S, Ramesh V, Locasale JW. Acetate Metabolism in Physiology, Cancer, and Beyond. Trends in Cell Biology. 2019 Sep;29(9):695–703.
8. Pees A, Chassé M, Lindberg A, Vasdev N. Recent Developments in Carbon-11 Chemistry and Applications for First-In-Human PET Studies. Molecules [Internet]. 2023 Jan 17;28(3):931.
9. Kamen MD. Chapter VIII - Short-Lived Radioactive Carbon (C11). In: Kamen MD, ed. Radioactive Tracers in Biology. 2nd ed. Academic Press; 1951. p. 224-243.
10. Bengt L, Antoni G, Gullberg P, Christer Halldin, Malmberg P, Kjell Någren, et al. Synthesis of L- and D-[methyl-11C]methionine. PubMed. 1987 Jun 1;28(6):1037–40
11. Larsen P, Ulin J, Dahlstrøm K, Jensen M. Synthesis of [11C]iodomethane by iodination of [11C]methane. Applied Radiation and Isotopes. 1997 Feb; 48(2):153–7.
12. Jewett DM. A simple synthesis of [11C]methyl triflate. International Journal of Radiation Applications and Instrumentation Part A Applied Radiation and Isotopes. 1992 Nov 1;43(11):1383–5.
13. Runkle AC, Shao X, Tluczek L, Henderson BD, Hockley BG, Peter. Automated production of [11C] acetate and [11C]palmitate using a modified GE Tracerlab FXC-Pro. Applied Radiation and Isotopes. 2011 Apr 1;69(4):691–8.
14. Shao X, Hoareau R, Runkle AC, Tluczek LJM, Hockley BG, Henderson BD, et al. Highlighting the versatility of the Tracerlab synthesis modules. Part 2: fully automated production of [11C]-labeled radiopharmaceuticals using a Tracerlab FXC-Pro. Journal of Labelled Compounds and Radiopharmaceuticals. 2011 Oct 20;54(14):819–38.
15. Scott PJH, Hockley BG, eds. Radiochemical Syntheses, Volume 1: Radiopharmaceuticals for Positron Emission Tomography- Part 2. 1st ed. John Wiley & Sons, Inc.; 2012.
16. Wenz J, Arndt F, Samnick S. A new concept for the production of 11C-labelled radiotracers. EJNMMI Radiopharmacy and Chemistry. 2022 Mar 28;7(1).
17. Wenz J, Arndt F, Samnick S. A robust [11C]acetate synthesis on a TRACERLab FX C pro module. Applied Radiation and Isotopes. 2022 Oct 1;188:110356–6.
18. European Pharmacopoeia. 11th Edition. Sodium acetate ([1-11C]) injection 04/2023:1920.
19. Soloviev D, Tamburella C. Captive solvent [11C] acetate synthesis in GMP conditions. Applied Radiation and Isotopes. 2006 Sep;64(9):995–1000.
20. Grassi I, Nanni C, Allegri V, Joshua James Morigi, Gian Carlo Montini, Castellucci P, et al. The clinical use of PET with (11)C-acetate. PubMed. 2012 Jan 1.
21. Shreve P, Chiao PC, Humes HD, Schwaiger M, Gross MD. Carbon-11-acetate PET imaging in renal disease. PubMed. 1995 Sep 1;36(9):1595–601.
22. Vāvere AL, Kridel SJ, Wheeler FB, Lewis JS. 1-11C-Acetate as a PET Radiopharmaceutical for Imaging Fatty Acid Synthase Expression in Prostate Cancer. The Journal of Nuclear Medicine. 2008 Jan 16;49(2):327–34.
23. Kato T, Tsukamoto E, Kuge Y, Takei T, Shiga T, Shinohara N, et al. Accumulation of [11C]acetate in normal prostate and benign prostatic hyperplasia: comparison with prostate cancer. European Journal of Nuclear Medicine and Molecular Imaging. 2002 Nov 1;29(11):1492–5.

24. Mena E, Baris Turkbey, Mani H, Adler SS, Valera V, Bernardo M, et al. 11C-Acetate PET/CT in Localized Prostate Cancer: A Study with MRI and Histopathologic Correlation. The Journal of Nuclear Medicine. 2012 Feb 17;53(4):538–45.
25. Heiko Schöder, Ong SC, Reuter VE, Cai S, Burnazi E, Guido Dalbagni, et al. Initial Results with 11C-Acetate Positron Emission Tomography/ Computed Tomography (PET/CT) in the Staging of Urinary Bladder Cancer. Molecular Imaging and Biology. 2011 Apr 14;14(2):245–51.
26. Jambor I, Borra R, Kemppainen J, Virva Lepomäki, Riitta Parkkola, Dean KI, et al. Improved detection of localized prostate cancer using co-registered MRI and 11C-acetate PET/CT. European Journal of Radiology. 2012 Nov 1;81(11):2966–72.
27. Spick C, Herrmann K, Czernin J. Evaluation of Prostate Cancer with 11C-Acetate PET/CT. Journal of Nuclear Medicine. 2016 Oct;57(Supplement 3):30S37S.
28. Hansjörg Vees, Franz Buchegger, Albrecht S, Khan H, Husarik D, Zaidi H, et al. 18F-choline and/or 11C-acetate positron emission tomography: detection of residual or progressive subclinical disease at very low prostate-specific antigen values (<1 ng/mL) after radical prostatectomy. BJU International. 2007 Apr 8;99(6):1415–20.
29. Dusing RW, Peng W, Sue Min Lai, Grado GL, Holzbeierlein JM, J. Brantley Thrasher, et al. Prostate-Specific Antigen and Prostate-Specific Antigen Velocity as Threshold Indicators in 11C-Acetate PET/CTAC Scanning for Prostate Cancer Recurrence. Clinical Nuclear Medicine. 2014 Sep 1;39(9):777–83.
30. Wachter S, Tomek S, Kurtaran A, Wachter-Gerstner N, Djavan B, Becherer A, et al. 11C-Acetate Positron Emission Tomography Imaging and Image Fusion With Computed Tomography and Magnetic Resonance Imaging in Patients With Recurrent Prostate Cancer. Journal of Clinical Oncology. 2006 Jun 1;24(16):2513–9.
31. Spick C, Polanec SH, Mitterhauser M, Wolfgang Wadsak, Anner P, Reiterits B, et al. Detection of Bone Metastases Using 11C-Acetate PET in Patients with Prostate Cancer with Biochemical Recurrence. PubMed. 2015 Dec 1;35(12):6787–91.
32. Regula N, Kostaras V, Johansson S, Trampal C, Lindström E, Lubberink M, et al. Comparison of 68Ga-PSMA-11 PET/CT with 11C-acetate PET/CT in re-staging of prostate cancer relapse. Scientific Reports. 2020 Mar 19;10(1).
33. Robert R. Sciacca, Olakunle Akinboboye, Ru Ling Chou, Shilpi Epstein and Steven R. Bergmann Measurement of Myocardial Blood Flow with PET Using 1-11C-Acetate Journal of Nuclear Medicine January 2001, 42 (1) 63-70.
34. Nesterov SV, Turta O, Han C, Mäki M, Lisinen I, Tuunanen H, Knuuti J. C-11 acetate has excellent reproducibility for quantification of myocardial oxidative metabolism. Eur Heart J Cardiovasc Imaging. 2015 May;16(5):500-6. https://doi.org/10.1093/ehjci/jeu289. Epub 2014 Dec 22. PMID: 25535214.
35. Song WS, Nielson BR, Banks KP, Bradley YC. Normal organ standard uptake values in carbon-11 acetate PET imaging. Nucl Med Commun. 2009 Jun;30(6):462-5. https://doi.org/10.1097/MNM.0b013e32832aa7ce. PMID: 19357549.
36. Ho C.L. Yu S.C.,Yeung D.W. 11C-acetate PET imaging in hepatocellular carcinoma and other liver masses. J Nucl Med. 2003; 44: 213-221.
37. Karanikas G, Beheshti M. ^{11}C-acetate PET/CT imaging: physiologic uptake, variants, and pitfalls. PET Clin. 2014 Jul;9(3):339-44. https://doi.org/10.1016/j.cpet.2014.03.006. Epub 2014 May 3. PMID: 25030397.
38. Seltzer MA, Jahan SA, Sparks R, et al. Radiation dose estimates in humans for [^{11}C]Acetate whole-body PET. J Nucl Med. 2004;45:1233–1236.

Pharmacopoeias and general monographs:

1. https://www.edqm.eu/en/european-pharmacopoeia-ph.-eur.-11th-edition
2. Eudralex Volume 4 - EU Guidelines for Good Manufacturing Practice for Medicinal Products for Human and Veterinary Use- Feb.2022.
3. Gillings N, Hjelstuen O, Ballinger J, Behe M, Decristoforo C, Elsinga P, Ferrari V, Peitl PK, Koziorowski J, Laverman P, Mindt TL, Neels O, Ocak M, Patt M, Todde S. Guideline on current good radiopharmacy practice (cGRPP) for the small-scale preparation of radiopharmaceuticals. EJNMMI Radiopharm Chem. 2021 Feb 12.
4. EU GMP Annex 15: Qualification and Validation.
5. ICH Q2(R2) Validation of analytical procedures - Scientific guideline. Mar 2024. https://www.ema.europa.eu/en/ich-q2r2-validation-analytical-procedures-scientific-guideline.
6. Pharm Eur, chapter 2.6.14- Bacterial Endotoxin.
7. Ph. Eur. monograph (0125) radionuclide precursor.

4

[^{18}F] FLURPIRIDAZ

by Giancarlo Gorgoni
Emiliano Cazzola

Department of Radiopharmacy, IRCCS Sacro Cuore, Negrar (VR), Italy

[18F]FLURPIRIDAZ

Nuclear cardiology has played an important role in the diagnosis of heart diseases since the 1970s, with thallium [201T] and technetium [99mTc]-labelled SPECT perfusion agents. In recent decades, however, there has been a reduction in PET applications due to certain drawbacks associated with PET radiopharmaceuticals, such as their very short half-life and throughput. In light of these limitations, fluorine [18F]-based radiopharmaceuticals might be able to fill the gap and increase cardiological applications in the PET field. [18F]flurpiridaz has all the characteristics required to be easy to prepare at high activity, with an attractive half-life allowing for examinations under stress and at rest on the same day. Furthermore, the high affinity for mitochondrial complex 1 of [18F]flurpiridaz suggests that the radiopharmaceutical may have promising applications in nuclear cardiology.

CHEMISTRY & PROPERTIES

[18F]flurpiridaz was identified by the Casabier group from a list of fluorinate pyridaben derivatives with high affinity for mitochondrial complex 1 (MC1). [1]

The molecule selected (Figure 1), with the high uptake, present three structural moieties, all of them are important for MC1 uptake. The three identified structural mojeties to obtain the high cardiac uptake are:

1. Hydrophobic heterocyclic pyridazinone (violet).

2. P-tert-butylphenyl moiety side chain (green).

3. Heteroatom-containing linker between 1 and 2 (orange).

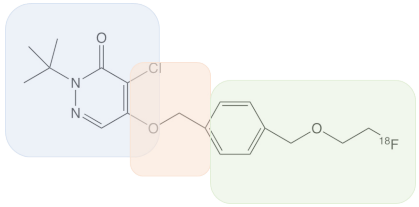

Figure 1. [18F]flurpiridaz chemical formula and biological groups.

To obtain the radiopharmaceutical, a one-pot nucleophilic substitution from a tosylate derivative was studied (Figure 2). No sensitive groups are present in the structure, so it was possible to prepare a deprotected precursor to use directly in production. The synthesised precursor is shown below and was isolated with a final yield of around 40% with 99.9% purity after semi-preparative HPLC. The precursor is not generally commercially available, but can be synthesised using various procedures. [2,3]

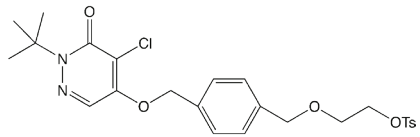

Figure.2. [18F]flurpiridaz precursor.

The radiochemical synthesis takes place in the synthesis module following the scheme shown below:

The step shown in Figure 3 can be summarised as follows [2]:

» Fluorine-18 trapping on QMA cartridge, followed by elution with TBA-HCO_3 solution and acetonitrile. The final solution was transferred to the reactor and dried.

» 10 mg of precursor in acetonitrile was added to the reactor and allowed to react for 10 minutes at 95°C.

» The crude reaction mixture was finally diluted and transferred to be purified in two different ways:

» HPLC purification: the reactor mixture was injected into a semi-preparative HPLC.

» SPE purification: the reactor mixture was passed through a TC18 cartridge (preconditioned with ethanol and rinsed by water). The cartridge was rinsed with ethanolic solution (40%) and ascorbic acid. Finally the product was eluted with ethanol 50% WFI.

» The final product was passed through a Sep-pack Allumina N plus to remove free fluorine-18, followed by a sterile 0.22 micron filter to remove the precipitate precursor, if present, and sterilise the product.

The product is isolated with a non-decay-corrected yield range of 25–35% after 110 min of solid phase purification and a non-decay-corrected yield range of 20–25% after 120 min of HPLC purification.

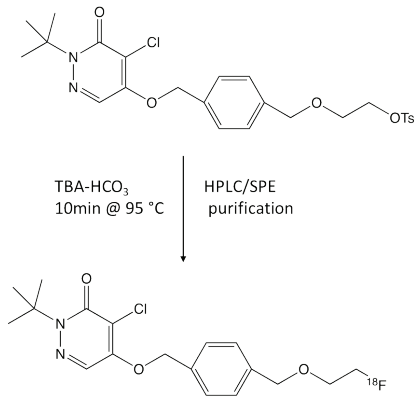

Figure. 3. Diagram of reaction scheme for the production of [18F]flurpiridaz.

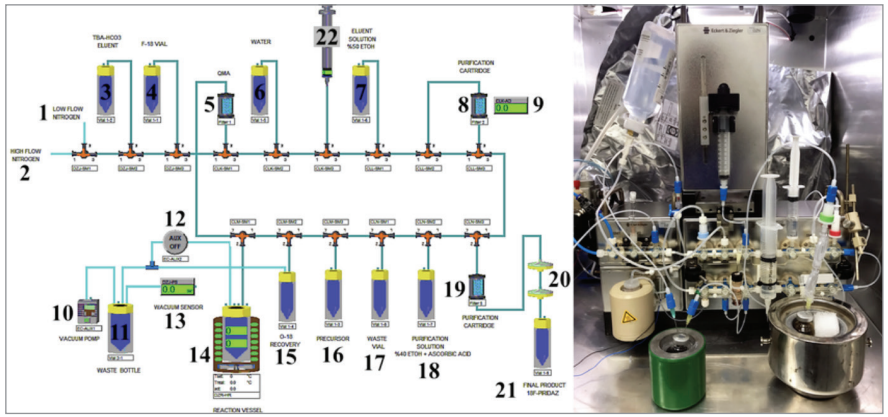

Figure 4. Schematic diagram and photo of module configuration for [18F]flurpiridaz production.[2]

Test	Method	Acceptance criteria	Results
Appearance	Visual	Clear, colourless	Clear, colourless
pH	pH-strip	4.5-8.5	6-7
Half-Life	Dose Calibrator	105-110 min	109 min
Radiochemical Purity	Radio-HPLC	> 95 %	> 98.5 %
Radionuclidic Purity	Gamma Spec	> 99.9 %	> 99.9 %
Chemical Purity	HPLC (precursor)	N.D.	N.D.
TBA	Spot Test	≤ 2.6 mg/V	≤ 2.6 mg/V
Residual Solvents	GC	EtOH ≤ 10 % (V/V) CH3CN ≤ 4.1 mg/V	EtOH ≤ 8.2 % (V/V) CH3CN ≤ 0.04 mg/V
BET	LAL	< 175 IU/V	< 175 IU/V
Sterility	Sterility test	Sterile	Sterile

Table 1. QC summary based on EU general monograph requirements.

QUALITY CONTROL PROCEDURES

Quality control (QC) procedures for the formulated radiopharmaceutical covering all the required parameters set out in the "Radiopharmaceuticals preparation" monograph in the current edition of the European Pharmacopoeia are summarised in Table 1:

The final product is collected in variable volumes depending on the desired formulation, but ascorbic acid is always present to prevent defluorination.

PHYSIOLOGICAL BIODISTRIBUTION

[18F]flurpiridaz was first tested on animals, with a heart uptake at 30 min of 3.4% ID/g. This data was confirmed in humans, showing a heart wall uptake ranging between 2.8% and 7.0% ID after 30 min in exercise stress and adenosine stress tests, respectively.

The radiopharmaceutical can be bolus injected and the physiological distribution shows uptake in brain, heart, kidneys and liver in a range of 2 to 3.7% of injected activity (%ID) at 17 min.

Due to the specificity of the application to myocardial perfusion imaging, stress test image collection was required, with exercise stress compared to pharmacological stress obtained with adenosine. Biodistribution in the two different tests was evaluated at different time points starting at 17 min up to 238 min by acquisition of total body images. The results were also used to calculate the radiation exposure of the patients and the maximum injected activity.

According to the test results, the major uptake was recorded in the organs listed in Table 2.

Organ	17 min	30 min	122 min	203 min	238 min
Brain	2.9[a]-6.0[b]	2.7-6.0	1.8-4.8	1.4-3.8	1.3-3.5
Heart wall	2.7-7.1	2.8-7.1	2.4-5.9	2.0-5.0	1.7-4.5
Kidneys	2.0-6.4	1.7-5.1	1.1-2.3	1.0-7.2	0.94-6.7
Liver	3.7-21	3.7-20	3.1-10	2.7-7.2	2.6-6.7

Table 2. a %ID vs. time in exercise stress subjects; b %ID vs. time in adenosine stress subjects1.

The differences in absolute values between the two tests can be explained by the different partitioning of the injected tracer generated by the two states.

The results for human biodistribution show an interesting organ uptake that makes this radiopharmaceutical ideal for myocardial perfusion imaging.

PATIENT PREPARATION & AFTERCARE

Stress-rest myocardial tomoscintigraphy is an examination that allows the evaluation of:

- perfusion at rest and under stress
- ventricular function (ejection fraction, volumes, phase analysis)
- the integrity/vitality of the myocardium.

The purpose of this examination, in the diagnostic phase, is to exclude and/or confirm the presence of ischaemic heart disease.

On the other hand, in patients with already established ischaemic heart disease (post-infarction, post-revascularisation) it defines the site, extent of infarction, viable myocardium and residual ischaemia of a coronary territory.

It should be emphasised that the examination does not study coronary artery anatomy, but coronary flow reduction (ischaemia) in the presence of suspected or known coronary stenosis. It should be remembered that there is often no correlation between anatomy and function: in other words, critical stenosis may not cause ischaemia or vice versa. This finding is critical for the cardiologist, to identify which coronary stenoses need to be treated, and—especially in cases of diffuse coronary artery disease—to recognise the most compromised artery.

The survey as a whole allows identification of patients at high or medium risk of cardiac events (angina, infarction), who are candidates for invasive procedures—e.g. coronarography, revascularisation—and patients who are low-risk (follow-up).

Patient preparation is similar to traditional methods. Investigation under "stress" conditions begins by preparing the patient for ECG recording, monitoring of blood pressure and insertion of a needle into an arm vein. Stress testing can be performed by stimulating coronary flow through physical exertion on a cyclo-ergometer or pharmacologically by administering an infusion of dipyridamole or adenosine.

At the peak of exertion (i.e., after reaching the target heart rate of ≥85% of the patient's theoretical max HR, 220 minus age), the radiopharmaceutical is injected.

During the at-rest test, the heart is not stimulated (through exercise or medication).

Supervision by a cardiologist is necessary during the stress test phase.

A review of contraindications to stress test should be performed (unstable angina not yet stabilised with medication, severe pulmonary hypertension, uncontrolled arrhythmia, inadequately controlled congestive heart failure, pulmonary embolism (a clot in the arteries of a lung), aortic dissection (a tear in the aorta), an acute illness of any sort, together with pregnancy status and body habitus.

Mostly required for the stress portion of the test:

- Nil by mouth for 4 hours prior to stress test in case of emergency;
- No caffeine for 12 hours prior to pharmacological vasodilator stress.

The patient should be advised to avoid direct contact with pregnant women and children during the 24 hours following the investigation.

IMAGING PROTOCOL

Due to the regulatory framework on radiopharmaceuticals, the investigational medicinal product (IMP) has not yet been authorised in Europe, so there are no standardised protocols at present. The following study was suggested in connection with the drug registration procedure [3]:

Same-day rest-stress examination using adenosine for stress protocol: activity ratio of 2.2 and injection delay of 30 minutes between the two injections. For same-day rest-stress with exercise protocol, exercise-to-rest activity ratio of three and one hour waiting time between the two injections was suggested.

Total rest-stress activity of 520 MBq (14 mCi) gave a good image quality and low patient radiation exposure. High signal-to-noise ratio is achievable with 74 MBq (2 mCi)[1].

[18F]flurpiridaz PET images showed reversible anterolateral wall defects in the distribution of the diseased left circumflex coronary artery. [7]

[1] https://classic.clinicaltrials.gov/ct2/show/study/NCT03354273

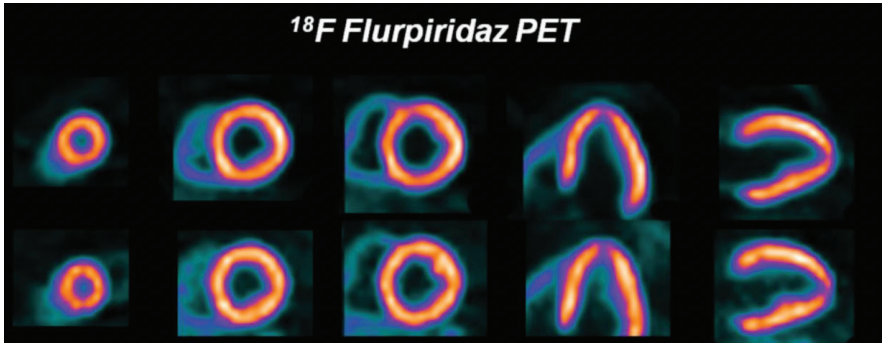

Figure 5. [18F]flurpiridaz PET images in a patient with significant disease in the left circumplex coronary artery.[7]

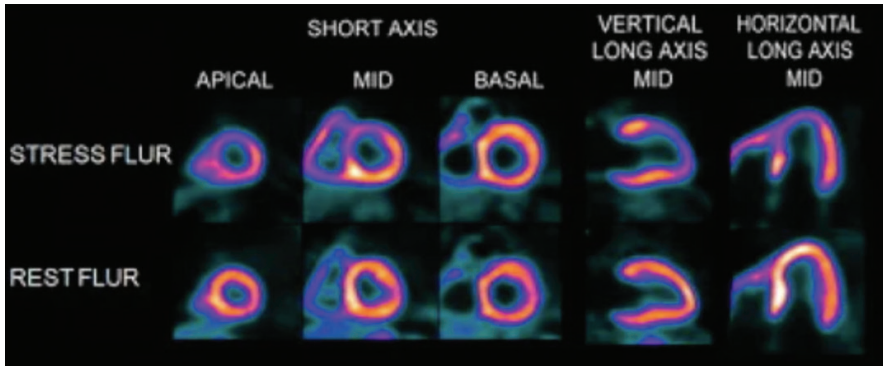

Figure 6. [18F]flurpiridaz PET images from an 82-year-old man.[8]

The [18F]flurpiridaz (top) PET images are from an 82-year-old man with shortness of breath, an occluded native proximal left anterior descending (LAD) coronary artery, an occluded left internal mammary graft to the LAD, and no other significant native CAD. The [18F]flurpiridaz images show a severe reversible perfusion defect throughout the territory of the occluded proximal LAD. [8]

RESULTS & INTERPRETATION

Imaging interpretation of [18F]flurpiridaz is only linked to clinical trials and reported in the listed publications. [4,5,6]

Radiation exposure

Based on the human biodistribution results, a dosimetry study was performed for each stress test procedure that can be applied for imaging acquisition.[3]

Exercise and adenosine stress tests gave different absolute values, but the relative distribution is comparable and was used to develop a complete dosimetry evaluation starting with the maximum injectable activity based on < 0.01 Sv effective dose to critical organ. This value is considered as a dose limit for the perfusion imaging study using technetium-99m agents.

Refer to 0.01 Sv, 685 MBq for exercise and 539 MBq was calculated as the maximum injectable activity of [18F]flurpiridaz examination.

Making the radiation dose evaluation due to rest-stress myocardial imaging protocols, comparing [18F]flurpiridaz with thallium-201, [99mTc]Tc-SESTAMIBI, Rubidium-82 and [13N] ammonia, only the ammonia combined effective dose is lower than [18F]flurpiridaz.

REFERENCES

1. A. Purohit, H. Radeke, M. Azure, K. Hanson, R. Benetti, F. Su, P.Yalamanchili, M. Yu, M. Hayes, M. Guaraldi, M. Kagan, S. Robinson, D. Casebier. Synthesis and Biological Evaluation of Pyridazinone Analogues as Potential Cardiac position Emission Tomography Tracers. J. Med. Chem 2008; 51, 2954–2970.
2. K. Eryilmaz and B Kilbas. A practical fully automated radiosynthesis of [18F]fluoropiridaz on the module modular lab-pharmtracer without external purification. EJNMMI Radiopharmacy and Chemistry. 2022; 7, 30.
3. J. Maddahi, F. Bengel, J. Czernin, P. Crane, M. Dahlbom, H. Schelbert, R. Sparks, M. Phelps, J. Lazewatsky. Dosimetry, biodistribution, and safety of flurpiridaz F 18 in healthy subjects undergoing rest and exercise or pharmacological stress PET myocardial perfusion imaging. J. Nuclear Cardiology. 2019; 26(6), 2018-2030.
4. Maddahi J, Agostini D, Bateman TM, Bax JJ, Beanlands RSB, Berman DS, Dorbala S, Garcia EV, Feldman J, Heller GV, Knuuti JM, Martinez-Clark P, Pelletier-Galarneau M, Shepple B, Tamaki N, Tranquart F, Udelson JE. Flurpiridaz F-18 PET Myocardial Perfusion Imaging in Patients With Suspected Coronary Artery Disease. J Am Coll Cardiol. 2023 Oct 17;82(16):1598-1610.
5. Matsumoto N. Progress of 18F-flurpiridaz in Clinical Trials. Ann Nucl Cardiol. 2023;9(1):91-93. doi: 10.17996/anc.23-00011. Epub 2023 Oct 31. PMID: 38058576; PMCID: PMC10696143.
6. Packard RRS, Votaw JR, Cooke CD, Van Train KF, Garcia EV, Maddahi J. 18F-flurpiridaz positron emission tomography segmental and territory myocardial blood flow metrics: incremental value beyond perfusion for coronary artery disease categorization. Eur Heart J Cardiovasc Imaging. 2022 Nov 17;23(12):1636-1644. doi: 10.1093/ehjci/jeab267. PMID: 34928321; PMCID: PMC9671402.
7. J. Maddahi, R. R. S. Packard,"Cardiac PET Perfusion Tracers: Current Status and Future Directions"Semin Nucl Med. 2014 September ; 44(5): 333–343.
8. T. Mou, X. Zhang," Research Progress on 18F-Labeled Agents for Imaging of Myocardial Perfusion with Positron Emission Tomography"Molecules 2017, 22(4), 562

[^{11}C]PE2I & [^{18}F]FE-PE2I

by Tea Crnic Bojkovic[1]
Jonathan Sigfridsson[1]
Vladimir Stepanov[2]
Jonas P. Eriksson[3]
My Jonasson[4]
Minyoung Oh[5]
Andrea Varrone[2]

[1]Molecular Imaging and Medical Physics, Department of Surgical Sciences, Uppsala University, Uppsala, Sweden / Medical Imaging Centre, Uppsala University Hospital, Uppsala, Sweden

[2] Department of Clinical Neuroscience, Centre for Psychiatry Research, Karolinska Institutet and Stockholm Health Care Services, Stockholm, Sweden

[3] Department of Medicinal Chemistry, Uppsala University, 751 23 Uppsala, Sweden / PET Centre, Uppsala University Hospital, 751 85 Uppsala, Sweden

[4]Molecular Imaging and Medical Physics, Department of Surgical Sciences, Uppsala University, Uppsala, Sweden / Medical Physics, Uppsala University Hospital, Uppsala, Sweden

[5] Department of Clinical Neuroscience, Centre for Psychiatry Research, Karolinska Institutet and Stockholm Health Care Services, Stockholm, Sweden / Departments of Nuclear Medicine, Asan Medical Center, University of Ulsan College of Medicine, Seoul, Republic of Korea

[11C]PE2I & [18F]FE-PE2I

Dopamine is the neurotransmitter that regulates motor functions, mood, and reward. Dopamine is released from axon terminals in the striatum or dendrites in the substantia nigra (SN). The action of dopamine on pre- and post-synaptic D1 and D2 dopamine receptors is terminated by the re-uptake of the neurotransmitter into presynaptic neuronal terminals through the dopamine transporter (DAT) (1). DAT density is higher in nigrostriatal axons and terminals but lower in the cell bodies and dendrites of the SN (2, 3).

[123I]FP-CIT (IOFLUPANE, DATSCAN) SPECT

is the most widely used modality for DAT imaging, authorised in Europe since 2000 and in the United States since 2011 (4, 5). DaTSCAN SPECT [123I] FP-CIT SPECT or DaTSCAN is indicated for the differential diagnosis of essential tremor from Parkinsonian syndromes related to idiopathic Parkinson's disease (PD), multiple system atrophy and progressive supranuclear palsy in patients with clinically uncertain Parkinsonian syndromes. It is also indicated to differentiate probable dementia with Lewy bodies from Alzheimer's dementia. Recently, PET imaging using [11C]PE2I and [18F]FE-PE2I has become a promising alternative offering high affinity and selectivity for DAT, favourable kinetics and improved spatial and temporal resolution (6, 7). This guide will provide an overview of the radiochemistry and in vivo properties of [11C]PE2I and [18F]FE-PE2I and how PET imaging with these radioligands is used in clinical practice.

CHEMISTRY & PROPERTIES

PE2I and FE-PE2I can both be viewed as structural derivatives of an earlier ligand, β-CIT, which has been extensively used for imaging DAT and SERT (serotonin transporters) (8). All three ligands share the same tropane backbone, commonly found in alkaloids contained in plants of the Erythroxylaceae and Solanaceae families. Many steps in the synthetic route for both PE2I and FE-PE2I are identical, as the compounds differ only in the alkyl chain on the tropane nitrogen. Much of the synthetic procedure is described in the original paper on PE2I synthesis by Emond and co-workers (9, 10), and it remains in use without significant changes. Given the complexities involved in building the tropane structure with the required stereochemistry from scratch, natural cocaine is used as a starting material for PE2I, FE-PE2I and their precursors due to its relative availability and low cost (Scheme 1).

PE2I(methyl-8-[(2E)-3-iodoprop-2-en-1-yl] -3-(4-methylphenyl)-8-azabicyclo[3.2.1] octane-2-carboxylate), along with the precursor for the synthesis of [11C]PE2I, desmethyl-PE2I (8-[(2E)-3-Iodoprop-2-en-1-yl]-3-(4-methylphenyl)-8-azabicyclo[3.2.1]

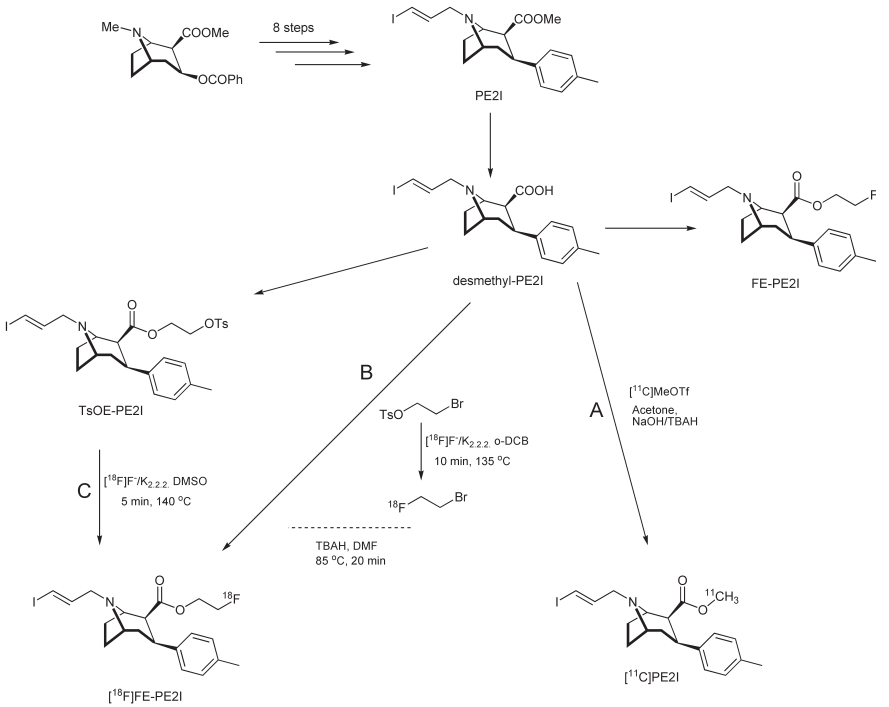

Scheme 1. Chemical structures of PE2I, FE-PE2I and synthesis of precursors. [11C]PE2I labelling (Pathway A). [18F]FE-PE2I 2-step labelling (Pathway B). [18F]FE-PE2I 1-step labelling (Pathway C).

octane-2-carboxylate), are solids with respective melting points of 75±5 °C and 167±5 °C. FE-PE2I (2-Fluoroethyl 8-[(2E)-3-iodoprop-2-en-1-yl]-3-(4-methylphenyl)-8-azabicyclo-[3.2.1]octane-2-carboxylate) and the precursor for [18F]FE-PE2I (tosylethyl-PE2I (2-(4-Methylphenylsulfonyl) ethyl 8-[(2E)-3-iodoprop-2-en-1-yl]-3-(4-methylphenyl)-8-azabicyclo-[3.2.1]octane-2-carboxylate)), are heavy-oil-like substances at room temperature that solidify at lower temperatures into a glassy material, a property that may complicate handling of small quantities. All four compounds are easily soluble in the majority of organic solvents; however, the tosylethyl-PE2I is unstable in aqueous solutions.

Radiosynthesis of [11C]PE2I

As with all carbon-11-labelled PET tracers, the radionuclide is produced by a cyclotron on-site. Carbon-11 is received as [11C]CO_2

or [^{11}C]CH_4 and the respective compound is then converted using the so-called wet method or the gas-phase method to [^{11}C] methyl iodide ([^{11}C]MeI), which in turn can be transformed into [^{11}C]methyl triflate ([^{11}C] MeOTf) for increased reactivity.

[^{11}C]PE2I can readily be synthesised from the O-desmethylated precursor, desmethyl-PE2I, using either [^{11}C]MeI or [^{11}C]MeOTf. The use of [^{11}C]MeOTf may be preferred due to the faster alkylation reaction and milder reaction conditions. The synthesis procedures were reported more than 20 years ago and are still widely used with minor modifications (11, 12) (Scheme 1, pathway A).

[^{11}C]PE2I is primarily synthesised using GBq quantities of [^{11}C]MeOTf transferred into a solution containing desmethyl-PE2I (0.4–0.6 mg) treated with a base (e.g., NaOH or TBAH) in acetone (300–600 µL). The reaction occurs nearly instantaneously at room temperature. In contrast, the use of [^{11}C]MeI typically requires heating to 80–90ºC and a reaction time of 5 minutes. The reaction mixture is then typically diluted, and obtained [^{11}C]PE2I is purified using HPLC (High Performance Liquid Chromatography), followed by reformulation and sterile filtration (11, 12) Since the early 2000s, when [^{11}C]PE2I was initially developed and reformulated by evaporation, reformulation methodologies have significantly advanced. More efficient solid phase extraction methods now dominate, offering high reliability and facilitating removal of residual polar impurities. These methods have largely replaced evaporation techniques. Similar approaches, or use of pharmaceutical HPLC-eluents that circumvents the reformulation step, have been applied to both [^{11}C]PE2I and [^{18}F]FE-PE2I (10, 13).

Radiosynthesis of [^{18}F]FE-PE2I

[^{18}F]FE-PE2I has been developed as a follow-up to [^{11}C]PE2I, partly because fluorine-18 offers several advantages for imaging and off-site preparation and distribution, and partly to overcome some unfavourable aspects of [^{11}C]PE2I kinetics (14, 15). The initial method, described by Schou and co-workers, is rather complex. It involves a reaction between desmethyl-PE2I and 2-bromo-1-[^{18}F]fluoroethane in dimethylformamide in the presence of sodium hydroxide (Scheme 1, pathway B) (14). The complexity of the original [^{18}F]FE-PE2I synthesis is largely attributed to the need for a simplified gas chromatography (GC) procedure for the purification of 2-bromo-1-[^{18}F]fluoroethane intermediate, making preparation of [^{18}F]FE-PE2I quite lengthy. However, development of a much simpler one-step labelling procedure (Scheme 1, pathway C) became possible with the introduction of a [^{18}F]FE-PE2I precursor suitable for direct labelling: tosylethyl-PE2I. This method was first published in 2012 by Stepanov et al. and was further refined by Bratteby and co-workers (13, 16).

Using the tosylethyl-PE2I precursor, [^{18}F]FE-PE2I can be obtained in a simple one-step, one-pot synthetic procedure performed in widely available solvents such as dimethylformaldehyde (DMF) and dimethyl sulfoxide (DMSO). This process involves trapping of the cyclotron-produced [^{18}F]fluoride on an anion-exchange cartridge, containing, for example, quaternary methylammonium resin (QMA), where it is concentrated and isolated from target water. The [^{18}F]fluoride is then typically eluted using a solution of Kryprofix$_{2.2.2}$/ potassium carbonate in a water and acetonitrile mixture, followed by removal of the solvent in a drying step. Following the addition of the tosylethyl-PE2I precursor solution, the fluorination reaction proceeds within 5 min at elevated temperatures (e.g. 140 ºC). The purification of [^{18}F]FE-PE2I is performed using HPLC, where a variety of approaches can be employed depending on the specifications of the synthetic module in use. It should be noted that [^{18}F]FE-PE2I is prone to radiolysis when trapped on SPE cartridges in large activity amounts (>1.5 GBq) or in aqueous solutions at high activity concentrations (>500 MBq/ml). Therefore, appropriate mitigation measures should be implemented, such as decreasing the activity concentration, increase of ethanol content, or addition of pharmaceutical-grade additives inhibiting radiolysis, such as sodium ascorbate and ascorbic acid.

QUALITY CONTROL PROCEDURES

Neither [^{11}C]PE2I nor [^{18}F]FE-PE2I are subjects of monographs in US or EU Pharmacopoeias. Therefore, in the absence of specifically described tests therein, general considerations for quality control apply (17). This includes a standard battery of quality control tests, such as tests for radiochemical purity, chemical purity, pH, filter integrity test, and residual solvents. Additionally, there are tests specifically for the [^{18}F]fluorine-labelled compounds, such as assessment of free [^{18}F]fluoride and Kryptofix content. Due to the short physical half-life of carbon-11 and fluorine-18, it is advised that lengthy quality control procedures should be conducted as post-release tests or on validation batches only (Table 1).

This is particularly relevant for radionuclide identification/radionuclidic purity tests and determination of endotoxins, and obviously a must for sterility tests on the formulated product. Other important control steps can only be carried out during the implementation of the production method. These can, for example, involve confirmation of the chemical structure using mass spectroscopy, ensuring high reproducibility of the synthesis, and ensuring that it yields sufficient activity amounts.

Comprehensive information on general procedures can, for example, be found in the general monograph on

Radiopharmaceutical Preparations (Ph. Eur 0125), in specific monographs written for other PET radiopharmaceuticals such as [18F]FDG and [11C]raclopride [Ph. Eur. 11.4, 1325 (01/2024); Ph. Eur. 11.4, 1924 (04/2023)] (18, 19), as well as in the scientific literature (13).

Quality control of [11C]PE2I

Due to the short half-life of carbon-11, pre-release testing is limited to the tests that are practically feasible to perform and mandatory for safe administration. Table 2 summarises the tests and analytical methods that can be used for quality control of [11C]PE2I.

Test	Pre-release	Post-release	Validation batches only
Radiochemical purity	X		
Product identification	X		
Radiochemical stability			X
Molar activity	X		
Filter integrity test	X		
Chemical purity	X		
pH	X		
Bacterial endotoxin test	X	X	
Residual solvents		X	
Sterility		X	
Radionuclidic purity			X
Confirmation of the carrier structure			X
Appearance			X
Residual Kryptofix	X		
Free [18F]fluoride	X		

Table 1. Pre-/post-release tests.

Test	Analytical method
Radiochemical purity	HPLC (with radiodetector)
Product identification	HPLC (with radiodetector)
Radiochemical stability	HPLC (with radiodetector)
Molar activity	With HPLC UV detector, scale and dose calibrator
Filter integrity test	as defined by Ph. Eur.
Chemical purity	HPLC (with UV detector)
pH	as defined by Ph. Eur.
Bacterial endotoxin test	as defined by Ph. Eur.
Residual solvents	GC
Sterility	as defined by Ph. Eur.
Radionuclidic purity	as defined by Ph. Eur.
Radionuclidic identity	as defined by Ph. Eur.
Appearance	as defined by Ph. Eur.

Table 2. Summary of tests and analytical methods for [11C]PE2I quality control.

Radiochemical purity of [11C]PE2I can be determined using Waters µ-Bondapak C18 10 µm, 3.9×300 mm column with acetonitrile/0.01 M H_3PO_4 35:65 as mobile phase at a flow rate of 3 ml/min with UV detector set to 254 nm. Chemical purity can be determined using ChromTech CP5-C18-25F 5 µm 4.6×250 mm column with acetonitrile/0.05M H_3PO_4 30:70 as mobile phase at flow rate 2 mL/min with UV detector set at 254 nm.

According to the European Pharmacopoeia monographs for other radiopharmaceuticals such as [18F]FDG and [11C]raclopride, the limit for bacterial endotoxins is 175 IU divided by the maximum recommended dose volume. Analysis can, for example, be performed using the Endosafe® nexgen-PTS™ system.

Quality control of [18F]FE-PE2I

A detailed description of Ph. Eur.-compliant Good Manufacturing Practice (GMP) quality control procedures can be found in (13) and Ph. Eur. 11.4, 1325 (01/2024) along with general considerations regarding quality control of radiopharmaceuticals described in (17). Table 3 summarises the tests and analytical methods that can be used for quality control of [18F]FE-PE2I.

Test	Analytical method
Radiochemical purity	HPLC (with radiodetector)
Product identification	HPLC (with radiodetector)
Radiochemical stability	HPLC (with radiodetector)
Molar activity	With HPLC UV detector, scale and dose calibrator
Filter integrity test	as defined by Ph. Eur.
Chemical purity	HPLC (with UV detector)
pH	as defined by Ph. Eur.
Bacterial endotoxin test	as defined by Ph. Eur.
Residual solvents	GC
Sterility	as defined by Ph. Eur.
Radionuclidic purity	as defined by Ph. Eur.
Radionuclidic identity	as defined by Ph. Eur.
Appearance	as defined by Ph. Eur.
Residual Kryptofix	as defined by Ph. Eur.
Free [18F]fluoride	as defined by Ph. Eur.

Table 3. Summary of tests and analytical methods for [18F]FE-PE2I quality control.

Radiochemical purity of [18F]FE-PE2I can be determined using Waters µ-Bondapak C18 10 µm, 3.9×300 mm column with acetonitrile/0.01 M H_3PO_4 35:65 as mobile phase at a flow rate of 2.5 ml/min with UV detector set to 254 nm. Chemical purity can be determined using Waters µ-Bondapak C18 10µm, 3.9×300 mm column with acetonitrile/0.01M H_3PO_4 30:70 as mobile phase at a flow rate of 2.5 ml/min with UV detector set to 254 nm. Alternative reverse-phase chromatography methods can be successfully employed as well (13, 16). Use of basic eluents for quality control of [18F]FE-PE2I can be beneficial, as it allows for LC determination of free [18F]fluoride (16, 20).

Residual Kryptofix is determined using a spot colorimetric threshold test as defined by Ph. Eur. The presence of sodium ascorbate, if added for improved stability of [18F]FE-PE2I in the formulation, can interfere with standard colorimetric tests, therefore it is imperative to perform a specificity test to confirm that Kryptofix can be successfully determined in the formulation used. Other quality control tests are performed to the standards defined in Ph. Eur. for [18F]FDG, where applicable [Ph. Eur. 11.4, 1325 (01/2024)] (19).

PHYSIOLOGICAL BIODISTRIBUTION

[11C]PE2I and [18F]FE-PE2I exhibit high affinity and remarkable selectivity for dopamine transporters (DAT) over serotonin and noradrenaline transporters (7).

[11C]PE2I

Several [11C]PE2I studies evaluated the whole-body biodistribution, radiation-absorbed doses and DAT quantification with PET in-vivo in humans (21-23). These studies have shown that ten minutes after administration of [11C]PE2I, the highest radioactivity concentration is observed in the kidneys, intestines, liver, stomach, salivary glands, vertebral bodies and the brain. Subsequently, 55–112 min after injection, most of the radioactivity accumulates in the urinary bladder.

[11C]PE2I undergoes rapid metabolism with predominant renal clearance and achieves peak blood–brain barrier penetration at 10 min post-injection. The highest uptake in the brain is observed in the striatum, where the concentration, in physiological conditions, remains constant from 10–60 min post-injection and decreases slowly between 1 and 2 h post-injection. The uptake of [11C]PE2I in the midbrain — SN — is lower than in the striatum. The thalamus shows some [11C]PE2I uptake, whereas the uptake in the cerebellum and other cortical regions is very low.

[18F]FE-PE2I

After intravenous administration of [18F]FE-PE2I, the highest activity concentration is observed in the liver between 10 and 30 min after injection, and in the gallbladder at 1 to 6 h after injection. At 6 h after injection, the gallbladder, the small intestine, the salivary glands, and the red marrow showed the highest activity concentration (24).

[18F]FE-PE2I rapidly enters the brain, with highest uptake in the striatum at approximately 10 min post-injection, and has a rapid washout of between 20 and 90 min post-injection. The metabolism of [18F]FE-PE2I is relatively fast. At 20 min, the unchanged radioligand in plasma is 20–25% of the total radioactivity, decreasing to 10–15% at 60 min after injection (24). [18F]FE-PE2I provides faster washout from the brain than [11C]PE2I and lower production of a radiometabolite that crosses the blood-brain barrier (25).

Overall, these properties permit the visualisation and quantification of DAT in the entire nigro-striatal system, which has been challenging due to the small size and low DAT density of the SN (26). The binding is predominantly distributed in the bilateral caudate nucleus and putamen, followed by the SN, with symmetrical and even distribution (27). Figure 1 shows the distribution of [11C]PE2I and [18F]FE-PE2I in the brain at different time points after injection in a healthy subject, together with time-activity curves in striatum

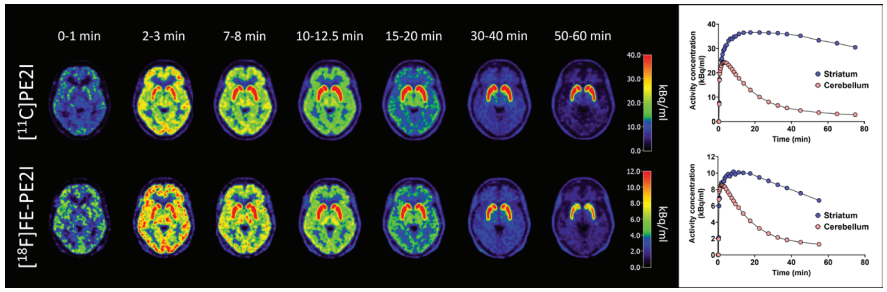

Figure 1. Distribution of [11C]PE2I (top row) and [18F]FE-PE2I (bottom row) in one healthy subject at different time points and time-activity curves in striatum (high-density region) and cerebellum (reference region).

(high-density region) and cerebellum (reference region).

PATIENT PREPARATION & AFTERCARE

Patient preparation for both [11C]PE2I and [18F]FE-PE2I is similar to the preparation before DAT SPECT examinations with [123I]β-CIT or [123I]FP-CIT. While the SPECT tracers also bind to the serotonin and noradrenaline transporters to some extent, the PE2I compounds are very selective for DAT. This means that medications that affect serotonin and noradrenaline re-uptake affect the DAT SPECT investigation, but they affect PE2I PET to a (much) lesser extent.

Before patient arrival, it is important to collect information about medications or drugs that bind competitively to DAT and could thus cause false positive results. Several drugs of abuse, mainly cocaine and amphetamine, have strong affinity for DAT and should be completely avoided before PE2I imaging. It is advised to refer to the EANM guideline/SNMMI procedure standard (27) for the list of drugs binding to the DAT that might interfere with the PET examinations. While discontinuation of medications targeting DAT should be considered, it is important to consider the risk to the patient, and such decisions should therefore be taken on an individual basis. In several cases, the risk outweighs the benefit of discontinuing medications before the examination.

Dynamic imaging with [11C]PE2I and [18F]FE-PE2I enables the measurement of relative cerebral blood flow (rCBF) and DAT availability in the same imaging session (see section on Quantification). If rCBF is measured, efforts should be made to reduce intake of food and common stimulants that affect the haemodynamics in the brain. Fasting for two to four hours before radiopharmaceutical injection is recommended and generally well tolerated. Caffeine, in its role as an adenosine receptor antagonist, can lower CBF and should be avoided before examination. Nicotine and alcohol are other blood flow-altering substances which should be avoided prior to a PE2I examination.

The patient should be positioned comfortably in the PET system using a head support and a support for the arms. Extra effort should be taken to secure the head position to reduce the risk of involuntary motion that might hamper image quality. The patient's brain should be positioned in the isocentre of the scanner. This is particularly important if a diagnostic CT scan is performed during the examination. When performing a dynamic scan to measure relative rCBF, it is preferable to dim the lights in the room and avoid loud noises during the early phase of the acquisition in order to reduce the impact on blood flow in the visual and auditory cortex, respectively.

IMAGING PROTOCOL (EQUIPMENT, IMAGING PARAMETERS)

[11C]PE2I and [18F]FE-PE2I PET can be performed using either dynamic or static acquisition. The most common protocol used in routine practice is static acquisition, since it is more clinically feasible, allows for higher patient throughput, and requires less post-processing. A static acquisition at 30–40 min p.i. is recommended for routine clinical use of both tracers (27).

Image reconstruction

Image reconstruction, whether for a dynamic or static scan, should be performed according to vendor recommendations. Reconstructions should, if possible, include time-of-flight (TOF) and point spread function (PSF) modelling. However, it is important that all patients in a given centre are evaluated using the same reconstruction parameters. To provide a reliable assessment when the interpretation is aided by comparison to a normal database, the reconstruction of PET data acquired in the patient should be equivalent to the reconstruction used for the PET data acquired in the subjects in the normal database. When performing dynamic acquisitions, shorter frame lengths of ≤60 s are used at the beginning of the acquisition, while 5–10-min frames are sufficient during the later phase. Short frame length in the early phase is especially relevant for the calculation of rCBF.

Quantification

Dynamic imaging allows for absolute quantification of DAT availability. The simplified reference tissue model (SRTM), using grey matter in the cerebellum or occipital cortex as the reference region, can provide the non-displaceable binding potential (BP_{ND}) without the need for

arterial sampling. BP_{ND} is directly proportional to the concentration of available dopamine transporters. From the same acquisition, it is also possible to calculate relative tracer delivery (R_1), providing an estimate of rCBF. Assessment of rCBF can aid in differentiation between idiopathic Parkinson's disease and atypical Parkinsonian syndromes (28).

Dynamic imaging for measurement of BP_{ND} using SRTM requires at least 80 min for [11C]PE2I (29), whereas an acquisition time of 60 min is sufficient for [18F]FE-PE2I due to its faster in vivo kinetics (25). Simplified measures can be estimated using shorter scan durations. Using a static acquisition at around 30–40 min p.i., it is possible to calculate the specific binding ratio (SBR) between striatum and a reference region (28, 30, 31). This is calculated as the ratio of the activity concentration in striatum minus the activity concentration in the reference region divided by the activity concentration in the reference region and equals the standardised uptake value ratio minus one. SBR corresponds well with BP_{ND} and allows for discrimination of patients with and without Parkinson's disease (30, 32). A 0–40 min dynamic acquisition can, in addition to SBR, also yield rCBF measurements for dual parameter investigation (32). Using a basis function implementation of SRTM, both BP_{ND} and rCBF can be estimated at the voxel level, allowing for visualisation of DAT availability and rCBF as parametric images (29). The hemisphere asymmetry index calculated as (Right-Left)/(Right+Left) or the putamen-to-caudate ratio can be useful in borderline cases (27).

RESULTS & INTERPRETATION (TYPICAL ABNORMAL FINDINGS / UPTAKE AND EXAMPLES)

An advantage of dynamic PET acquisitions lies in the ability to perform pharmacokinetic analyses, thus obtaining quantitative parameters. For both [11C]PE2I and [18F]FE-PE2I, BP_{ND} or SBR to measure DAT availability, as well as rCBF, corresponding to overall brain function, can be calculated and visualised as parametric images (28).

A comparative analysis investigated the use of dynamic [11C]PE2I PET as a stand-alone method versus the dual-modality approach using [123I]FP-CIT SPECT and 2-[18F]FDG PET (28). Strong consistency between [11C]PE2I BP_{ND} and [123I]FP-CIT SPECT images was observed, showing superior image quality for [11C]PE2I BP_{ND}. Moreover, there was a strong correlation between rCBF and 2-[18F]FDG PET images. The relationship between rCBF and 2-[18F]FDG across the regions was slightly inhomogeneous, with somewhat higher correlations in cortical regions than in subcortical regions, but with similar disease patterns overall. This implies that the disease patterns for [123I]FP-CIT SPECT and 2-[18F]FDG PET described in recent EANM guidelines are applicable to dynamic [11C]PE2I PET in differential diagnosis of Parkinsonian disorders (27, 33).

Integration with structural imaging (CT, MRI) expands the diagnostic potential, providing a comprehensive one-stop solution for patients with Parkinsonian disorders. In a recent study, a within-subject comparison of [11C]PE2I and [18F]FE-PE2I was performed, showing a high correlation regarding both measures of DAT availability and rCBF (34).

Evaluation of PE2I PET images involves careful visual examination in the axial, sagittal and coronal planes, and the interpretation should also take account of anatomical information from structural imaging (CT, MR). Visual interpretation can be supported by semi-quantification methods, such as the three-dimensional stereotactic surface projections (3D SP) method developed for [18F]FDG (35, 36). To enhance visual analysis, a 3D SP perfusion map can be generated through voxel-based analysis of rCBF, by normalising activities against a reference region and comparing them to a normal control database. Reference to the 3D-SSP images (Figure 3 and 4).

Ideally, the reference region should be unaffected by the disease and cerebellum is used in most cases. Alternatively, the occipital cortex may be used. A simplified

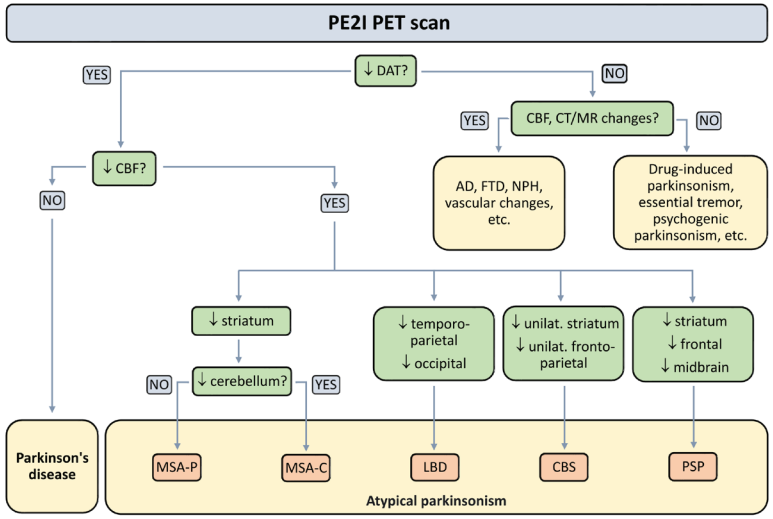

Figure 2. A simplified diagnostic algorithm chart for dynamic [11C]PE2I PET and [18F]PE2I PET scans. Image adopted from recent EANM guidelines (2, 3). DAT, dopamine active transporter; CBF, cerebral blood flow; AD, Alzheimer's disease; FTD, frontotemporal dementia; NPH, normal pressure hydrocephalus; MSA-P, multiple system atrophy-Parkinsonian type; MSA-C, multiple system atrophy-cerebellar type; LBD, dementia with Lewy bodies; CBS, corticobasal syndrome; PSP, progressive supranuclear palsy.

diagnostic algorithm chart for dynamic [^{11}C]PE2I PET and [^{18}F]PE2I PET scans is presented in Figure 2.

In general, DAT ligand binding is observed in Parkinson's disease and atypical Parkinsonian syndromes. However, differentiation at this level is challenging due to the significant overlap between disease patterns. To distinguish Parkinson's disease from different types of atypical Parkinsonian syndrome, the evaluation of rCBF images is essential for detecting typical topographic patterns of blood flow alterations. Furthermore, structural imaging helps evaluate other types of changes that could be causing symptoms, such as vascular changes or normal pressure hydrocephalus. Figures 3 and 4 depict typical abnormal findings in a patient with Parkinson's disease and progressive supranuclear palsy, respectively.

Longitudinal DAT changes measured with [^{18}F]FE-PE2I or [^{11}C]PE2I PET

Age-related DAT decline has been reported in several single-centre studies; however, the largest pool of normative data has been generated by two large multicentre studies performed in healthy subjects. The first is the ENC-DAT (European Normal Control Database of DaTSCAN) database, which includes [^{123}I]FP-CIT SPECT data acquired in 13 different centres from 139 healthy controls (74 men, 65 women) with an age range between 20 and 83 years (37). The second database was acquired as part of the Parkinson's Progression Marker Initiative (PPMI) and includes [^{123}I]FP-CIT SPECT data of 196 healthy controls examined longitudinally over 3 to 4 years (38). The age-related DAT decline reported by these two multicentre studies was 5.5–6% per decade (0.6%/year).

In Parkinson's disease, the average annualised DAT decline measured with [^{18}F]FE-PE2I was 5% to 8.5% for the caudate, putamen and sensorimotor striatum, whereas negligible DAT changes have been reported for the substantia nigra (31, 39). Figure 5 shows [^{18}F]FE-PE2I BP_{ND} images in a PD patient with longitudinal follow-up and an age-matched healthy control. Similar results have been reported for [^{11}C]PE2I PET.

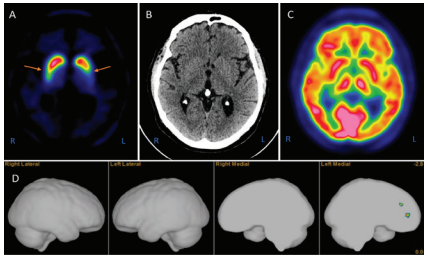

Figure 3. Example of [^{11}C]PE2I PET/CT images in a patient with Parkinson's disease with predominantly right-sided clinical symptoms. (A) [^{11}C]PE2I images of DAT availability showing asymmetrically reduced uptake in striatum (orange arrows), more pronounced on the left side. (B) CT image at the level of striatum showing no abnormalities. (C) [^{11}C]PE2I image of rCBF showing normal perfusion in the cortex and striatum. (D) 3D surface projection map showing perfusion z-scores compared to a healthy control database, indicating perfusion in the normal range in all cortical regions.

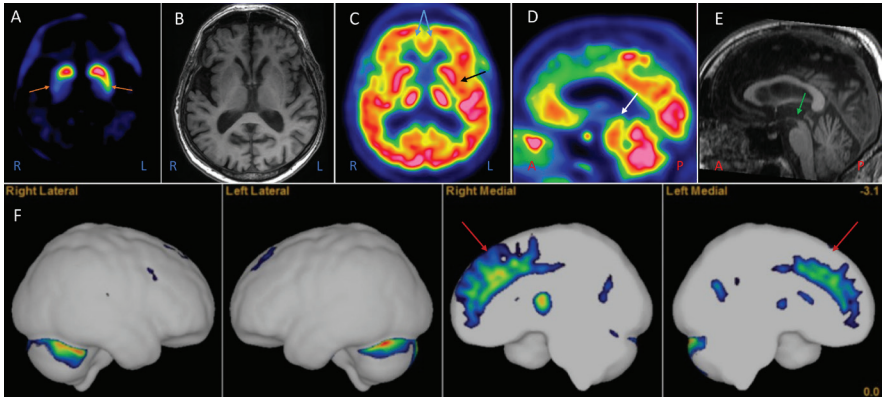

Figure 4. Example of [^{11}C]PE2I PET/MR images in a patient with progressive supranuclear palsy with predominantly left-sided clinical symptoms, axial rigidity and impaired eye gaze. (A) [^{11}C]PE2I images of DAT availability showing reduced uptake in striatum (orange arrows), more pronounced on the right side. (B) MR image (T1-weighted sequence) showing no abnormalities in the striatum. (C) [^{11}C]PE2I image of rCBF showing decreased perfusion bilaterally in medial frontal cortex (blue arrows) and in left putamen (black arrow). (D) [^{11}C]PE2I image of rCBF showing decreased perfusion in midbrain (white arrow). (E) MR image (T1-weighted sequence) showing midbrain atrophy (green arrow). (F) 3D surface projection map showing perfusion z-scores compared to a healthy control database, indicating decreased perfusion bilaterally in medial frontal cortex and anterior cingulate gyrus (red arrows).

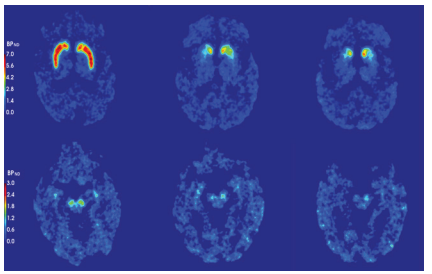

Figure 5. Representative images of [^{18}F]FE-PE2I BP_{ND} in the striatum (upper section) and substantia nigra (lower section) of 67-year-old healthy male control (on the left) and a 68-year-old male patient with Parkinson's disease, with a UPDRS motor score of 23 and a disease duration of 2 years at the baseline (in the centre) and after a 2-year follow-up (on the right).

RADIATION EXPOSURE

[11C]PE2I

The effective dose from [11C]PE2I is 0.0064 mSv/MBq, and the organs receiving the highest equivalent doses are the urinary bladder wall, kidneys, and stomach (19). The tracer is mainly eliminated through renal clearance (Table 4). Typical administered activity is 350 MBq per 70 kg body weight.

[18F]FE-PE2I

The effective dose from [18F]FE-PE2I is 0.023 mSv/MBq, and the organs receiving the highest equivalent doses are the urinary bladder wall, liver, and pancreas (21). These values are comparable with other 18F-labelled radioligands for brain imaging. The tracer is eliminated via both gastrointestinal and renal clearance (Table 4). Typical administered activity is 185–200 MBq per 70 kg body weight.

Radiotracer	Organs receiving the highest absorbed dose	mGy/MBq	Effective dose per injected activity
[11C]PE2I	Urinary bladder wall	0.018	0.0064
	Kidneys	0.016	
	Stomach	0.014	
[18F]FE-PE2I	Urinary bladder wall	0.119	0.023
	Liver	0.046	
	Pancreas	0.031	

Table 4. Critical organs, equivalent and effective dose for [11C]PE2I and [18F]FE-PE2I.

REFERENCES

1. Giros B, Caron MG. Molecular characterization of the dopamine transporter. Trends Pharmacol Sci. 1993;14(2):43-9.
2. Nirenberg MJ, Vaughan RA, Uhl GR, Kuhar MJ, Pickel VM. The dopamine transporter is localized to dendritic and axonal plasma membranes of nigrostriatal dopaminergic neurons. J Neurosci. 1996;16(2):436-47.
3. Hersch SM, Yi H, Heilman CJ, Edwards RH, Levey AI. Subcellular localization and molecular topology of the dopamine transporter in the striatum and substantia nigra. J Comp Neurol. 1997;388(2):211-27.
4. DATSCAN (ioflupane I 123 injection), for intravenous use [cited 2024 JAN 19]. Available from: https://www.accessdata.fda.gov/drugsatfda_docs/label/2022/022454s010lbl.pdf.
5. DaTSCAN, Ioflupane (I-123) [cited 2024 JAN 19]. Available from: https://www.ema.europa.eu/en/documents/product-information/datscan-epar-product-information_en.pdf.
6. Varrone A, Halldin C. Molecular imaging of the dopamine transporter. J Nucl Med. 2010;51(9):1331-4.
7. Varrone A, Halldin C. New developments of dopaminergic imaging in Parkinson's disease. Q J Nucl Med Mol Imaging. 2012;56(1):68-82.
8. Muller L, Halldin C, Farde L, Karlsson P, Hall H, Swahn CG, et al. [11C] beta-CIT, a cocaine analogue. Preparation, autoradiography and preliminary PET investigations. Nucl Med Biol. 1993;20(3):249-55.
9. Emond P, Garreau L, Chalon S, Boazi M, Caillet M, Bricard J, et al. Synthesis and ligand binding of nortropane derivatives: N-substituted 2beta-carbomethoxy-3beta-(4'-iodophenyl)nortropane and N-(3-iodoprop-(2E)-enyl)-2beta-carbomethoxy-3beta-(3',4'-disubstituted phenyl)nortropane. New high-affinity and selective compounds for the dopamine transporter. J Med Chem. 1997;40(9):1366-72.
10. Stepanov V, Schou M, Jarv J, Halldin C. Synthesis of 3H-labeled N-(3-iodoprop-2E-enyl)-2beta-carbomethoxy-3beta-(4-methylphenyl) nortropane (PE2I) and its interaction with mice striatal membrane fragments. Appl Radiat Isot. 2007;65(3):293-300.
11. Dolle F, Bottlaender M, Demphel S, Emond E, Fuseau C, Coulon C, et al. Highly efficient synthesis of [11C] PE2I, a selective radioligand for the quantification of the dopamine transporter using PET. J Labelled Cpd Radiopharm. 2000;43:997-1004.
12. Halldin C, Erixon-Lindroth N, Pauli S, Chou YH, Okubo Y, Karlsson P, et al. [(11)C]PE2I: a highly selective radioligand for PET examination of the dopamine transporter in monkey and human brain. Eur J Nucl Med Mol Imaging. 2003;30(9):1220-30.
13. Bratteby K, Denholt CL, Lehel S, Petersen IN, Madsen J, Erlandsson M, et al. Fully Automated GMP-Compliant Synthesis of [(18)F]FE-PE2I. Pharmaceuticals (Basel). 2021;14(7).
14. Schou M, Steiger C, Varrone A, Guilloteau D, Halldin C. Synthesis, radiolabeling and preliminary in vivo evaluation of [18F]FE-PE2I, a new probe for the dopamine transporter. Bioorg Med Chem Lett. 2009;19(16):4843-5.
15. Varrone A, Toth M, Steiger C, Takano A, Guilloteau D, Ichise M, et al. Kinetic analysis and quantification of the dopamine transporter in the nonhuman primate brain with 11C-PE2I and 18F-FE-PE2I. J Nucl Med. 2011;52(1):132-9.
16. Stepanov V, Krasikova RN, Raus L, Loog O, Hiltunen J, Halldin C. An efficient one-step radiosynthesis of [18F]FE-PE2I, a PET radioligand for imaging of dopamine transporters. Journal of Labelled Compounds and Radiopharmaceuticals. 2012;55:206-10.
17. Elsinga P, Todde S, Penuelas I, Meyer G, Farstad B, Faivre-Chauvet A, et al. Guidance on current good radiopharmacy practice (cGRPP) for the small-scale preparation of radiopharmaceuticals. European journal of nuclear medicine and molecular imaging. 2010;37:1049-62.
18. EDQM. Raclopride ([11C]Methoxy) injection European Pharmacopoeia 11.4 ed. Strasbourg, France: European Directorate for the Quality of Medicines & HealthCare; 2023.
19. EDQM. [18F]Fludeoxyglucose injection. European Pharmacopoeia 11.4 ed. Strasbourg, France: European Directorate for the Quality of Medicines & HealthCare; 2024.

20. Ory D, Van den Brande J, de Groot T, Serdons K, Bex M, Declercq L, et al. Retention of [(18)F]fluoride on reversed phase HPLC columns. J Pharm Biomed Anal. 2015;111:209-14.
21. Hirvonen J, Johansson J, Teras M, Oikonen V, Lumme V, Virsu P, et al. Measurement of striatal and extrastriatal dopamine transporter binding with high-resolution PET and [11C]PE2I: quantitative modeling and test-retest reproducibility. J Cereb Blood Flow Metab. 2008;28(5):1059-69.
22. Ribeiro MJ, Ricard M, Lievre MA, Bourgeois S, Emond P, Gervais P, et al. Whole-body distribution and radiation dosimetry of the dopamine transporter radioligand [(11)C]PE2I in healthy volunteers. Nucl Med Biol. 2007;34(4):465-70.
23. Seki C, Ito H, Ichimiya T, Arakawa R, Ikoma Y, Shidahara M, et al. Quantitative analysis of dopamine transporters in human brain using [11C] PE2I and positron emission tomography: evaluation of reference tissue models. Ann Nucl Med. 2010;24(4):249-60.
24. Lizana H, Johansson L, Axelsson J, Larsson A, Ogren M, Linder J, et al. Whole-Body Biodistribution and Dosimetry of the Dopamine Transporter Radioligand (18)F-FE-PE2I in Human Subjects. J Nucl Med. 2018;59(8):1275-80.
25. Fazio P, Svenningsson P, Forsberg A, Jonsson EG, Amini N, Nakao R, et al. Quantitative Analysis of (1)(8)F-(E)-N-(3-Iodoprop-2-Enyl)-2beta-Carbofluoroethoxy-3beta-(4'-Methyl-Phenyl) Nortropane Binding to the Dopamine Transporter in Parkinson Disease. J Nucl Med. 2015;56(5):714-20.
26. Fazio P, Svenningsson P, Cselenyi Z, Halldin C, Farde L, Varrone A. Nigrostriatal dopamine transporter availability in early Parkinson's disease. Mov Disord. 2018;33(4):592-9.
27. Morbelli S, Esposito G, Arbizu J, Barthel H, Boellaard R, Bohnen NI, et al. EANM practice guideline/SNMMI procedure standard for dopaminergic imaging in Parkinsonian syndromes 1.0. Eur J Nucl Med Mol Imaging. 2020;47(8):1885-912.
28. Appel L, Jonasson M, Danfors T, Nyholm D, Askmark H, Lubberink M, et al. Use of 11C-PE2I PET in differential diagnosis of parkinsonian disorders. J Nucl Med. 2015;56(2):234-42.
29. Jonasson M, Appel L, Engman J, Frick A, Nyholm D, Askmark H, et al. Validation of parametric methods for [11C] PE2I positron emission tomography. Neuroimage. 2013;74:172-8.
30. Sonni I, Fazio P, Schain M, Halldin C, Svenningsson P, Farde L, et al. Optimal Acquisition Time Window and Simplified Quantification of Dopamine Transporter Availability Using 18F-FE-PE2I in Healthy Controls and Parkinson Disease Patients. J Nucl Med. 2016;57(10):1529-34.
31. Brumberg J, Kerstens V, Cselenyi Z, Svenningsson P, Sundgren M, Fazio P, et al. Simplified quantification of [(18)F]FE-PE2I PET in Parkinson's disease: Discriminative power, test-retest reliability and longitudinal validity during early peak and late pseudo-equilibrium. J Cereb Blood Flow Metab. 2021;41(6):1291-300.
32. Jonasson M, Appel L, Danfors T, Nyholm D, Askmark H, Frick A, et al. Development of a clinically feasible [(11)C]PE2I PET method for differential diagnosis of parkinsonism using reduced scan duration and automated reference region extraction. Am J Nucl Med Mol Imaging. 2017;7(6):263-74.
33. Guedj E, Varrone A, Boellaard R, Albert NL, Barthel H, van Berckel B, et al. EANM procedure guidelines for brain PET imaging using [(18)F]FDG, version 3. Eur J Nucl Med Mol Imaging. 2022;49(2):632-51.
34. Jonasson M, Appel L, Roslin S, Antoni G, Nyholm D, Danfors T, et al. Within-subject comparison of 11C-PE2I and 18F-FE-PE2I PET for dopamine transporter availability and relative blood flow measures. EANM'23 Abstract Book Congress Sep 9-13, 2023. European Journal of Nuclear Medicine and Molecular Imaging. 2023;50(1):1-898.
35. Minoshima S, Frey KA, Koeppe RA, Foster NL, Kuhl DE. A diagnostic approach in Alzheimer's disease using three-dimensional stereotactic surface projections of fluorine-18-FDG PET. Journal of Nuclear Medicine. 1995;36(7):1238-48.
36. Ishii K, Kono AK, Sasaki H, Miyamoto N, Fukuda T, Sakamoto S, et al. Fully automatic diagnostic system for early-and late-onset mild Alzheimer's disease using FDG PET and 3D-SSP. European journal of nuclear medicine and molecular imaging. 2006;33:575-83.
37. Varrone A, Dickson JC, Tossici-Bolt L, Sera T, Asenbaum S, Booij J, et al. European multicentre database of healthy controls for [123I]FP-CIT SPECT (ENC-DAT): age-related effects, gender differences and evaluation of different methods of analysis. Eur J Nucl Med Mol Imaging. 2013;40(2):213-27.
38. Marek K, Jennings D, Lasch S, Siderowf A, Tanner C, Simuni T, et al. The Parkinson progression marker initiative (PPMI). Progress in neurobiology. 2011;95(4):629-35.
39. Kerstens VS, Fazio P, Sundgren M, Brumberg J, Halldin C, Svenningsson P, et al. Longitudinal DAT changes measured with [(18)F]FE-PE2I PET in patients with Parkinson's disease; a validation study. Neuroimage Clin. 2023;37:103347.

6

^{89}ZIRCONIUM–LABELLED ANTIBODIES

by Carla Abreu[1]
Chiara da Pieve[2]

[1]JNuclear Medicine and PEC/CT Department, Royal Marsden NHS Foundation Trust, London UK

[2]Preclinical Molecular Imaging Group, The Institute of Cancer Research, Sutton, UK

^{89}ZIRCONIUM–LABELLED ANTIBODIES

^{89}Zr is an emerging radionuclide that plays an important role in immuno-positron emission tomography (PET) imaging. The long half-life of ^{89}Zr (t1/2 = 78.41h) is favourable for assessing the in vivo distribution of monoclonal antibodies. Thus, for instance, the use of ^{89}Zr is promising for the monitoring of antibody-based cancer therapies. Immuno-PET combines the sensitivity of PET with the specificity of the antibodies. Several studies [1,2] have been conducted to investigate the feasibility of ^{89}Zr-immuno-PET imaging for predicting the efficacy of radioimmunotherapy and antibody therapies, imaging target expression, detecting target-expressing tumours, and the monitoring of anti-cancer chemotherapy treatment.

Monoclonal antibodies

Antibodies are proteins produced for protection by the body's immune system in response to harmful substances.

Monoclonal antibodies (mAbs), and in particular the most common, immunoglobulin G (IgG), are Y-shaped proteins formed by two identical heavy (HCs, ca. 50 kDa/chain) and two light (LCs, ca. 25 kDa/chain) polypeptide chains linked together by disulphide bonds. Both chains include fragments with a constant and a variable sequence of amino acids. Additionally, the Y structure is formed of one crystallisable fragment (Fc), which interacts with other components of the host immune system, and two identical antigen-binding fragments (Fab) for binding to the specific target (Figure 1) [3].

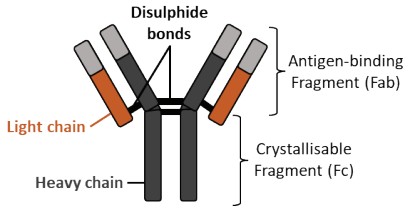

Figure 1. Structure and main features of an IgG antibody [1]

Man-made mAbs used for therapy and imaging are produced mostly in mice, and once introduced into the human body, they can induce a neutralising immune response (allergic reaction) in the form of human anti-mouse antibodies (HAMAs). To achieve more human-compatible and hence more robust mAbs, some or most of the amino acid sequences are engineered without compromising the functionality of the protein. The result is the production of chimeric (mouse antibody with human Fc region) and humanised antibodies (most of the rodent-derived protein sequence is identical to that of a human variant). Recently, technological advances have allowed the production of fully human mAbs using transgenic mice [3].

Monoclonal antibodies with high affinity and specificity for various targets—including growth factors, cell surface receptors and cytokines—have been developed and are currently used in the clinic for the treatment of a variety of conditions [4].

IMMUNOTHERAPY AND IMMUNO-PET

In recent years, owing to their high affinity and specificity for their target, mAbs have become the most investigated drug class for conditions such as cancer, inflammatory diseases, and autoimmune disorders. Following their binding to the antigen, functioning either as agonists or inhibitors, mAbs can modulate the function of cell membrane-associated receptors, either directly or by recruiting the body's immune system. In any case, the result is cell death [5].

Unfortunately, not all patients respond to immunotherapy. Insights into the pharmacokinetics, distribution and uptake in the targeted tissue of such therapeutic agents could be crucial for selecting patients who would benefit from the therapy, as well as monitoring response and predicting toxicities.

PET imaging using mAbs and analogues as imaging agents (immuno-PET) can provide that information non-invasively. Immuno-PET has additional advantages compared to conventional diagnostic procedures such as biopsies and immunohistochemistry, which are invasive and can only assess limited areas of the tissue of interest. Immuno-PET can identify heterogeneity and changes in antigen expression and distribution during disease progression and after treatments, as well as metastases. Furthermore, immuno-PET is a useful tool for drug development. It can assess target accessibility, which is crucial for the success of immunotherapies and antibody-drug conjugates and allows dosimetry prediction and optimisation for radioimmunotherapies [6].

Due to their nature, size, and structure, mAbs have some limitations. They accumulate non-specifically in the liver and require a long time to reach the tissue of interest and to clear from the blood and body. This prolonged biological half-life can affect the target-to-background ratio and the production of good-contrast images. Additionally, the costly production of both mAbs and their derivatives negatively impacts their availability and use in developing countries. Despite that, radiolabelled full-length antibodies can produce excellent PET images and have achieved indisputable clinical success [7].

In general, for the development of protein-based imaging agents it is fundamental to match the physical half-life of the radioisotope to the biological half-life of the vector. As previously mentioned, full-size antibodies are characterised by slow pharmacokinetics and can require several days to reach the target tissue. Therefore, long-lived radioisotopes such as copper-64 (^{64}Cu, T1/2 = 12.7h), zirconium-89 (^{89}Zr, T1/2 = 78.4h) and iodine-124 (^{124}I, T1/2 = 4.2d) are the most suitable for antibody-based immuno-PET [8].

^{89}Zr-immuno-PET

^{89}Zr radiochemistry and general properties of ^{89}Zr-mAbs

^{89}Zr is produced in a medical cyclotron, using a commercially available metal target (yttrium-89), via either a ^{89}Y(p,n)^{89}Zr or a ^{89}Y(d,2n)^{89}Zr reaction. ^{89}Zr decays with a half-life of 78.4h via both positron emission (23%) and electron capture (77%) to metastable yttrium-89m (^{89m}Y), which decays to stable yttrium-89 (^{89}Y) via gamma emission (909 keV). The relatively low-energy positrons emitted by ^{89}Zr (E_{mean} = 395 keV) allow for high-resolution images and, if a suitable energy window is set during the scan, the 909 keV gamma rays are not in coincidence with the 511 keV photons [9].

Zirconium is a metal present as a positively charged +4 ion (Zr^{4+}) in aqueous solutions. The cation usually forms complexes with a coordination number of 8 and is coordinated preferentially by oxygen donor atoms. Consequently, ^{89}Zr is supplied in its stable oxalate form in a 1 M oxalic acid solution.

Generally, procedures developed to radiolabel proteins with radiometals like ^{89}Zr require the attachment of chelators to the protein (i.e., conjugation), purification of the product (i.e., conjugate), and then the subsequent radiolabelling and purification of the radioconjugate.

Ideally, ^{89}Zr-labelled antibodies should have the same pharmacokinetics and affinity for the target as the unlabelled antibodies. Furthermore, they should be stable and should not release the radiometal. These characteristics can be achieved by selecting the most appropriate chelator for ^{89}Zr and by optimising the conjugation reaction.

Currently, the most-used chelator for ^{89}Zr is desferrioxamine B (DFO). DFO is a bacterial iron-sequestering molecule which contains three metal-chelating hydroxamate groups and a terminal primary amine which, once suitably modified, can be used to conjugate DFO to the antibody (Figure 2). Importantly, DFO shows rapid and efficient coordination of ^{89}Zr under mild conditions (i.e., pH 7 and room temperature), forming a stable complex involving eight oxygen atoms (six binding oxygen atoms from the chelator and two from water molecules) (Figure 3) [6].

Preparation of ^{89}Zr-antibodies

The preparation of ^{89}Zr-antibodies is a two-step process consisting of the initial production of the DFO-mAb conjugate (using the commercially available chelator which reacts with lysine residues, Figure 2) followed by its radiolabelling (Figure 3) [10].

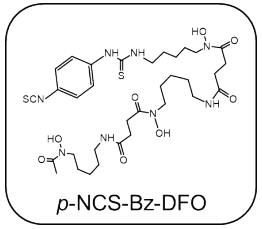

Figure 2. Molecular structure of chelator p-NCS-Bz-DFO [6].

A typical antibody has approximately 80 lysine residues distributed throughout the whole protein structure. Therefore, conjugation methods via lysine residues are non-selective (i.e., random) and generate products characterised by twofold heterogeneity (i.e., attachment of different number of chelators per antibody and yield of conjugates with the same number of chelators but coupled to different lysine residues) [11]. If the chelators are attached at the antigen site, the target recognition ability of the antibody can potentially be compromised.

A site-specific conjugation would increase control of the number and location of the chelators on the protein, resulting in conjugates with more homogeneous and reproducible structures. However, site-specific approaches have not shown any significant advantage regarding distribution and targeting affinity compared to the random conjugation procedure [6].

Importantly, the conjugation strategy should be selected based on the requirements, the availability of the components and the feasibility of the process. In most cases, the random conjugation on lysine residues is more than adequate for the purpose as it is rapid, straightforward, and requires commercially available material. The more site-specific conjugation method should be considered only in the event of proven and concerning interference with target recognition.

The radiolabelling of the DFO-mAb conjugate is carried out by incubating it with commercially available ^{89}Zr-oxalate under mild conditions (i.e., pH 7 and room temperature) (Figure 3). The radiolabelled product is then purified from free radiometal, and oxalic acid and buffer are exchanged using commercially available pre-packed columns.

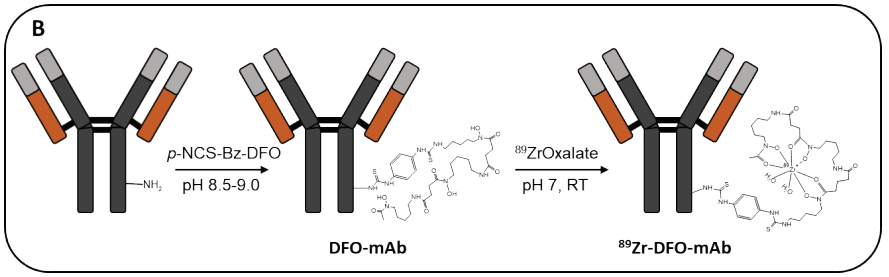

Figure 3. Structure of lysine-based conjugate and ^{89}Zr-radioconjugate as well as the reaction conditions for their preparation (B) [6].

Quality control of ^{89}Zr-immunoconjugates for clinical use

Quality control of ^{89}Zr-mAbs includes the conventional standard quality tests performed for any PET radiopharmaceutical, such as visual appearance, pH, radionuclide identity and purity, chemical purity, specific activity, membrane filter integrity, bacterial endotoxin and sterility. Chemical and radiochemical purity is assessed by size-exclusion high-pressure liquid chromatography (SE-HPLC). In addition, instant thin-layer chromatography (ITLC) can be used to check the radiochemical purity of the product. Importantly, the retained ability to bind adequately to the target antigen is confirmed by immunoreactivity testing. Either cell-based tests following the method proposed by Lindmo et al. [12] or isolated antigen-based techniques (such as ELISA or functionalised magnetic beads) [13,14] can be used to estimate the immunoreactive fraction. The sterility test and immunoreactivity assay can be performed after the release of the ^{89}Zr-mAb.

PET imaging with ^{89}Zr-mAbs

For the achievement of optimal image contrast, imaging is usually performed several days after the administration of zirconium-89-mAbs to allow for their clearance from the blood and accumulation in the target tissue. Importantly, zirconium-89 is trapped inside the cell (i.e., residualisation) following the antigen-antibody complex internalisation, contributing to increased uptake in the target tissue and the production of high-contrast images [15]. Additionally, ^{89}Zr-immuno-PET images usually show high liver uptake as a consequence of the non-specific hepatobiliary clearance of full-length antibodies.

Preclinical studies have demonstrated the release of the radiometal from ^{89}Zr-radiolabelled antibodies as the free ^{89}Zr localises in the bone, especially in zones of growing and remodelling (e.g., epiphyses). The main reason for the metal release can be attributed to the structure of the chelator. DFO is a good chelator for ^{89}Zr, but not a perfect one: it provides only six donor atoms out of the eight preferred by the metal to form the most stable complex. Water molecules contribute the missing two extra oxygen atoms (Figure 3). The resulting non-perfect configuration can trigger some release of ^{89}Zr, and a subsequently high radioactive signal in the mineral bone [17]. To resolve the issue, considerable radiochemistry research is dedicated to developing new chelators for the formation of more stable complexes with ^{89}Zr [17]. However, the high degree of bone uptake shown in preclinical images has not been identified in clinical trials with ^{89}Zr-antibodies, therefore it does not pose a significant concern.

Another consideration for the clinical use of long-lived radionuclides such as ^{89}Zr, and radiopharmaceuticals with slow body clearance, is the considerable radiation dose that is delivered to the patients. However, PET systems with increased sensitivity (e.g., digital PET/CT and whole-body scanners) can guarantee optimal image quality even after administration of lower activities, therefore reducing the radiation exposure to the patient [18]. The amount of dose administered and the interval between tracer administration and imaging acquisition warrant investigation in order to obtain an optimised contrast between lesions and background. In the case of [^{89}Zr]Zr-trastuzumab, the optimal imaging time for a ~37 MBq (50 mg) intravenous injection was observed as being between 4–5 days after injection [19,20]. At this point, low blood-pool activity and high tumour avidity was established. Imaging after longer periods >6 days can compromise the spatial resolution and image quality [19]. At higher administered activities (~185 MBq/50 mg), [^{89}Zr]Zr-trastuzumab still generated high-quality spatial resolution in images acquired between 5–6 days post-injection [19,20,21]. Scan periods of 3–8 days, depending on the dose, are typical for other full-length mAb tracers in clinical trials.

In conclusion, at present, the benefits of ^{89}Zr-immuno-PET for drug development, patient stratification and response to therapy assessment outweigh any of the above-mentioned concerns.

^{89}ZR-LABELLED RADIOPHARMACEUTICALS

Oncology

Immuno-PET with ^{89}Zr-labelled antibodies has demonstrated great potential in evaluating the in vivo distribution of monoclonal antibodies in cancer therapies. A large variety of ^{89}Zr-mAbs have been developed for a wide range of tumour-associated antigens (e.g., EGFR, HER2, CD44v6, PSMA, CD20, VEGF-A, PD-1 and PD-L1) [22,23].

For example, [^{89}Zr]Zr-trastuzumab has been used to assess human epidermal growth factor 2 (HER2) expression status and to predict patients' response to HER2-targeted therapy in breast cancer as well as gastric cancer patients [7].

Pilot clinical studies were carried out to test the feasibility and safety of EGFR imaging agent [^{89}Zr]Zr-cetuximab in non-small cell lung cancer (NSCLC). Additionally, both [^{89}Zr]Zr-cetuximab and [^{89}Zr]Zr-panitumumab were used to image EGFR expression in head and neck squamous cell carcinoma (HNSCC) and colorectal cancer.

[^{89}Zr]Zr-atezolizumab, targeting programmed death-ligand 1 (PD-L1), and [^{89}Zr]Zr-nivolumab and [^{89}Zr]Zr-pembrolizumab, both targeting programmed death 1 (PD-1), were investigated with regard to selection of patients for therapy with immune-checkpoint inhibitors in breast and lung

cancer as well as in melanoma clinical studies [7]. [^{89}Zr]Zr-atezolizumab was also used in clinical studies of patients with advanced or metastatic bladder cancer, NSCLC, triple negative breast cancer [24] and glioblastoma (GBM) [25]. An example of a [^{89}Zr]Zr-atezolizumab scan in a GBM patient is shown in Figure 4.

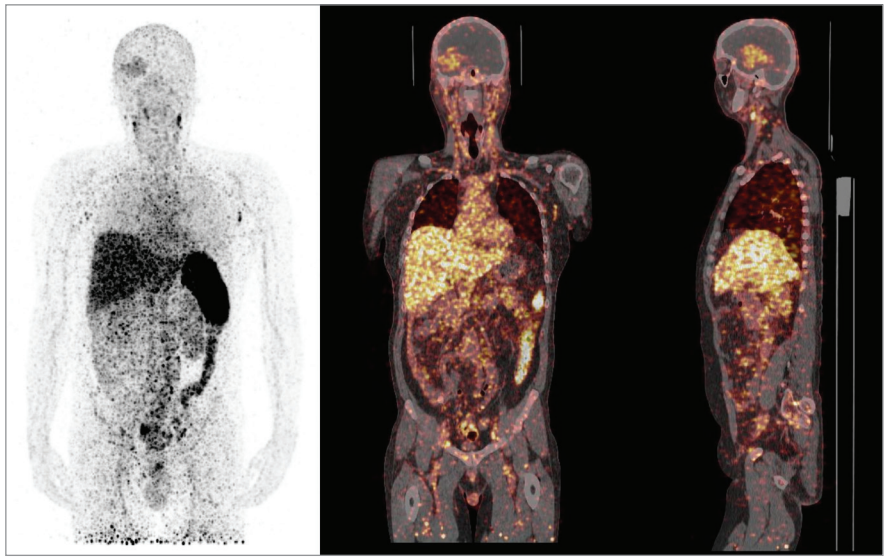

Figure 4. Whole-body MIP (left) and PET/CT (middle & right) of [^{89}Zr]Zr-atezolizumab (ca. 37 MBq, co-injection of 10 mg of unlabelled atezolizumab) in a patient with GBM at 72 h post-injection showing uptake of the imaging agent in the brain (lesion), in the liver (clearance), and in PD-L1-expressing lymphoid tissues (e.g., spleen and lymph nodes). The studies (NCT05235737) were performed at Maria Sklodowska-Curie National Research Institute of Oncology in Gliwice, Poland. Images: courtesy of Prof. Gabriela Kramer-Marek, MSCNRIO, Gliwice, Poland and the ICR, London, UK.

[^{89}Zr]Zr-zevalin PET imaging was used to determine the dose-limiting organs for [^{90}Y]Y-zevalin treatment (the FDA-approved radioimmunotherapy [^{90}Y]Y-ibritumomab tiuxetan) in patients with non-Hodgkin lymphoma (NHL) [22].

^{89}Zr-immuno-PET has so far shown high specificity and sensitivity: for example, [^{89}Zr]Zr-bevacizumab PET (anti-VEGF-A) showed a high sensitivity (96%) for detecting VEGF-expressing primary breast cancers and high specificity (100%) for lymph node metastasis [26], and [^{89}Zr]Zr-girentuximab demonstrated high sensitivity and specificity in clear cell renal cell carcinoma [27]. More recently, Shuch et al. [28] published results of PET imaging with [^{89}Zr]Zr-girentuximab detecting clear cell renal cell carcinoma in patients with a tumour mass ≤7cm, demonstrating a mean sensitivity of 85.5% and mean specificity of 87%.

Autoimmune diseases

Autoimmune diseases include multiple sclerosis, rheumatoid arthritis, Crohn's and Graves' disease. They are caused by an overactive immune system that mistakenly attacks and destroys normal cells. Generally, diagnosis is based on classical signs of inflammation (e.g., swelling, redness, pain, and heat) which usually appear at late stages of the condition when the tissue damage might already be irreversible. Blood and urine analysis as well as biopsies are currently the most reliable tests performed for early diagnosis, estimation of the condition's severity, and assessment of disease progress. However, patients with autoimmune diseases may benefit from ^{89}Zr-immuno-PET [29].

Leukocytes are actively involved in the condition, and treatments targeting and depleting B-cells using the anti-CD20 mAb rituximab were shown to alleviate the inflammation and improve the overall disease symptoms [30]. [^{89}Zr]Zr-rituximab PET showed promising results in the selection of rheumatoid arthritis responders to rituximab therapy and could detect active lesions in multiple sclerosis patients. The same radiopharmaceutical was tested on orbital inflammatory disease patients, confirming its potential in the diagnosis of this complex condition [23].

Patient preparation, Imaging and Dosimetry

^{89}Zr-labelled mAbs are usually administered intravenously, slowly over 3–10 minutes to avoid any adverse reactions. The injection (37–74 MBq) is done either on the day of the scan (e.g., 1h or 3h post-injection) or several days before (e.g., 4- or 7-days post-injection), depending on the clinical study. Unlabelled antibody is usually administered together with the radiopharmaceutical to prevent rapid clearance (mostly hepatobiliary) and to allow the agent to accumulate in the lesions [21, 24].

Patients should be instructed to void prior to imaging. The scan range is dependent on the clinical study and/or on whether the patient has known or suspected lower extremity disease involvement. The scan range should be consistent across the different scanning time points.

No special dieting or fasting have so far been required for an ^{89}Zr PET scan, and patients are allowed to go home even if the scan is scheduled for 4–7 days post-injection.

To advise on how to limit close contact with others after administration of ^{89}Zr, an effective half-life of 78.4 hours was assumed for ^{89}Zr based on the literature [31] and

a number of contact patterns (partner/spouse, children, infant) describing the time and distance spent in proximity to a patient injected with 37 MBq ^{89}Zr were analysed to estimate the total dose that would be received in the absence of restrictions.

The restriction period is highly dependent on the assumption made regarding contact with others. The following wording is suggested for inclusion in patient discharge information:

For a few days after each injection of ^{89}Zr your body will contain some radioactivity. During this time, anyone who spends time in regular close contact with you will get a small dose of radiation, which is best avoided. You will reduce the radiation dose to other people if you follow these instructions:

For the first 3 nights after the injection:

» Sleep in a separate bed from your partner.

For the first 4 days after the injection:

» Try to stay more than an arm's length away from other people and limit the time you spend close to them.

» Maintain a high level of personal hygiene, sit down when urinating, and wash hands thoroughly afterwards.

» Clothes, bed linen etc. can be washed as usual.

Depending on the clinical study specifications, blood samples are collected, and tumour biopsies performed for pharmacokinetics assessment and post-imaging immunohistochemistry staining, respectively [24].

As mentioned before, ^{89}Zr has a half-life of 78.4 hours, which makes it suitable for antibody imaging as it matches the pharmacokinetics of antibody biodistribution [22,32]. The whole-body effective dose for ^{89}Zr-labelled antibodies is estimated to be between 0.264–0.330 mSv/MBq [2]. Dosimetry analysis showed that the organs receiving the highest doses (mean ± SD) were the liver (1.86 ± 0.40 mGy/MBq), the kidneys (1.50 ± 0.22 mGy/MBq) and the heart wall (1.45 ± 0.19 mGy/MBq), with a mean whole-body effective dose of 0.57 ± 0.08 mSv/MBq [33]. For a typical injected dose of 37–74 MBq of ^{89}Zr-labelled antibody, patients generally receive a total radiation dose of approximately 20–40 mSv [22]. The long half-life of ^{89}Zr allows for imaging at later time points to assess antibody biodistribution [32].

^{89}Zr decays by positron emission (23%) and electron capture (77%), emitting 909 keV and 511 keV gamma rays [22]. The relatively low positron energy (396 keV average) of ^{89}Zr allows for high-resolution PET imaging [24]. Recent technical advancements have allowed the development of whole-body PET/CT scanners with exceptional sensitivity and high spatial resolution. Such systems, together with the less costly digital PET/CT systems, enable the injection of lower activities of radioactive agents without compromising the image quality, thus reducing the radiation burden on the patients. Whole-body PET scanners with high sensitivity enable ^{89}Zr-labelled antibody imaging for up to 30 days after injection, compared to only 7–10 days with conventional PET systems [34]. This allows imaging time points to better match antibody biodistribution half-lives in humans and tissue pharmacokinetics.

CONCLUSIONS

Following promising preclinical data, ^{89}Zr was successfully used in several clinical trials. The beneficial imaging properties combined with the long half-life make ^{89}Zr a versatile PET imaging tool, especially for radiolabelling mAbs to assess antigen expression, analyse biodistribution, plan treatment and assess response to anticancer therapies. Although oncology is by far the largest field of application, ^{89}Zr-radiolabelled mAbs have been proposed for possible use in inflammation and autoimmune disorders, with interesting results.

REFERENCES

1. Heskamp S, Raavé R , Boerman O, Rijpkema M, Goncalves, Franck Denat, F. 89Zr-Immuno-Positron Emission Tomography in Oncology: State-of-the-Art 89Zr Radiochemistry. Bioconjugate Chemistry. 2017; 28 (9), 2211-2222.
2. Liberini V, Laudicella R, Capozza M, Huellner MW, Burger IA, Baldari S, Terreno E, Deandreis D. The Future of Cancer Diagnosis, Treatment and Surveillance: A Systemic Review on Immunotherapy and Immuno-PET Radiotracers. Molecules. 2021; 26(8):2201.
3. Chiu ML, Goulet DR, Teplyakov A, Gilliland GL. Antibody Structure and Function: The Basis for Engineering Therapeutics. Antibodies. 2019; 8(4):55.
4. Sharma P, Joshi RV, Pritchard R, Xu K, Eicher MA. Therapeutic Antibodies in Medicine. Molecules. 2023; 28(18):6438.
5. Kaifeng H, Zeng S, Qian L. Recent progress in the molecular imaging of therapeutic monoclonal antibodies. Journal of Pharmaceutical Analysis. 2020; 10(5): 397-413.
6. Heskamp S, et al. 89Zr-Immuno-Positron Emission Tomography in Oncology: State-of-the-Art 89Zr Radiochemistry. Bioconjugate Chemistry. 2017; 28 (9):2211-2223.
7. Manafi-Farid R. ImmunoPET: Antibody-Based PET Imaging in Solid Tumors. Frontiers in Medicine. 2022; 9:916693.
8. Deri M, et al. PET imaging with 89Zr: From radiochemistry to the clinic. Nuclear Medicine and Biology. 2013; 40(1):3-14.
9. Holland JP, Sheh Y, Lewis JS. Standardized methods for the production of high specific-activity zirconium-89. Nuclear Medicine and Biology. 2009 Oct;36(7):729-739.
10. Perk, L.R., Vosjan, M.J.W.D., Visser, G.W.M. et al. p-Isothiocyanatobenzyl-desferrioxamine: a new bifunctional chelate for facile radiolabeling of monoclonal antibodies with zirconium-89 for immuno-PET imaging. Eur J Nucl Med Mol Imaging. 2010; 37:250–259.
11. Dennler P, Fischer E, Schibli R. Antibody Conjugates: From Heterogeneous Populations to Defined Reagents. Antibodies. 2015; 4(3):197-224.
12. Lindmo T et al. Determination of the immunoreactive fraction of radiolabeled monoclonal antibodies by linear extrapolation to binding at infinite antigen excess. Journal of Immunological Methods. 1984; 72(1):77-89.
13. Moreno I, Domínguez M, Toraño A. A kinetic ELISA to determine the immunoreactive fraction of monoclonal antibodies. Journal of Immunological Methods. 2020. 476: 112689.
14. Sharma SK, Lyashchenko SK, Park HA et al. A rapid bead-based radioligand binding assay for the determination of target-binding fraction and quality control of radiopharmaceuticals. Nucl Med Biol. 2019;71:32-38.
15. Van Dongen G, Beaino W, Windhorst A et al. The Role of 89Zr-Immuno-PET in Navigating and Derisking the Development of Biopharmaceuticals. Journal of Nuclear Medicine. 2021; 62(4):438-445.
16. Abou D, Ku T, Smith-Jones P. In vivo biodistribution and accumulation of 89Zr in mice. Nuclear Medicine and Biology. 2011; 38(5):675-681.
17. Bhatt NB, Pandya DN, Wadas TJ. Recent Advances in Zirconium-89 Chelator Development. Molecules. 2018; 23(3):638.
18. Lasnon C, Coudrais N, Houdu B, et al. How fast can we scan patients with modern (digital) PET/CT systems? European Journal of Radiology. 2020; 129:109144.
19. Dijkers EC, Oude Munnink TH, Kosterink JG, et al. Biodistribution of 89Zr-trastuzumab and PET imaging of HER2-positive lesions in patients with metastatic breast cancer. Clin. Pharmaco.l Ther. 2010; 87(5):586–592.
20. Jauw YW, Zijlstra JM, de Jong D, et al. Performance of 89Zr-Labeled-Rituximab-PET as an Imaging Biomarker to Assess CD20 Targeting: A Pilot Study in Patients with Relapsed/Refractory Diffuse Large B Cell Lymphoma. PLoS One. 2017; 12(1):e0169828.
21. Menke-van der Houven van Oordt CW, Gootjes EC, Huisman MC, et al. 89Zr-cetuximab PET imaging in patients with advanced colorectal cancer. Oncotarget. 2015; 6(30):30384–30393.
22. Yoon J-K, Park B-N, Ryu E-K, et al. Current Perspectives on 89Zr-PET Imaging. International Journal of Molecular Sciences. 2020; 21(12):4309.
23. De Feo, M.S., Pontico, M., Frantellizzi, V. et al. 89Zr-PET imaging in humans: a systematic review. Clin Transl Imaging. 2022; 10: 23–36.
24. Bensch F, van der Veen EL, Lub-de Hooge MN, Jorritsma-Smit A, Boellaard R, Kok IC, Oosting SF, Schröder CP, Hiltermann TJN, van der Wekken AJ, Groen HJM, Kwee TC, Elias SG, Gietema JA, Bohorquez SS, de Crespigny A, Williams SP, Mancao C, Brouwers AH, Fine BM, de Vries EGE. 89Zr-atezolizumab imaging as a non-invasive approach to assess clinical response to PD-L1 blockade in cancer. Nat Med. 2018 Dec;24(12):1852-1858.
25. Dar D, Rodak M, Da Pieve C, Gorczewska I, Sharma G, Chmielik E, Niedbala M, Bzowski P, d'Amico A, Bobek-Billewicz B, Nowicka E, Tarnawski R, Kaspera W and Kramer-Marek G. Imaging PD-L1 in the brain – journey from the lab to the clinic. Manuscript in preparation.
26. Gaykema S, Brouwers A, Lub-de Hooge et al. 89Zr-Bevacizumab PET Imaging in Primary Breast Cancer. Journal of Nuclear Medicine. 2013; 54 (7):1014-1018.
27. Shuch B, Pantuck A, Bernhard J C et al. Results from phase 3 study of 89 Zr-DFO-girentuximab for PET/CT imaging of clear cell renal cell carcinoma (ZIRCON). Journal of Clinical Oncology. February 2023; 41(6_suppl):LBA602-LBA602.
28. Shuch B, Pantuck AJ, Bernhard JC, Morris MA, Master V, Scott AM, et al. [89Zr]Zr-girentuximab for PET–CT imaging of clear-cell renal cell carcinoma: a prospective, open-label, multicentre, phase 3 trial. The Lancet Oncology. 2024 Sep 10.
29. Dammes N, Peer D. Monoclonal antibody-based molecular imaging strategies and theranostic opportunities. Theranostics. 2020;10(2):938-955.
30. Randall KL. Rituximab in autoimmune diseases. Aust Prescr. 2016;39(4):131-134
31. P. K. E. Börjesson, Radiation Dosimetry of 89Zr-Labeled Chimeric Monoclonal Antibody U36 as Used for Immuno-PET in Head and Neck Cancer Patients. J Nucl Med. 2009; 50 (11): 1828-1836.
32. Lindenberg L, Adler S, Turkbey IB, Mertan F, Ton A, Do K, et al. Dosimetry and first human experience with 89Zr-panitumumab. American Journal of Nuclear Medicine and Molecular Imaging. 2017 Sep 7(4):195–203.
33. Merkx, R.I.J., Lobeek, D., Konijnenberg, M. et al. Phase I study to assess safety, biodistribution and radiation dosimetry for 89Zr-girentuximab in patients with renal cell carcinoma. Eur J Nucl Med Mol Imaging. 2021; 48, 3277–3285.
34. Berg E, Gill H, Marik J, Ogasawara A, William S, Van Dongen G, Vugts D, Cherry S R, Tarantal A F. Total-Body PET and Highly Stable Chelators Together Enable Meaningful 89Zr-Antibody PET Studies up to 30 Days After Injection. Journal of Nuclear Medicine. 2020, 61 (3) 453-460.

CHAPTER 6

^{89}ZIRCONIUM–LABELLED ANTIBODIES

7

^{64}CU-LABELLED RADIOPHARMA-CEUTICALS FOR ONCOLOGICAL APPLICATIONS

by Elisabeth Eppard
Michelle Degen

Faculty of Medicine, University Clinic for Radiology and Nuclear Medicine, Otto von Guericke University (OvGU), 39120 Magdeburg, Germany

^{64}CU-LABELLED RADIOPHARMACEUTICALS FOR ONCOLOGICAL APPLICATIONS

Copper is an essential trace element, the metabolism of which is associated with a variety of diseases. Beside dementia, cancer and inflammation, both nutritional dysfunctions and hereditary diseases of copper metabolism exhibit potential for imaging and, under certain circumstances, therapy using copper-labelled radionuclides. Unfortunately, this potential is largely untapped.

Within the group of suitable radionuclides of copper, copper-64 stands out with several unique properties that qualify it for a large number of potential applications. However, the advantage of copper-64 as a multipurpose radionuclide can also be perceived as a disadvantage. For each potential application, other more common radionuclides (e.g. fluorine-18, gallium-68, lutetium-177) may be superior. The availability of copper-64 is stagnating for several reasons, including high production costs, short shelf-life of the finished radiopharmaceutical, and competition from established radionuclides.

PROPERTIES

Radionuclide properties

Copper (Z = 29) has two stable isotopes (copper-63 (69.15 %), copper-65 (30.85 %)) and a total of 27 radionuclides. Within this multitude are four positron emitters (copper-60 (T1/2 = 23.7 min, 93 % β+), copper-61 (T1/2 = 3.33 h, 61 % β+), copper-62 (T1/2 = 9.7 min, 98 % β+) copper-64 (T1/2 = 12.7 h, 19 % β+, 38 % β–)) and one electron emitter (copper-67 (T1/2 = 61.83 h, 100 % β–) which are suitable for nuclear medicine applications.

Within the group of medically relevant copper radionuclides, copper-64 stands out with its unique properties. The half-life of copper-64 is 12.7 h. It undergoes three modes of decay: 17.5 % positron emission (β+), 38.5 % beta emission (β–), and 44.0 % electron capture (EC), as shown schematically in Figure 1. The electron capture is accompanied by the emission of high- linear-energy-transfer Auger electrons, which can increase its cytotoxic potency given that the radionuclide is located inside cells within or close to cell nuclei.

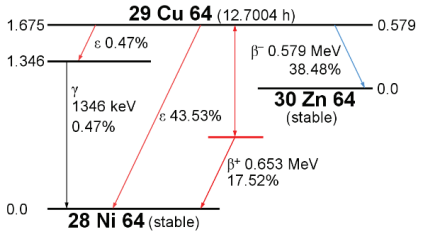

Figure 1. Decay scheme for the decay of copper-64 [1].

Copper chemistry

Copper can exist in oxidation states ranging from +1 to +4 due to its electron configuration. However, in stable copper complexes, the oxidation states +1 and +2 are dominant. Cu(I), which has a d10 configuration, forms diamagnetic complexes and prefers a tetrahedral geometry. Cu(I) complexes are often stabilised by ligands, such as carbon in isocyanides, uncharged sulphur in thioethers (e.g. methionine), phosphorus in phosphines, or sulphur anions of thiolates (e.g. cysteine). However, due to their instability under physiological conditions, Cu(I) complexes are generally unsuitable for in vivo applications. On the other hand, Cu(II) complexes have coordination numbers of four, five, and six. The d9 configuration of the complex leads to paramagnetism and a tetragonally distorted geometry [2]. As a result, the axial ligands become elongated in an octahedral geometry. In extreme cases, a loss of ligands can occur along the z-axis. This results in a square-planar or square-pyramidal structure of the corresponding Cu(II) complex. Ligands that contain nitrogen, such as amines, imines, or heteroaromatics like pyridines, bipyridines, or imidazoles, are typically preferred.

Although copper-64 is an attractive option for nuclear medicine, its use is limited by the prevalent chelators in radiopharmacy. These chelators are developed and optimised for use with the most common radiometals, and complexes with these chelators may result in unwanted radiation doses to the patient due to lowered in vivo stability. Furthermore, trans-chelation to copper proteins can pose a challenge to the copper complex of the radiopharmaceutical. Facilitating this process involves intracellular reduction of copper from Cu(II) to Cu(I). Copper proteins tend to accumulate in the liver and kidneys, which can result in an unwanted radiation dose. It is therefore essential to develop copper-specific chelators and carefully select dedicated radiopharmaceuticals.

Chelators can be classified into three general groups. The first group are the acyclic chelators, which are known for their fast copper complexation kinetics. However, their comparably low stability constants are challenged in vivo by copper proteins. The most important acyclic chelators are bis(thiosemicarbazones) (BTSCs). Neutral, stable copper complexes can easily react with BTSCs, which can be functionalised and have potential for hypoxy, myocardial, and cerebral perfusion imaging [3]. The most important derivatives of BTSCs for this purpose are Cu-GTSM, Cu-ATSM, and Cu-PTSM.

Macrocyclic chelators are preferred due to their higher stability. Various polyaza chelators based on N-macrocycles bearing functionalisation on the nitrogen atoms are available. One example is 1,4,7-triazacyclononane-1,4,7-triacetic acid (NOTA), which is a convenient candidate for Cu-radiopharmaceuticals due to its ability to form in vivo stable complexes with fast complexation kinetics, even at room temperature. However, 1,4,7,10-tetraazacyclododecane-1,4,7,10-tetraacetic acid (DOTA, cyclen family)

is more prevalent in radiopharmacy. DOTA complexation requires relatively mild heating and provides sufficient thermodynamic stability and large in vivo stability with respect to the half-life of copper-64 [4]. Nevertheless, the stability of its derivatives depends heavily on the number and structure of the side arms. The stability of DO3A is comparable, while DO2A is significantly less stable. Phosphonate analogues (DO2P, DO3P, DOTP) are generally more stable. 1,4,8,11-tetraazacyclotetradecane-1,4,8,11-tetraacetic acid (TETA), which belongs to the cyclam family, is highly stable but suffers from dissociation in vivo. Various N-functionalised mono- and bifunctional chelators based on cyclen and cyclam are commercially available to some extent [5]. The kinetic inertness of cyclen and cyclam ligands can be improved by introducing a cross-bridge. However, chelators that contain cross-bridges have limited use because they require harsher radiolabelling conditions that not every biovector can tolerate. Currently, the most effective copper chelates are derivatives of sarcophagine (SAR), which is a cross-bridged bicyclic cyclam derivative. SAR-derivatives exhibit fast kinetics at room temperature, can complex in a pH range from 4 to 9, and possess high thermodynamic stability [6]. Several bifunctional chelators have been reported as having excellent copper chelation properties.

Porphyrins present the latest group of suitable copper chelators. The porphyrin molecule's tetrapyrrole structure is present in various natural compounds, including chlorophyll, vitamin B12, and cofactor F430. The clinical application of Cu-porphyrins is restricted due to the radiolabelling requirements: harsh temperatures, reductive stabilisers, and the presence of dimethyl sulfoxide (DMSO) [7].

FROM THE RADIONUCLIDE TO THE RADIOPHARMACEUTICAL

Radionuclide production

Various methods for producing copper-64 using a reactor or cyclotron have been published over time, resulting in copper-64 of varying quantity and quality. The latter's usefulness for medical applications may be limited by factors such as radionuclide, radiochemical and chemical purity, as well as specific activity. More recently, methods have been reported that result in medically acceptable purity and specific activities [8, 9, 10, 11, 12, 13, 14, 15, 16]. Among these methods, the ^{64}Ni(p,n)^{64}Cu reaction is noteworthy because it can be applied even on the low-energy medical cyclotrons that are commonly used for the production of PET radionuclides. The use of enriched ^{64}Ni-targets is necessary to achieve maximum specific activities, but this can be very expensive. An effective and efficient recovery and recycling process is therefore essential.

In terms of the final medical application, it is important to comply with current good manufacturing practice (cGMP) or good radiopharmaceutical practices as proposed by the EANM, even at this early stage [17]. This may involve obtaining starting materials from suppliers who provide GMP-compliant certificates of analysis, and ideally also a fully automated process of target post-processing. Alves et al. recently described an automated GMP-compliant process [18].

As with other radiometals, the complexation reaction can be easily influenced by the presence of other competing metals. It is therefore crucial to ensure trace-level concentrations of metal impurities and accurately identify and quantify them. The preferred analytical method for this purpose is inductively coupled plasma mass spectrometry (ICP-MS). To ensure that subsequent problems resulting from the presence of different ionic species of the radionuclide are avoided, the use of thin-layer chromatography (TLC) is strongly recommended to identify the radiochemical purity of the final radionuclide solution.

Radiolabelling

As for all radiometals, radiolabelling with copper-64 depends on the chelator and the biovector used. Due to the huge variety of both, only general recommendations can be proposed for radiolabelling with copper-64.

For radiolabelling of a precursor, the regulatory frameworks are the same as those for radionuclide production. Consequently, it is important to comply with current good manufacturing practices (cGMP) to fulfil pharmaceutical requirements as well as complying with the national radiation protection legislation.

As previously stated, the complexation reaction can be influenced by the presence of competing metals, depending on the specificity of the chelator used. To minimise this effect, it is highly recommended that measures be taken to prevent metal contamination of the reaction mixture. This can be achieved by using the highest quality chemicals with low metal content (if available, use grade trace metal analysis) for all synthesis steps involved in complexation. It is advisable to avoid the use of metal accessories such as spatulas, cannulas, or regular laboratory glassware and to use special coated glassware or cannulas instead.

Quality Control

Quality control is indispensable to guarantee the quality of the final product. This should be along the lines of the general requirements for radiopharmaceuticals and PET radiopharmaceuticals, for which a variety of monographs are already available in the European Pharmacopoeia [19-21]. However, no specific monograph for a ^{64}Cu-radiopharmaceutical is available to date. Quality control processes therefore have

to be established carefully with reference to the general chapters and monographs, such as the general monograph on "Radiopharmaceutical preparations".

The quality control process comprises all standard quality tests, including appearance, pH, radionuclidic identity and purity, (radio)chemical purity, filter integrity, bacterial endotoxins and sterility. Suitable methods and acceptance criteria need to be established and thoroughly validated for every radiopharmaceutical, depending on its structure and chemistry. As a result of the relatively long half-life of the radionuclide, all tests except the test for sterility should be completed before release of the product. The test for sterility must be started as soon as practically possible.

CLINICAL APPLICATION OF ^{64}CU-RADIOPHARMACEUTICALS

Hypoxia Imaging

Hypoxia, a common condition in 50–60% of locally advanced solid tumours, occurs when cells are deprived of oxygen [22]. Hypoxia is associated with increased resistance to radiotherapy, chemotherapy and risk of metastasis [23, 24] which makes the hypoxic microenvironment an attractive target for radiopharmaceuticals. Fujibayashi et al. found the lipophilic radioactive Cu(II)-complex of Cu-ATSM to play a critical role in the selective accumulation of the tracer at hypoxic sites [25, 26]. Further investigations confirmed its ability to detect tumour hypoxia with high specificity and selectivity [27-31], although the accumulation mechanism is still not fully comprehended. It is assumed that the tracer, after passive diffusion into the cell driven by its high permeability, is trapped after reduction due to the specific conditions in hypoxic cells.

Two of the most promising hypoxia tracers are ^{64}Cu-radiopharmaceuticals: [^{64}Cu]Cu-ATSM and [^{64}Cu]Cu-PTSM. [^{64}Cu]Cu-ATSM accumulates depending on the oxygen level of a cell and has faster clearance than its analogue, therefore providing a more stable accumulation [32].

A clinical study with 10 patients suffering from cervical cancer found the signal-to-noise ratio for [^{64}Cu]Cu-ATSM superior to [^{60}Cu]Cu-ATSM, with imaging reproducibility even at advanced time points [33]. This enables centralised production, as well as a wider distribution range and more flexible patient management than radiopharmaceuticals with shorter physical half-life.

Another case report of a glioblastoma multiform (GBM) patient showed steady accumulation in hypoxic sites over the chosen examination period and high correlation between PET/CT data and HIF-1α expression [34]. A clinical study comprising 11 patients with head and neck cancer treated with chemoradiotherapy compared [^{64}Cu]Cu-ATSM and [^{18}F]FDG in terms of efficacy. It was shown to be comparable in terms of biological tumour volume (BTV) estimation, with higher sensitivity and lower specificity in predicting neoadjuvant chemoradiotherapy response [35].

Tumour targeting: Antibodies

Antibodies possess a unique characteristic of localisation to tumours due to their extended accumulation time at the tumour site and clearance time from the blood, which can range from hours to days. An example of such an antibody with relevance to nuclear medicine is trastuzumab. Trastuzumab is a humanised antibody that binds to the extracellular domain of HER2, inhibiting proliferation [36]. It has already been approved as a first-line treatment for HER2-positive advanced breast cancer (BC) [37]. The uptake of [^{64}Cu]Cu-trastuzumab in lesions is a promising criterion for patient management in terms of treatment planning [38]. It has also shown potential for diagnosing metastases of several other malignancies [38]. Radiolabelled trastuzumab can be considered a standard tracer for HER2-positive gastric or gastro-oesophageal junction cancer patients [39], as it provides comparable results to [^{18}F]FDG in patients with HER2-positive primary gastric cancer with liver metastases [40]. Six liver metastases larger than 1 cm were detected using both radiopharmaceuticals. Two metastases smaller than 0.5 cm were only detected using [^{18}F]FDG and not easily with [^{64}Cu]Cu-NOTA-trastuzumab, despite the SUV_{max} of the ^{64}Cu-compound in the primary lesion being estimated at 28.6±0.50 compared to 13.5±0.30 for [^{18}F]FDG [40]. Therefore, further clinical evaluation is necessary.

Another relevant antibody is rituximab, a chimeric human/murine monoclonal antibody that targets CD20-positive B-cell malignancies. It was the first antibody with approval for cancer therapy and is widely used in clinical routine. Additional radiolabelling with β-/β+ emitters augment the clinical potential of the antibody. Copper-64, in particular, has to be noted in this context, as it enables simultaneous treatment enhancement and monitoring. [^{64}Cu]Cu-DOTA-rituximab was evaluated in a pre-clinical trial to determine the tracer's pharmacokinetics, biodistribution, stability, uptake, and radiation dosimetry in CD20-positive B-cell NHL patients compared to [^{18}F]FDG PET/CT [41]. A paper on the GMP-compliant production of the radiopharmaceutical was subsequently published [42]. In recent years, the efficacy of [^{64}Cu]Cu-rituximab for imaging B-cells in a mouse model of multiple sclerosis (MS) gave hope for MS patients responsive to anti-B-cell therapy for detection and early diagnosis of the disease [43].

Ongoing research is being conducted to develop and evaluate new ^{64}Cu-antibodies, such as [^{64}Cu]Cu-DOTA-pembrolizumab, in view of their high potential as radiolabelled antibodies. This will expand their application range.

Tumour targeting: Somatostatin Derivatives

Somatostatin receptors (SSTRs) are known to be suitable targets for synthetic somatostatin analogues, which are already well established in the treatment of patients with neuroendocrine tumours (NETs). Due to its radionuclide properties, copper-64 is expected to be superior to the current gold standard gallium-68 for imaging with somatostatin analogues. It promises easier distribution and patient management and higher spatial resolution. Several clinical trials have aimed to evaluate the advantage of ^{64}Cu-radiolabelled compounds over ^{68}Ga-labelled compounds. A head-to-head comparison of [^{68}Ga]Ga-DOTA-TOC and [^{64}Cu]Cu-DOTA-TATE PET/CT in 59 NET patients showed that [^{64}Cu]Cu-DOTA-TATE had higher specificity and sensitivity compared to [^{68}Ga]Ga-DOTA-TOC [44]. However, this lesion-to-lesion comparison between the two radiopharmaceuticals had some limitations. One of these is the use of DOTA-TOC instead of DOTA-TATE for the ^{68}Ga scans. As no clear superiority of one over the other was reported, the authors concluded that the differences seen were radionuclide-induced [44]. This conclusion seems plausible in view of the different chemical properties, especially in terms of complex formation, as different complex geometries and total complex charge also affect biodistribution.

Further studies confirmed the superiority of [^{64}Cu]Cu-DOTA-TATE over 99mTc-and 111In-derivatives and its utility in the diagnosis, treatment and follow-up of NETs [45-50]. In September 2020, the FDA approved [^{64}Cu]Cu-DOTA-TATE, which is now commercially available. Thanks to its properties and robust manufacturing process, [^{64}Cu]Cu-DOTA-TATE is now the most appropriate choice for NET diagnosis in the United States. However, EMA approval and availability in Europe are still pending.

In a retrospective study, 33 NET patients with surgically removed primary lesions underwent [^{64}Cu]Cu-DOTA-TOC PET/CT which showed that lesions can be detected with high target-to-background contrast [51]. These results correlate with a follow-up evaluation in a different group of patients using [^{177}Lu]Lu-DOTA-TATE [56]. Further studies within larger populations are needed to identify the most appropriate ^{64}Cu-radiolabelled somatostatin derivative for NET diagnosis.

Another somatostatin analogue under clinical evaluation is [^{64}Cu]Cu-SAR-TATE. It contains MeCOSar as a Cu-chelate, the complexes of which are more stable with copper than DOTA. In a clinical trial, [^{64}Cu]Cu-SAR-TATE demonstrated its potential to provide high contrast up to at least 24 hours p.i., to improve patient management, and to allow pre-therapeutic estimation of dosimetry at multiple time points [52].

Tumour targeting: Prostate Cancer

In the last decade, prostate-specific membrane antigen (PSMA) inhibitors have been successfully employed in the targeted treatment of prostate cancer (PC) for diagnostic and therapeutic purposes. Among all radiolabelled PSMA inhibitors, [^{68}Ga]Ga-PSMA-11 has demonstrated the most promising results to date. A comparative clinical trial revealed that the biodistribution of [^{64}Cu]Cu-PSMA-617 and [^{68}Ga]Ga-PSMA-11 is similar, with the exception of the excretion route. [^{64}Cu]Cu-PSMA-617 is excreted through the gastrointestinal tract, rather than the renal system as is the case with [^{68}Ga]Ga-PSMA-11. A further clinical study demonstrated the high potential of [^{64}Cu]Cu-PSMA-617 in the detection of recurrent cases or progressive local lesions in primary staging of PC, with superior uptake compared to [^{68}Ga]Ga-PSMA-11 [53].

Another established radiopharmaceutical for PC is [^{18}F]Choline ([^{18}F]FCH), which is used for the detection of bone metastases in PC patients of high risk. A comparison of [^{64}Cu]Cu-PSMA-617 with [^{18}F]FCH in a cohort of 43 patients with biochemical recurrence (BC) revealed no statistically significant differences between the tracers in terms of detection rate. However, [^{64}Cu]Cu-PSMA-617 demonstrated superior performance, particularly in BC with low PSA levels [54].

In addition, [^{64}Cu]Cu-PSMA-617 [^{64}Cu]$CuCl_2$ has been identified as a suitable tracer for PC diagnostics. Copper is an essential element that plays a significant role in electron transport within key enzymatic pathways. It is therefore logical to suggest that higher uptake is to be expected in cancer cells with uncontrolled growth and a high proliferation rate. A clinical study involving 50 patients with BC PC after surgery or external-beam radiation therapy evaluated the diagnostic value of [^{64}Cu]$CuCl_2$ in comparison to [^{18}F]FCH [55]. The results demonstrated that [^{64}Cu]$CuCl_2$ is more suitable for exploring the prostate and pelvic bed and has a higher detection rate in patients with relapsed PC with low PSA levels.

Patient preparation & aftercare

Patient preparation and the expected length of stay in the department depend on the target of the radiopharmaceutical as well as on the on-site workflow.

Radiation protection must be applied, together with assessment of pregnancy status as needed. Measures must be taken to avoid unnecessary radiation dose to the patient, the patient's social environment and staff. Accompanying persons are allowed only in exceptional cases. The patient should be instructed to ensure adequate hydration before and after administration of the radiopharmaceutical. This ensures that the tracer is flushed out of the patient's body as soon as possible and thus lowers the radiation dose.

The patient should be aware that their body will be inside the camera for the duration of the scan, the length of which depends on the examination goal, type (whole body scan or not) and device (for the latest generation of PET/CT scanners, shorter scan times may apply). The head will not be enclosed most of the time, but patients with severe claustrophobia or other concerns may need to talk to the doctor about sedation.

Side-effects for diagnostic radiopharmaceuticals are rare due to their extremely low level of pharmacological active substance. If they do occur, they are normally limited to hypersensitivity reactions.

For the approved radiopharmaceutical [^{64}Cu]Cu-DOTA-TATE it is recommended to leave a sufficient period before the scan (2 to 28 days) for the wash-out of other somatostatin analogues that are part of the patient's treatment. This ensures that the patient's regular treatment does not negatively influence the imaging quality and results. In this respect, patient handling is analogous to other somatostatin-receptor-targeting diagnostic radiopharmaceuticals.

For acceptable image quality, administered activities from 105–192 MBq of ^{64}Cu-radiopharmaceuticals are sufficient. Nevertheless, much depends on the technical characteristics of the PET scanner and patient body weight. The administered dose should be as low as reasonably possible to obtain good image quality. The administered activity should be determined considering the applicable radiation protection regulations (e.g. Directive 97/43 EURATOM, national legislation, Diagnostic Reference Levels).

An indwelling catheter or indwelling venous cannula should be used for administration to reduce the risk of extravasation.

Patients should void before imaging to reduce background noise and radiation dose to kidneys and bladder.

Imaging Protocol

In the case of the approved [^{64}Cu]Cu-DOTA-TATE, the image acquisition protocol purported by the license holder in the summary of product characteristics (spc) is again analogous to that of the approved ^{68}Ga-analogue NETSPOT. Whole-body acquisition (skull vertex to mid-thigh) is recommended, and can be performed 45 to 90 minutes post injection. Uptake time should be adjusted in line with scanner and patient characteristics. However, literature data indicate that uptake time can be extended up to 3 hours without significant differences in the diagnostic value of the scan [56]. The iterative reconstruction algorithm for image reconstruction should use the system settings. If available, time-of-flight information should be acquired and considered.

For other investigational or not-yet-approved ^{64}Cu-based radiopharmaceuticals it may be helpful to assess in-house experiences with ^{68}Ga-analogues in order to integrate the compound into the clinical routine.

Interpretation

As with other somatostatin-receptor-targeting radiopharmaceuticals, uptake of [^{64}Cu]Cu-DOTA-TATE correlates with the level of somatostatin receptor expression in neuroendocrine tumours. Attention should be paid to the fact that a variety of tumours also express somatostatin receptors in non-cancerous pathologies and under normal physiological conditions. Therefore, increased uptake is not necessarily an indication of a NET. Tumour heterogeneity, differentiation or lesion size may also cause false-negative results.

Radiation exposure of ^{64}Cu-radiopharmaceuticals

Effective doses for the total body were found to be in a range of 0.01 to 0.06 mSv/MBq [58]. From the radiation protection point of view, these levels are acceptable and lower than for other similar radiopharmaceuticals.

The average effective dose of [^{64}Cu]Cu-ATSM was estimated to be 0.036 mSv/MBq, with the liver as a dose-limiting organ (0.39 mGy/MBq) [37]. It should be noted that due to the inherent properties of copper-64, detailed and accurate dosimetry is challenging and still remains to be established [57].

The average effective dose of [^{64}Cu]Cu-DOTA-trastuzumab was estimated to be 0.036±0.009 mSv/MBq, with the heart as a dose-limiting organ (0.34 mGy/MBq) [39]. An animal study estimating the dose via Monte Carlo simulation determined the liver as a dose-limiting organ (0.079 mGy/MBq) for [^{64}Cu]Cu-NOTA-trastuzumab [44].

The average effective dose of [^{64}Cu]Cu-DOTA-rituximab was estimated via animal study to be 0.024 mSv/MBq, with the spleen as the organ with the highest absorbed dose (0.051 mGy/MBq) [44].

The mean effective dose of [^{64}Cu]Cu-DOTA-TATE after injection of 193–232 MBq was found to be 0.032 mSv/MBq, with the pituitary gland as the organ with the highest absorbed dose (0.19 mGy/MBq), even higher than the liver (0.16 mGy/MBq) or kidneys (0.14 mGy/MBq) [50]. For the approved drug, 148 MBq are injected as intravenous bolus within approximately 1 minute.

The mean effective dose of [^{64}Cu]Cu-SAR-TATE after injection of 192 MBq was found to be 0.045 mSv/MBq, with absorbed doses to organs at risk of 0.36 mGy/MBq (spleen), 0.20 mGy/MBq (kidneys) and 0.17 mGy/MBq (adrenals) [52].

The mean effective dose of [^{64}Cu]Cu-PSMA-617 following injection of 119–160 MBq was found to be 0.029 mSv/MBq, with absorbed doses to organs at risk of 2.04 mGy/MBq (gallbladder wall), 0.014 mGy/MBq (liver) and 0.009 mGy/MBq (kidneys) [54].

The mean effective dose of [^{64}Cu]$CuCl_2$ following an injection of 4.0 MBq/kg was found to be 0.051 mSv/MBq, with absorbed doses of 0.32 mGy/MBq (liver) and 0.153 mGy/MBq (lower large intestine wall) [59].

REFERENCES

1. http://www.nucleonica.net/wiki/index.php?title=Decay_Schemes
2. Jahn HA; Teller E. Stability of polyatomic molecules in degenerate electronic states. I. Orbital degeneracy. Proc. Royal Soc. London A. 1937; 161:220-235.
3. Delaloye AB. The Role of Nuclear Medicine in the Treatment of Non-Hodgkin's Lymphoma (NHL). Leukemia & Lymphoma. 2003; 44:S29-S36.
4. Sun X, et al. In vivo behavior of copper-64-labeled methanephosphonate tetraaza macrocyclic ligands. J. Biol. Inorg. Chem. 2003; 8:217.
5. IAEA. Copper-64 radiopharmaceuticals: production, quality control and clinical applications. IAEA radioisotopes and radiopharmceuticals series. 2022; 7.
6. Ma MT, et al. A new bifunctional chelator for copper radiopharmaceuticals: A cage amine ligand with a carboxylate functional group for conjugation to peptides. Chem. Commun. 2009; 14:3237.
7. Mukai H, et al. The synthesis of 64Cu-chelated porphyrin photosensitizers and their tumor-targeting peptide conjugates for the evaluation of target cell uptake and PET image-based pharmacokinetics of targeted photodynamic therapy agents. Ann. Nucl. Med. 2013; 27:625.
8. Maziere B, et al. [55Co]- and [^{64}Cu]DTPA: New radiopharmaceuticals for quantitative tomocisternography. Int. J. Appl. Radiat. Isot. 1983; 34:595.
9. Ometakova J, et al. Automated production of 64Cu prepared by 18 MeV cyclotron. J. Radioanal. Nucl. Chem. 2012; 293:217.
10. Rajec P, et al. Preparation and characterization of nickel targets for cyclotron production of 64Cu. J. Radioanal. Nucl. Chem. 2010; 286:665.
11. McCarthy DW, et al. Efficient production of high specific activity 64Cu using a biomedical cyclotron. Nucl. Med. Biol. 1997; 24:35.
12. Al Rayyes AH, Ailouti Y. Production and quality control of 64Cu from high current Ni target. World J. Nucl. Sci. Technol. 2013; 3:72.
13. Tang L. Radionuclide production and yields at Washington University School of Medicine. Q. J. Nucl. Med. Mol. Imaging. 2008; 52:121.
14. Szeleczsenyi F, Blessing G. Qaim SM. Excitation functions of proton induced nuclear reactions on enriched 61Ni and 64Ni: Possibility of production of no-carrier-added 61Cu and 64Cu at a small cyclotron. Appl. Radiat. Isot. 1993; 44:575.
15. Obata A, et al. Production of therapeutic quantities of 64Cu using a 12 MeV cyclotron. Nucl. Med. Biol. 2003; 30:535.
16. Avila-Rodriguez MA, Nye JA, Nickles R.J. Simultaneous production of high specific activity 64Cu and 61Co with 11.4 MeV protons on enriched 64Ni nuclei. Appl. Radiat. Isot. 2007; 65:1115.
17. Gillings, N., et al., Guideline on current good radiopharmacy practice (cGRPP) for the small scale preparation of radiopharmaceuticals. EJNMMI Radiopharmacy and Chemistry. 2021. 6:1-22.
18. Alves V. et al. Automated purification of radiometals produced by liquid targets. Instruments. 2018;2:17.
19. Huang, Y.-Y., An overview of PET radiopharmaceuticals in clinical use: regulatory, quality and pharmacopeia monographs of the United States and Europe. Nucl. Med. Phys. 2019:35-58.
20. Lange, R., Schreuder N., Hendrikse H., Radiopharmaceuticals, in Practical Pharmaceutics: An International Guideline for the Preparation, Care and Use of Medicinal Products. 2023, Springer. 531-550.
21. van Dommelen, T., Radiopharmaceuticals–How to Register in EU? 2019.
22. Hao G, et al. Recent advances in copper radiopharmaceuticals. Current radiopharm. 2011; 4:109.
23. Jing X, et al. Role of hypoxia in cancer therapy by regulating the tumor microenvironment. Mol. Canc. 2019; 18:1.
24. Sørensen BS, Horsman MR. Tumor hypoxia: impact on radiation therapy and molecular pathways. Front. Oncol. 2020; 10:562.
25. Fujibayashi Y, et al. Copper-62-ATSM: a new hypoxia imaging agent with high membrane permeability and low redox potential. J. Nucl. Med. 1997; 38:1155.
26. Fujibayashi Y, et al. Comparative studies of Cu-64-ATSM and C-11-acetate in an acute myocardial infarction model: ex vivo imaging of hypoxia in rats. Nucl. Med. Biol. 1999; 26:117.
27. Dearling JL, Blower PJ. Redox-active metal complexes for imaging hypoxic tissues: structure-activity relationships in copper (II) bis (thiosemicarbazone) complexes. Chem. Commun. 1998; 2531.
28. Tanaka T, et al. Double-tracer autoradiography with Cu-ATSM/FDG and immunohistochemical interpretation in four different mouse implanted tumor models. Nucl. Med. Biol. 2006; 33:743.
29. Yuan H, et al. Intertumoral differences in hypoxia selectivity of the PET imaging agent 64Cu (II)-diacetyl-bis (N4-methylthiosemicarbazone). J. Nucl. Med. 2006; 47:989.
30. Dence CS, et al. Autoradiographic and small-animal PET comparisons between 18F-FMISO, 18F-FDG, 18F-FLT and the hypoxic selective 64Cu-ATSM in a rodent model of cancer. Nucl. Med. Biol. 2008; 35:713.
31. Holland JP, et al. Spectroelectrochemical and computational studies on the mechanism of hypoxia selectivity of copper radiopharmaceuticals. Chem. Eur. J. 2008; 14:5890.
32. Liu T, et al. Hypoxia imaging and theranostic potential of [^{64}Cu][Cu (ATSM)] and ionic Cu (II) salts: a review of current evidence and discussion of the retention mechanisms. EJNMMI Res. 2020; 10:1.
33. Lewis JS, et al. An imaging comparison of 64Cu-ATSM and 60Cu-ATSM in cancer of the uterine cervix. J. Nucl. Med. 2008; 49:1177.
34. Gangemi V, et al. Impact of [^{64}Cu][Cu(ATSM)] PET/CT in the evaluation of hypoxia in a patient with Glioblastoma: a case report. BMC Canc. 2019; 19:1.
35. Grassi I, et al. Usefulness of 64Cu-ATSM in head and neck cancer: a preliminary prospective study. Clin. Nucl. Med. 2014; 39:e59.
36. Jarrett AM, et al. Towards integration of 64Cu-DOTA-trastuzumab PET-CT and MRI with mathematical modeling to predict response to neoadjuvant therapy in HER2+ breast cancer. Sci. Rep. 2020; 10:1.
37. Giordano SH, et al. Systemic therapy for patients with advanced human epidermal growth factor receptor 2–positive breast cancer: ASCO clinical practice guideline update. J. Clin. Onc. 2018; 36:2736.
38. Mortimer JE, et al. Use of HER2-directed therapy in metastatic breast cancer and how community physicians collaborate to improve care. J. Clin. Med. 2020; 9:1984.
39. Tamura K, et al. 64Cu-DOTA-trastuzumab PET imaging in patients with HER2-positive breast cancer. J. Nucl. Med. 2013; 54:1869.
40. Bang Y-J, et al. Trastuzumab in combination with chemotherapy versus chemotherapy alone for treatment of HER2-positive advanced gastric or gastro-oesophageal junction cancer (ToGA): a phase 3, open-label, randomised controlled trial. Lancet. 2010; 376:687.
41. Chopra A. 64Cu-Labeled DOTA-conjugated rituximab, a chimeric murine/human anti-CD20 monoclonal antibody. MICAD [Internet]. 2012.
42. Natarajan A, et al. Positron emission tomography of 64Cu-DOTA-Rituximab in a transgenic mouse model expressing human CD20 for clinical translation to image NHL. Mol. Imag. Biol. 2015; 14:608.
43. Woo S-K, et al. Development of 64Cu-NOTA-trastuzumab for HER2 targeting: a radiopharmaceutical with improved pharmacokinetics for human studies. J. Nucl. Med. 2019; 60:26-33.
44. Johnbeck CB, et al. Head-to-head comparison of 64Cu-DOTATATE and ^{68}Ga-DOTATOC PET/CT: a prospective study of 59 patients with neuroendocrine tumors. J. Nucl. Med. 2017; 58:451.
45. Delpassand ES, et al. 64Cu-DOTATATE PET/CT for Imaging Patients with Known or Suspected Somatostatin Receptor–Positive Neuroendocrine Tumors: Results of the First US Prospective, Reader-Masked Clinical Trial. J. Nucl. Med. 2020; 61:890.
46. Carlsen EA, et al. 64Cu-DOTATATE PET/CT and prediction of overall and progression-free survival in patients with neuroendocrine neoplasms. J. Nucl. Med. 2020; 61:1491.
47. de Camargo Etchebehere ECS, et al. ^{68}Ga-DOTATATE PET/CT, 99mTc-HYNIC-octreotide SPECT/CT, and whole-body MR imaging in detection of neuroendocrine tumors: a prospective trial. J. Nucl. Med. 2013; 55:1598.

48. Bodei L, et al. Current concepts in ^{68}Ga-DOTATATE imaging of neuroendocrine neoplasms: interpretation, biodistribution, dosimetry, and molecular strategies. J. Nucl. Med. 2017; 58:1718.
49. Pfeifer A, et al. 64Cu-DOTATATE PET for neuroendocrine tumors: a prospective head-to-head comparison with 111In-DTPA-octreotide in 112 patients. J. Nucl. Med. 2015; 56:847.
50. Pfeifer A, et al. Clinical PET of neuroendocrine tumors using 64Cu-DOTATATE: first-in-humans study. J. Nucl. Med. 2012; 53:1207.
51. Mirzaei S, et al. 64Cu-DOTATOC PET-CT in patients with neuroendocrine tumors. Oncol. Ther. 2020; 8:125.
52. Hicks RJ, et al. 64Cu-SARTATE PET imaging of patients with neuroendocrine tumors demonstrates high tumor uptake and retention, potentially allowing prospective dosimetry for peptide receptor radionuclide therapy. J. Nucl. Med. 2019; 60:777.
53. Grubmüller B, et al. 64Cu-PSMA-617 PET/CT imaging of prostate adenocarcinoma: first in-human studies. Canc. Biotherapy Radiopharm. 2016; 31:277.
54. Liu T, et al. 64Cu-PSMA-BCH: a new radiotracer for delayed PET imaging of prostate cancer. Eur. J. Nucl. Med. Mol. Imaging. 2021; 48:4508.
55. Piccardo A, et al. 64CuCl2 PET/CT in prostate cancer relapse. J. Nucl. Med. 2018; 59:444.
56. Loft M, et al. 64Cu-DOTATATE PET in Patients with Neuroendocrine Neoplasms: Prospective, Head-to-Head Comparison of Imaging at 1 Hour and 3 Hours After Injection J Nucl Med. 2021; 62(1):73-80
57. Laforest R, et al. Dosimetry of 60/61/62/64Cu-ATSM: a hypoxia imaging agent for PET. Eur. J. Nucl. Med. Mol. Imag. 2005; 32:764.
58. Vahidfar, N., et al., Recent Advances of Copper-64 Based Radiopharmaceuticals in Nuclear Medicine. In Dosimetry and Radiopharmaceuticals – New Advances and Needs InTechOpen 2024.
59. Avila-Rodriguez M, et al. Biodistribution and radiation dosimetry of [64Cu] copper dichloride: first-in-human study in healthy volunteers. EJNMMI Res. 2017; 7:1.

8

[^{13}N] AMMONIA

by Tonantzin Samara Martinez-Lucio[1]
Oscar Isaac Mendoza-Ibañez[1]
Johannes H. Van Snick[1]
Sergiy V. Lazarenko[2]

[1]*University Medical Center Groningen (UMCG), Department of Nuclear Medicine and Molecular Imaging*

[2]*Northwest Clinics Alkmaar, Department of Medical Imaging*

[13N]AMMONIA

^{13}N was discovered approximately 90 years ago by Irene Curie and Frederic Joliot. The production of this new radiotracer was achieved by alpha-particle irradiation and heating of boron nitride, as described in the publication "Artificial Production of a New Kind of Radio-Element" (1934) [1]. The first in-cyclotron production of ^{13}N was performed in the same year by Cockcroft et al. by bombarding Acheson graphite with high-energy protons.[2] There were differences in the estimated half-life of the tracer, as Curie and Joliot estimated a half-life of 14 minutes, whereas Cockcroft calculated a time of 10.5 ±0.5 minutes, much more similar to the current accepted time of 9.97 minutes.[3] All this work on ^{13}N and other radioactive molecules led to the award of the Nobel Prize to both Irene Curie and Frederic Joliot (Chemistry, 1935) for their work on the synthesis of new radioactive elements, and to John Cockcroft (together with Ernest Walton, Physics1951) for his work on the transmutation of atomic nuclei by artificially accelerated atomic particles.[4, 5] After this pioneering work, further research on the production and possible clinical indications of ^{13}N have taken place, and ^{13}N is currently a validated radio compound with clinical indications within positron emission tomography (PET) examinations. This chapter aims to review the properties, production, quality control methods and biodistribution of this tracer, as well as presenting the current clinical uses and possible future applications of ^{13}N.

CHEMISTRY AND PROPERTIES

Currently, ^{13}N is produced by the nuclear reaction ^{16}O(p,α)^{13}N via proton irradiation of H_2O. This reaction results in the creation of a mixture of [^{13}N]ammonia, [^{13}N]nitrogen, [^{13}N]nitrite, and [^{13}N]nitrate. When water is irradiated, the predominant products obtained are [^{13}N]nitrite and nitrate ([^{13}N]NO_x), but [^{13}N]NH_3 ([^{13}N]ammonia) is preferred as it has a direct application in the imaging of the heart. Different processes can be applied in order to increase the percentage of obtained [^{13}N]NH_3 (discussed later).[6-8] Moreover, [^{13}N]NH_3 allows for further chemical manipulation and has been used for the synthesis of [^{13}N]-labelled amines, [^{13}N]-labelled amino acids, ([^{13}N]-labelled L-glutamate, [^{13}N]-labelled L-glutamine, [^{13}N]-labelled L-aspartate and [^{13}N]-labelled L-alanine), [^{13}N]cisplatin, [^{13}N] carbamates/ureas, [p-nitrophenyl [^{13}N]carbamate ([^{13}N]NPC), [^{13}N]-labelled carbamazepine, and [^{13}N]labelled thalidomide].[9-11] Nevertheless, only [^{13}N]NH_3 is approved by the Food and Drug Administration and used in routine clinical practice.[12] Figure 1 summarises the chemical pathway for the synthesis of ^{13}N compounds.

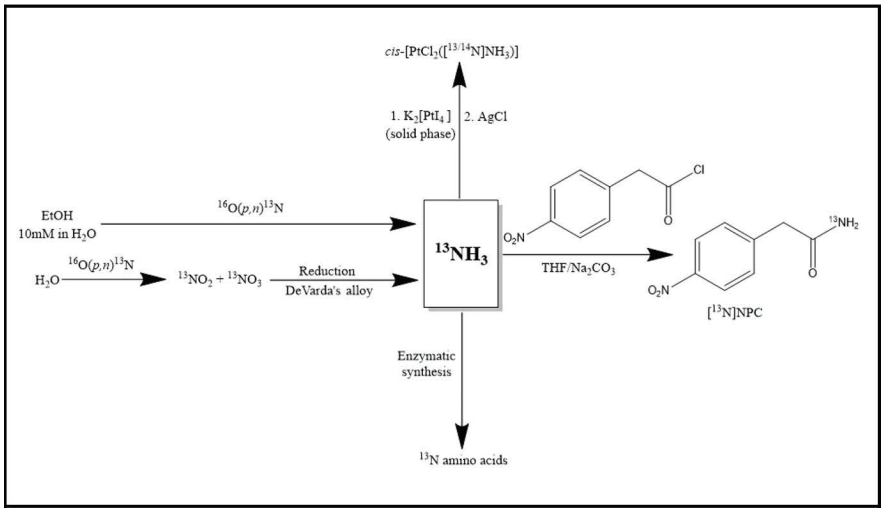

Figure 1. Chemical pathways for the synthesis of ^{13}N-labelled compounds.

[^{13}N]NH_3 is a short-lived radiotracer with a half-life of 9.96. Because of the aforementioned, clinical production and use requires an on-site cyclotron. Properties of [^{13}N]NH_3 are summarised in Table 1.[13, 14] The physiological properties of [^{13}N]NH_3 were studied extensively before the clinical application of the radiotracer, both in pre-clinical and clinical settings. Within the vascular space, [^{13}N]NH_3 was described as existing primarily in its ionic form [^{13}N]NH4+. However, it diffuses freely across cell membranes due to the fact that it is lipid-soluble and has a rapid conversion to [^{13}N]NH_3 after leaving the blood pool. Due to this last property, [^{13}N]NH_3 has a really high single-pass extraction fraction. Further, it was proposed and proven that [^{13}N]NH_3 undergoes subsequent amidation by glutamic acid to glutamine (glutamine synthetase reaction), and that this was the main route for metabolic trapping and fixation within the myocardial wall. The radiotracer was also shown to have a rapid blood pool clearance, which combined with the high myocardial retention would make it feasible to accurately image the heart wall. All of the aforementioned proved that [^{13}N]NH_3 concentrations in the myocardium were related to the myocardial blood flow and that this tracer was suitable for the performance of myocardial perfusion imaging (MPI), with better kinetics than most of the other radiotracers used in MPI. [15-18]

Half-life	9.96 min
Positron energy	1.19 MeV
Production	On-site cyclotron
Mean positron range in water (mm)	1.5
Mean positron range in tissue (mm)	0.4
Effective dose	0.002 mSv/MBq
Kinetics	Metabolically trapped

Table 1. Properties of [^{13}N]NH_3

LABELLING AND PRODUCTION

Since the first discovery of ^{13}N in 1934, several methods have been proposed for obtaining ^{13}N compounds, mainly for the final production of [^{13}N]N_2 and [^{13}N]NH_3. A summary of these different techniques is presented in Table 2.

Authors	Year	Target	Nuclear Reaction	In-target Product
Joliot and Curie	1934	BN	^{10}B(α,n)^{13}N	[^{13}N]
Cockcroft et al.	1934	Graphite	^{12}C(d,n)^{13}N	[^{13}N]CN
Cockcroft et al.	1934	^{13}C-enriched charcoal	^{13}C(p,n)^{13}N	Trapped [^{13}N]CN
Ruben et al.	1940	Charcoal	^{12}C(d,n)^{13}N	[^{13}N]N_2 + trapped [^{13}N]CN
Hunter and Monahan	1971	Al_4C_3	^{12}C(d,n)^{13}N	Matrix-trapped [^{13}N]
Monahan et al.	1972	CH_4 (flowing)	^{12}C(d,n)^{13}N	[^{13}N]NH_3 + [^{13}N] HCN + [^{13}N] $CH3NH_2$
Krizek et al.	1973	H_2O	^{16}O(p,α)^{13}N	[^{13}N]NH3 + [^{13}N] NO3- + [^{13}N]NO-
Wieland et al.	1991	H_2O/ethanol	^{16}O(p,α)^{13}N	[^{13}N]NH_3

Table 2. Historical review of the main production methods for [^{13}N] compounds

After the pioneering work by Cockcroft et al., subsequent techniques were described using the ^{12}C(d,n)^{13}N nuclear reaction in charcoal, aluminium and methane gas. However, these methods were proven not to be easily implemented and most did not have the required purity, mainly with respect to the obtained [^{13}N]NH_3.[2, 19-21] The use of liquid targets began in 1973, when Krizek et. al. proposed the irradiation of liquid water via the ^{16}O(p,α)^{13}N reaction to produce [^{13}N]-compounds. However, this technique achieved a maximum percentage of ≈40% [^{13}N]NH_3.[22] Further refinements to this method showed how subsequent reduction with De Varda alloy (Al/Cu/Zn alloy) or $TiCl_3$ could improve [^{13}N]NH_3 production and led to the first description of a fully automated process for [^{13}N]NH_3 production.[6] A major breakthrough took place in 1991, when Wieland et al. proved that adding a small amount of ethanol (5–10 mM) to the irradiated water resulted in the production of more than 96% of radioactivity in the form of [^{13}N]NH_3.[23]

Currently, the most used and widely established method worldwide is the production of [^{13}N]NH_3 by proton irradiation of ethanol/water solutions. Below we present a summary of the general production protocol for [^{13}N]NH_3 for routine clinical use from the University Medical Center, Groningen, The Netherlands. It must be stated that these protocols may vary between centres, with some of them available to access in the scientific literature. [24, 25]

General description: [^{13}N]NH_3 is produced after radiation of the ^{13}N target with protons; the target contains about 1.8 ml of 5 mmol/l ethanol in water. Ethanol is added to prevent the formation of nitrite and nitrate. The nuclear reaction is ^{16}O(p,α)^{13}N.

Material to be irradiated: ethanol in water (5 mM) [30 µl of ethanol into a bottle containing 100 ml of water for injection], a fresh solution must be prepared every week.

Product: [^{13}N]NH_3 in 5 mM ethanol in physiological salt

Production process: The preparation must be placed in the designated container connected to the ^{13}N target. After setting the [^{13}N]NH_3 route to the respective laminar airflow workstation (LAF) in the system, the ^{13}N target is filled by the loading system. The cyclotron dries the line and verifies that the pathway is not blocked. After this the target is filled with approximately 2200 µl of 5 mmol/l ethanol in water. The route to the designated LAF cabinet is selected and this process is repeated until 5 rinses have been made. The final rinse will be reserved for analysis of germs and pyrogens.

On preparation day, the battery of the activity meter must be tested and the calibration date checked. Before radiation of the target, all the tubing is rinsed and disinfected with 20 ml of ethanol and then with 20 ml of sterile water. Afterwards, the syringe-filling module must be replaced.

Pictures taken in the Department of Nuclear Medicine and Molecular Imaging of the UMCG, Groningen, The Netherlands

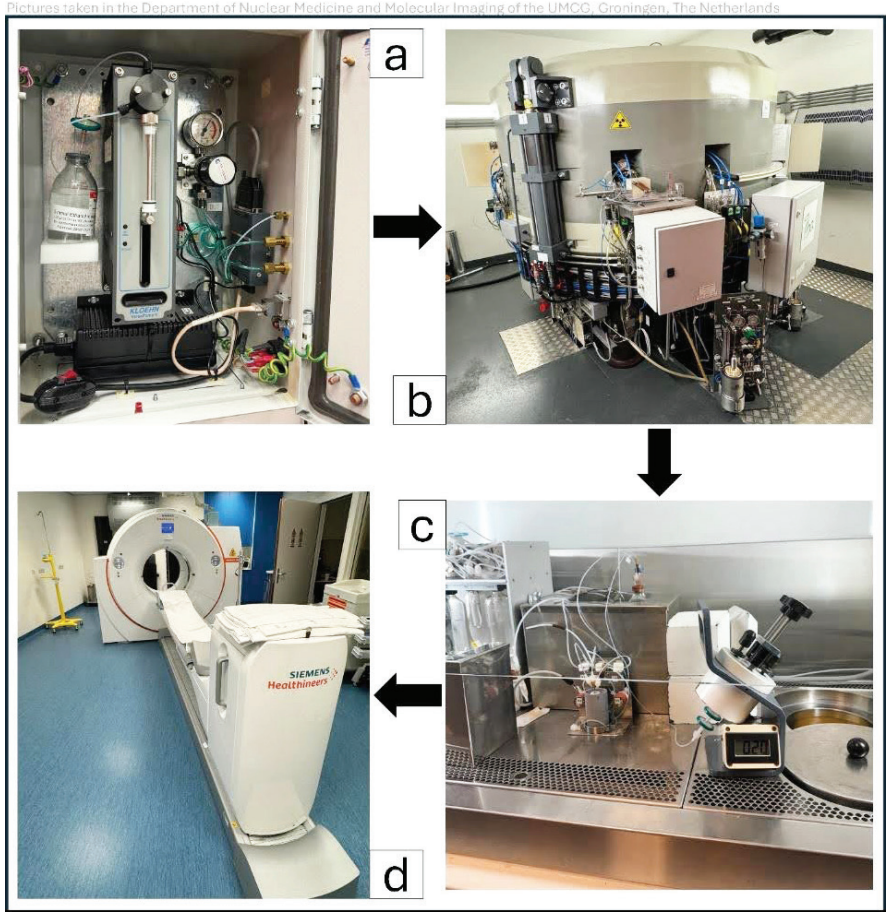

Figure 2. General workflow of [^{13}N]NH3 production. a) Container of ethanol in H_2O (5 mM), b) Cyclotron, c) Laminar air flow workstations, d) PET/CT scanner.

Before starting each run, the line to the syringe must be empty and dry so the filters do not clog up.

For radiation (by cyclotron operator), the route of [^{13}N]NH_3 to the designated LAF cabinet is selected and the target is filled using the cyclotron system. Irradiation of the ^{13}N target will then start. The system is emptied after irradiation. Approximately 1.8 ml of the produced liquid is transported to a LAF cabinet with compressed air (~2.5 bar). When all the activity is in the tubing, it is pushed into the syringe with overpressure. Via a QMA SepPak cartridge, it is then transferred into an empty sterile 25 ml vial containing 12 ml of 0.9% NaCl. A 12 ml sterile syringe is filled in a designated syringe holder. The syringe filters are then disconnected from the syringe, the pH is measured, and bubble point tests are performed on the remaining liquid in the filters. The facilities for [^{13}N]NH_3 production are depicted in Figure 2.

Quality control

Radiopharmaceuticals are different from other pharmaceutical formulations as they have a short half-life and will decay over time. This means that final preparations must be produced just before being administered to patients.[26] Strict and homogeneous regulations are therefore required to ensure proper and safe administration to patients, as well to minimise any potential risk to medical or hospital staff. Quality control procedures play a vital role within this task, ensuring compliance with good practice for the production and release of [^{13}N]NH_3. Figure 3 shows a radiochemistry laboratory where some of the quality control processes are tested.[26, 27]

The European Pharmacopoeia describes the specific quality control tests that [^{13}N]NH_3 must undergo and pass in order to be considered safe for human use within the European Union. These requirements encompass a wide range of characteristics, such as appearance, pH, radiochemical purity and sterility, among others. However, not all the requirements must be tested for every patient and only a couple of them are required before release of the pharmaceutical for clinical use. Moreover, institutions may opt to include additional tests within their internal protocol. Table 3 shows the quality control requirements for the production of [^{13}N]NH_3 at an academic institution [University Medical Center Groningen (UMCG)] and compares these with the ones included in the European Pharmacopoeia. It should be emphasised that institutions can apply different thresholds or test these parameters with different frequencies, as long as they comply with the general recommendations stated in the European Pharmacopoeia.

[13N]NH3	UMCG standards	Release require-ment1	Frequency	European Pharmaco-poeia
Appearance	Clear, colourless	No	Every patient	Clear, colourless
pH	6-8	Yes	Every patient	5.5-8.5
Bubble point test syringe-filter 1 (bar)	> 3,7	No	Every patient	-
Bubble point test syringe-filter 2 (bar)	> 3,7	No	Every patient	-
Radiochemical purity (%) impurities: $[^{13}N]NO_2^-$ $[^{13}N]NO_3^-$ $[^{13}F]F^-$ $[^{13}O]H_2O$	> 99%	No	1x per even week if operational	> 99%
Radionuclide purity (%): gamma spectrum (keV) t1/2 (min)	1973	No	4x/year	> 99%
Ethanol (g/l) 2	< 100	No	Validation only	-
Osmolarity (mosmol/kg) (for information only)	240-800	No	1x per even week if operational	-
Sterility	Sterile	No	1x per even week if operational	Sterile
Endotoxins (EU/ml)	< 5.0	No	1x per even week if operational	< 5.8
Germ count after 1 time gp filtration 4	Max. 1 cfu/ml	No	Validation only	-
Germ count after 2 times gp filtration 4	0	No	Validation only	-
Al (µg/l)	< 2000	No	Validation only	< 2000

Table 3. Quality control requirements established in the European Pharmacopoeia and in the procedural guidelines of a teaching hospital.

Pictures taken in the NGMB Department of the UMCG, Groningen, The Netherlands

Figure 3. General workflow of $[^{13}N]NH_3$ production. a) Container of ethanol in H_2O (5 mM), b) Cyclotron, c) Laminar air flow workstations, d) PET/CT scanner.

PHYSIOLOGICAL BIODISTRIBUTION AND CLINICAL INDICATIONS

Biodistribution

Different studies have explored the biodistribution of [^{13}N]NH_3 within the human body after injection of the radiotracer, as the adequate characterisation of the behaviour of the tracer can help in improving radiation protection and optimising dosimetry. As stated above, [^{13}N]NH_3 has been described as a highly diffusible tracer with a high extraction fraction and good retention, mainly in the myocardial wall.[15-18] There are other organs classically associated with high extraction rates of [^{13}N]NH_3, such as the liver, brain, kidneys and urinary bladder.[28] However, there have been differences in the reported results from specific studies of [^{13}N]NH_3 biodistribution in the human body.

Three major, relatively recent studies have extensively characterised [^{13}N]NH_3 biodistribution [(Stabin, 2008), (Yi, 2015), (Yu, 2023)] in the body.[29-31] Stabin reported that the organs with the highest absorbed doses are the urinary bladder wall, followed by the kidneys, brain and liver. Interestingly, the myocardial wall was the organ with the seventh-highest absorption, surpassed also by the lungs and the adrenal glands.[29] On the other hand, Yi concluded that the organs with highest absorption were the myocardial wall, followed by the kidneys, bone marrow and liver.[30] Finally, in 2023 Yu et al. used a whole-body PET (uEXPLORER) with better spatial resolution and simultaneous whole-body parametric dynamic acquisition instead of whole-body imaging by multi-bed multi-pass acquisition protocol. For males, the authors reported the pancreas, thyroid gland, spleen, heart wall and kidneys as the organs with highest absorption, whereas in women it was the pancreas, heart wall, spleen, lungs and kidneys. Even when using only a fraction of the data to simulate a short-axis PET acquisition, the five organs with highest absorbed radiation remain the same for men (but in a different order), whereas in women the liver occupied third place, displacing the lungs from the top-five absorbing organs.[31]

Clinical indications

The particularities of [^{13}N]NH_3 physiology and biodistribution explain why this tracer has been validated and is used routinely in clinical practice for MPI PET/CT examinations. The European Society of Cardiology (ESC) guideline on Chronic Coronary Syndromes (2019) recommends the use of MPI PET/CT in patients with intermediate to high risk of coronary artery disease (CAD), and in patients already diagnosed with CAD for whom a detailed physiological assessment is needed. The same guideline recommends examining patients by PET/CT if there is suspicion of microvascular angina, as it allows the non-invasive measurement of impaired microcirculatory function. Finally, it also suggests MPI PET/CT for the evaluation of patients with recurrence of chest pain after percutaneous coronary intervention or coronary artery bypass graft surgery.[32] Moreover, the ESC Working Group on Coronary Pathophysiology & Microcirculation encourages the use of PET/CT for the evaluation and diagnosis of coronary microvascular dysfunction (CMD) and myocardial infarction with non-obstructive coronary artery disease (MINOCA). The EANM Procedural Guidelines (2021) highlight the different benefits of performing MPI PET examinations with [^{13}N]NH_3 instead of 82Rb or [^{15}O]H_2O, such as lower activity than 82Rb, which reduces the risk of overflow and dead-time losses; higher quality of the uptake images with better definition of the volumes of interest (VOIs) than 82Rb; and less spill-over fraction with the possibility of determining validated values of left ventricle volumes and ejection fraction (LVEF) when compared to [^{15}O]H_2O.[14]

PATIENT PREPARATION AND AFTERCARE

Adequate preparation

Proper preparation of the patient is crucial prior to conducting the [^{13}N]NH_3 cardiac scan. The purpose of the scan must be carefully explained to the patient by the ordering physician. Clear instructions on how to prepare for the scan and a detailed description of the examination will be provided to the patient by the nuclear medicine department. These instructions will be provided in written format and/or through the use of digital media such as instructional videos on platforms such as YouTube.

To ensure accurate results, it is crucial for the patient to prepare for the examination in advance. The following medications must be stopped prior to the examination: Persantin® and Asasantin® three days in advance; Cedocard, Isosorbide mononitrate and Promocard, 12 hours in advance. These medications can affect heart rate and may interfere with the effects of adenosine.

A light breakfast is allowed before 9:00 a.m., consisting of one rusk or half a slice of bread with jam, accompanied by a glass of water or fruit juice. To ensure the best results, it is crucial that the patient follows these guidelines before the examination. It is important to instruct the patient on avoiding the consumption of coffee, tea, chocolate, cocoa, cola, and other caffeinated drinks, food (e.g. banana) or caffeine-containing medical drugs (e.g. paracetamol/caffeine combination) for 24 hours prior to the examination, as these products may interfere with the effect of the adenosine. The patient is allowed to drink some water, but not too much, otherwise there is a possibility that the patient may need to go to the bathroom during the examination. Regarding radiation protection, pregnancy is a contraindication for performing [^{13}N]NH_3 cardiac PET/CT. Lactation must be briefly suspended as small amounts of

the radiotracer might be excreted to the milk. The scan is usually delayed until breastfeeding has been suspended. However, if the scan must be performed, the patient is advised to collect milk prior to the scan, and to collect and eliminate milk for 2 hours after the scan. Breastfeeding can be resumed after that.[33]

IMAGING PROTOCOL

Performing the scan

After the patient's name and date of birth have been verified, the technologist will give a detailed explanation of the procedure. With regard to the duration of the scan, 90 minutes are indicated, consisting of of a rest phase and a stress phase. Two intravenous lines are placed in each anterior surface of the elbow joint, one to administer adenosine/regadenoson and the other to administer the radiotracer. In addition, the patient is connected to two ECGs: one for the triggering of the PET scan and the other for monitoring the heart during the stress phase. Finally, the patient will have a Bau manometer for blood pressure monitoring during the rest and stress scans. Figures 4 and 5 illustrate patient preparation, with the devices indicated by coloured arrows.

There are different acquisition protocols (administered activity, scan duration, time interval between rest and stress scans, etc.) depending on the used PET scanners and software. The administered activity can vary between 200 and 800 MBq. The recommended time interval between rest and stress scans is at least 40 minutes, to avoid the influence of residual activity from the first injection. The acquisition duration is approximately 10 min (for optimal dynamic, static and gated images), but can vary between 5 minutes (sufficient for dynamic series) and 20 minutes (older scanners without list mode acquisition but with predefined frames). A short acquisition protocol can be implemented by applying residual activity correction to the second scan. For an example of a short acquisition protocol (only one minute between the end of rest and start of stress scans) performed at the Northwest Clinics, Alkmaar, The Netherlands, see Figure 6.

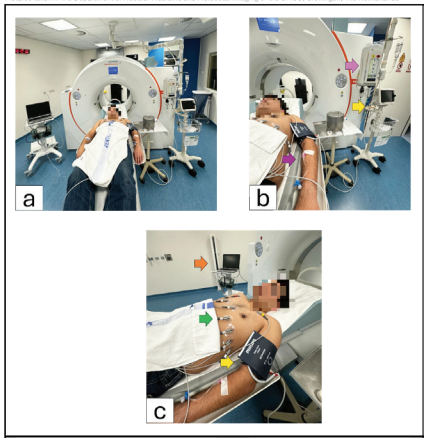

Figure 4. a) Patient preparation for cardiac [^{13}N]NH_3 PET/CT rest acquisition. When inside the PET/CT ready for the start of the scan, arms must be above the head to avoid artefacts. b) Light pink arrow indicates the radiotracer injection system, dark pink arrow indicates the intravenous line for radiotracer administration, and yellow arrow points out the heart rate and blood pressure monitor. c) The green arrow indicates the electrodes connected to the ECG monitor (orange arrow) and to the scanner. The yellow arrow points out the bracelet of the Bau manometer.

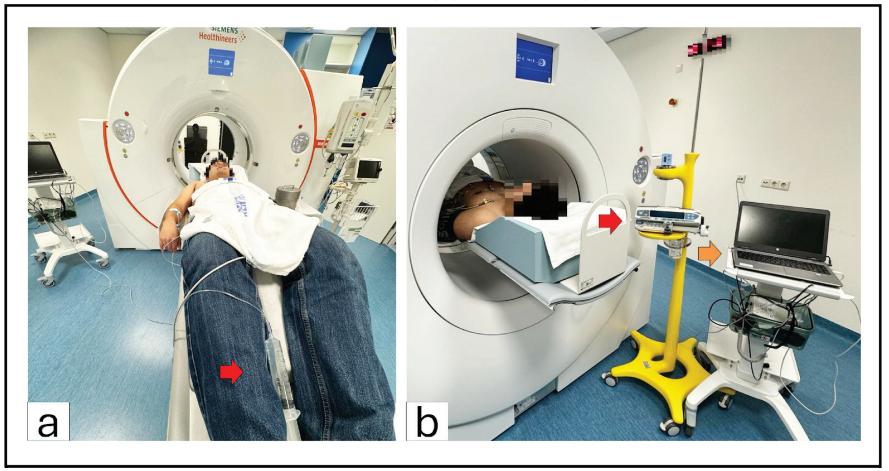

Figure 5. Patient preparation for cardiac PET/CT stress acquisition. When inside the PET/CT ready for the start of the scan, arms must be above the head to avoid artefacts. a) Patient position before the preparation for stress acquisition. The red arrow indicates the syringe of adenosine. b) Patient preparation for stress acquisition. The red arrow indicates adenosine infusions system, and orange arrow points out the ECG monitor.

Protocol:

- Scout CT for patient positioning
- Low-dose CT
- 12 min rest scan with 300 MBq [13N] NH_3 (effective dose of 0.6 mSv) administered via automated injection system (Medrad), including ECG gating
- Immediately after rest scan start an intravenous adenosine* infusion 140 µg. kg-1 / min
- One minute later start 12 min stress acquisition, including ECG gating
- 3 minutes after start of intravenous adenosine infusion inject 400 MBq [13N]NH_3 (effective dose of 0.8 mSv) via automated injection system (Medrad)

*The protocol with regadenoson instead of adenosine is also frequently used. Regadenoson is administered using a single bolus of 400 µg (5 mL in 10 seconds) followed by a 10-mL saline flush (in 10 seconds).

The first two minutes of the stress scan are used to correct for residual activity from the rest scan.

Adenosine may cause short-term symptoms. These may include chest pain, facial flushing, dry mouth, headache, or weakness in the arms or legs.

Protocol provided by the Department of Nuclear Medicine of Northwest Clinics Alkmaar, The Netherlands

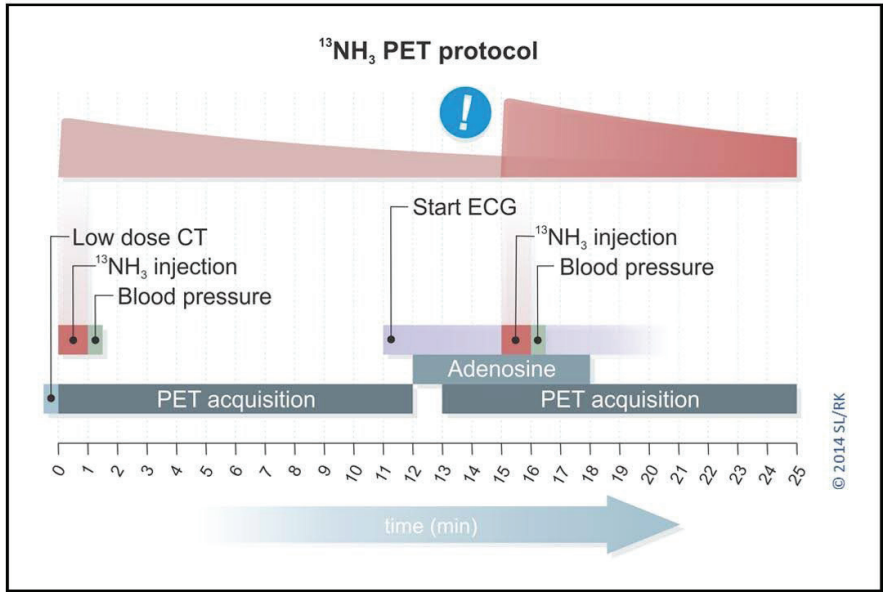

Figure 6. Protocol from Northwest Clinics, Alkmaar.

Anonymized PET/CT results' snapshots from the Department of Nuclear Medicine of Northwest Clinics Alkmaar, The Netherlands

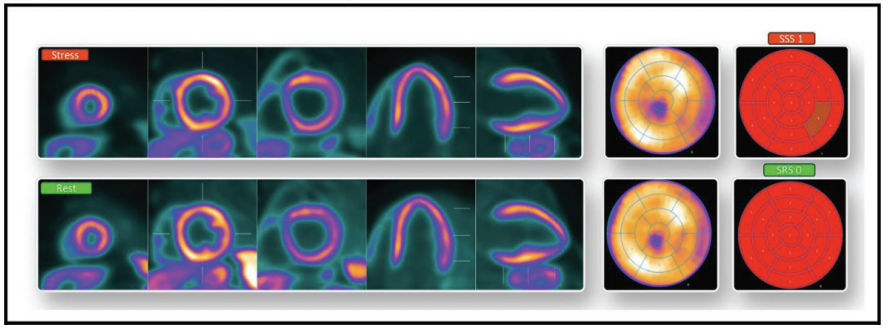

Figure 7a. Patient with a normal myocardial perfusion.

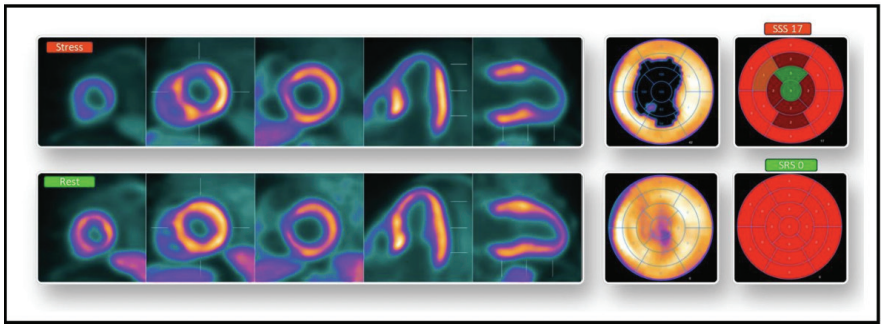

Figure 7b. Myocardial perfusion PET showing a perfusion defect in the LAD territory, corresponding to the significant stenosis of the LAD on invasive angiography.

RESULTS AND INTERPRETATION

A final check of all data by the technologist is needed before transferring it to the nuclear medicine physician / medical imaging specialist. The results can be grouped according to the acquisition series they come from: static, gated and dynamic.

Static Series

From the static series, it is possible to perform a visual semi-quantitative analysis. In this approach the MPI PET/CT images are divided into 17 segments (AHA model). Each segment is scored on a 5-point scale, where 0 is a normal perfusion, 1 is a mildly reduced perfusion, 2 is a moderately reduced perfusion, 3 is a severely reduced perfusion and 4 is an absent perfusion. This is done automatically by dedicated cardiac software and is performed for both rest and stress images. The 17 segment scores are then summed, resulting in a summed rest score (SRS), a summed stress score (SSS) and a summed difference score (SDS). Different thresholds have been proposed: the most frequently used describes an SSS of less than 4 as normal perfusion; 4–8 is considered mildly abnormal, 9–13 is moderately abnormal and more than 13 is severely abnormal.[14, 34] Another approach by Dorbala et al. proposes converting SRS, SSS and SDS into percentages using the formula summed score x 100/68 (maximal possible score), giving as a result the percentage of scarred (SRS), abnormal (SSS), and ischaemic (SDS) myocardium.[35] Figures 7a and 7b show examples with normal and abnormal results.

Gated series

From the gated series, dedicated cardiac software—with possible manual adjustments— automatically provides the values of the left ventricular (LV) volumes, specifically LV end-systolic volume and LV end-diastolic volume, both at rest and in stress, together with the LVEF at rest and in stress, wall motion and thickening, and synchrony.

One of the most important measurements from the gated series, due to its prognostic value, is LVEF, for which a normal value ranges from 50% to 70%. Dorbala et al. reported that a positive LVEF reserve (LVEF stress - LVEF rest) of more than 5% had an excellent negative predictive value for excluding severe left main or 3-vessel CAD.[36]

Cardiac Magnetic Resonance is the gold standard for the evaluation of left ventricular function, and diverse studies have compared LV volumes, LVEF and wall motion values and the concordance of PET with the gold standard, generally reporting strong correlations between the parameters acquired using the two modalities.[37-39] Alongside the numeric results, the cine mode display in PET allows visual evaluation of the LV wall contraction. Some examples of gated results are shown in Figure 8.

Anonymized PET/CT results' snapshots from the Department of Nuclear Medicine of Northwest Clinics Alkmaar, The Netherlands

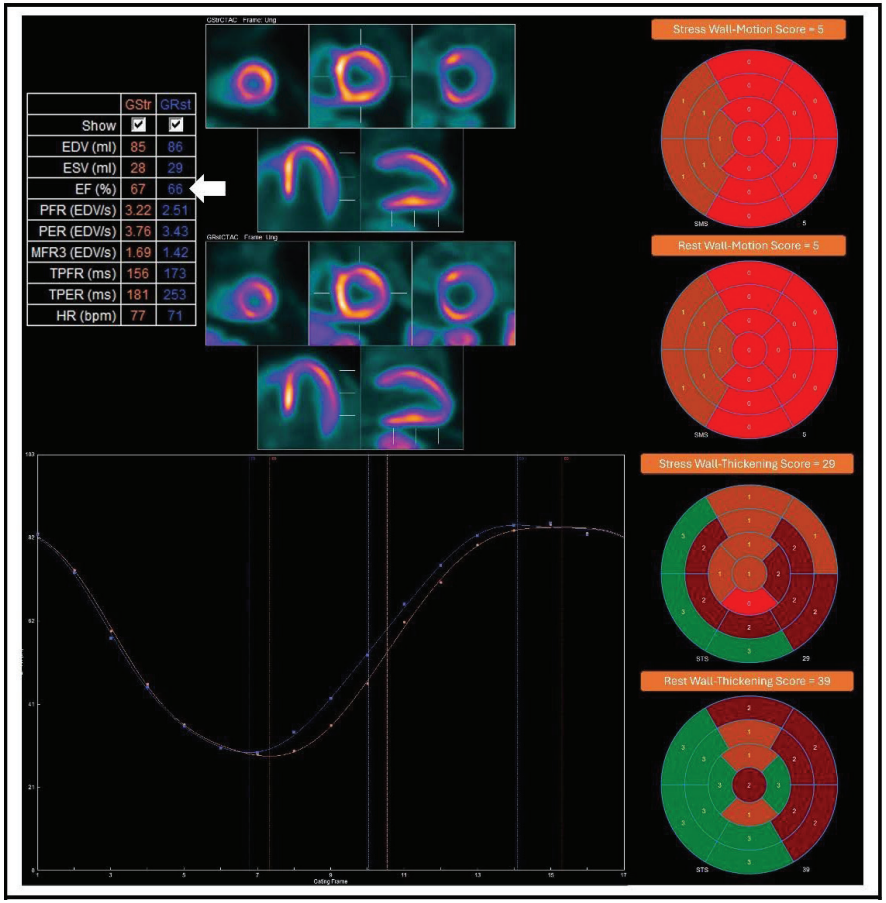

Figure 8. Myocardial perfusion PET showing gated-series results from a normal patient. Note the LVEF (white arrow) values higher than 50% both in rest and stress phases.

Dynamic Series

From the dynamic series it is possible to perform absolute quantification of myocardial perfusion in millilitres per gram per minute (ml/g/min) and obtain the values for myocardial blood flow (MBF) at rest and in stress for every coronary artery region [left anterior descendant (LAD), circumflex (Cx), and right coronary arteries (RCA)] and for the total of the myocardial wall (global rest & stress MBF). Rest MBF will be corrected for rate pressure product if rest heart rate and/or baseline blood pressure is abnormally elevated. Global rest & stress MBF will further be used to calculate the values of coronary flow reserve (CFR) globally and per region by calculating the ratio between MBF in stress and MBF at rest. Various studies have proposed different thresholds for normal-abnormal MBF stress and CFR, as changes in these values of MBF and CFR have been reported depending on the radiotracer used.[40-42] The current specific thresholds for [^{13}N]NH_3 recommended by the EANM are 1.85 ml/g/min for the MBF values in stress, and 2.00 for CFR.[14] At present there are no suggested thresholds for MBF values at rest. Figures 9a and 9b showed some examples of the myocardial flows from normal and abnormal patients.

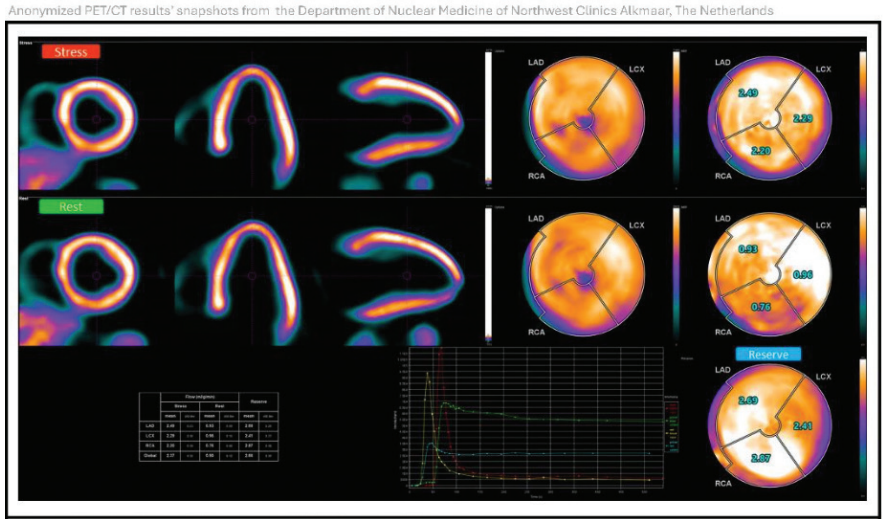

Figure 9a. Patient with a normal MBF and CRF.

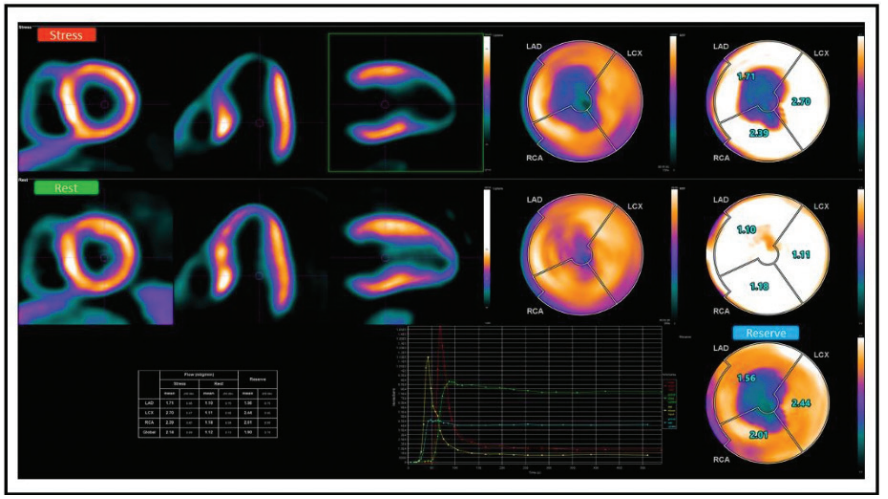

Figure 9b. MBF and CRF showing a severe ischaemia in the left anterior descendant (LAD) coronary artery territory, corresponding to a significant stenosis of the LAD on invasive angiography.

CURRENT AND POTENTIAL LINES OF RESEARCH

As stated earlier, [^{13}N]NH_3 is the only ^{13}N-labelled compound that is FDA approved and currently used in routine clinical practice for the evaluation of patients with suspected CAD, MVA, CMD and MINOCA. [30-33] Although other ^{13}N-labelled compounds have been synthesised (e.g. ^{13}N-labelled L-glutamate, ^{13}N-labelled L-glutamine, ^{13}N-labelled L-aspartate, ^{13}N-labelled L-alanine, [^{13}N]cisplatin, [^{13}N]NPC, ^{13}N-labelled carbamazepine), these tracers have been used solely in laboratory settings and for research purposes only. [9, 10, 43, 44]

The main limitation on the production and evaluation of other ^{13}N-labelled compounds is the short half-life of this product (9.96 minutes), which means that an on-site cyclotron is needed. For this reason, even [^{13}N]NH_3 is not widely available for the performance of MPI PET examinations. This could change in the coming years, however, as cyclotron technology has evolved rapidly in the last decade with the availability of new-generation cyclotrons of smaller size and with lower logistical and operational requirements. This would reduce the cost of acquisition and operation, hopefully leading to a wider availability of [^{13}N]NH_3.[45] Moreover, the availability of new-generation

long-axial field-of-view PET scanners with higher resolution and sensitivity opens up the potential for shorter scan times with low radiation doses, even in tracers with a short half-life such as [^{13}N] compounds.[26] In fact, there are open lines of research for the application of [^{13}N]NH_3 in areas other than MPI. For example, Albano et al. (2019) have recently reviewed the application of [^{13}N]NH_3 in different oncological diseases. From the articles found, they concluded that [^{13}N]NH_3 showed a good discriminating capacity to differentiate between gliomas and non-neoplastic brain lesions, and even to differentiate between high- and low-grade gliomas. This diagnostic performance in gliomas was even superior to the performance of [^{18}F]FDG. Furthermore, a positive impact was found in preliminary research on the use of [^{13}N]NH_3 in liver and prostate cancer. Despite the promising results, the authors also highlight the need for more research in larger populations before this modality can be introduced into clinical oncological practice. [46]

With respect to other ^{13}N-labelled compounds, the short half-life of the tracer also requires rapid and efficient methods for the preparation of molecules other than [^{13}N]NH_3, to prevent radioactive decay. The selection of the physiological process to be examined is also difficult, as processes with slow kinetics are unfeasible to track.[47] However, the fact that the stable isotope of nitrogen (^{14}N) is present in the vast majority of biologically active molecules makes this an attractive tracer with a wide range of molecules available for labelling.[16] More recently, a method was developed for proton beam activation of aluminium oxide nanoparticles (NPs) using the $^{16}O(p,\alpha)^{13}N$ nuclear reaction.[48] Given all of this, we can expect a revival of interest in exploring the role of different ^{13}N compounds in the near future.

REFERENCES

1. Joliot, F. and I. Curie, Artificial production of a new kind of radio-element. Nature, 1934. 133: p. 2021-202.
2. Cockcroft, J.D., C.W. Gilbert, and E.T.S. Walton, Production of Induced Radioactivity by High Velocity Protons. Nature, 1934. 133(3357): p. 328-328.
3. Weiss, M., et al., Determinants of [13N]ammonia kinetics in hepatic PET experiments: a minimal recirculatory model. Eur J Nucl Med Mol Imaging, 2002. 29(12): p. 1648-56.
4. Aston, F., Nobel Lecture, Chemistry 1922-1941. 1966, Elsevier Publishing Company, Amsterdam, London, New York.
5. Oliphant, M.L.E. and W.G. Penney, John Douglas Cockcroft, 1897-1967. 1968, The Royal Society London.
6. Ido, T.a.I., R, Fully automated synthesis of $^{13}NH_3$, in Third International Symposium on Radiopharmaceutical Chemistry, J.L.C. Radiopharm, Editor. 1981. p. 244-246.
7. Lindner, L., J. Helmer, and G. Brinkman, Water "loop"-target for the in-cyclotron production of ^{13}N by the reaction ^{16}O (p, α) ^{13}N. The International Journal of Applied Radiation and Isotopes, 1979. 30(8): p. 506-507.
8. Vaalburg, W., et al., An improved method for the cyclotron production of ^{13}N-labelled ammonia. Int J Appl Radiat Isot, 1975. 26(5): p. 316-8.
9. Cooper, A.J.L. and A.S. Gelbard, The use of immobilized glutamate dehydrogenase to synthesize ^{13}N-labeled l-amino acids. Analytical Biochemistry, 1981. 111(1): p. 42-48.
10. Finn, R.D., D.R. Christman, and A.P. Wolf, A rapid synthesis of nitrogen-^{13} labelled amphetamine. Journal of Labelled Compounds and Radiopharmaceuticals, 1981. 18(6): p. 909-913.
11. Tominaga, T., et al., Synthesis of ^{13}N-labelled amines by reduction of ^{13}N-labelled amides. International Journal of Radiation Applications and Instrumentation. Part A. Applied Radiation and Isotopes, 1986. 37(12): p. 1209-1212.
12. Al-Mallah, M.H., et al., Assessment of myocardial perfusion and function with PET and PET/CT. J Nucl Cardiol, 2010. 17(3): p. 498-513.
13. Raijmakers, P., ^{13}N-ammonia and H2 15O PET/CT of Myocardial Perfusion, in Procedure Guidelines Nuclear Medicine. Dutch Society of Nuclear Medicine, J.P. Esser, Editor. 2016, HGP Vullers.
14. Sciagra, R., et al., EANM procedural guidelines for PET/CT quantitative myocardial perfusion imaging. Eur J Nucl Med Mol Imaging, 2021. 48(4): p. 1040-1069.
15. Krivokapich, J., et al., ^{13}N ammonia myocardial imaging at rest and with exercise in normal volunteers. Quantification of absolute myocardial perfusion with dynamic positron emission tomography. Circulation, 1989. 80(5): p. 1328-37.
16. Rosenspire, K.C., et al., Metabolic Fate of [^{13}N] ammonia in human and canine blood. J Nucl Med, 1990. 31(2): p. 163-167.
17. Schelbert, H.R., et al., N-13 ammonia as an indicator of myocardial blood flow. Circulation, 1981. 63(6): p. 1259-72.
18. Schelbert, H.R., et al., Regional myocardial perfusion assessed with N-13 labeled ammonia and positron emission computerized axial tomography. Am J Cardiol, 1979. 43(2): p. 209-18.
19. Hunter, W. and W. Monahan, ^{13}N-ammonia: A new physiologic radiotracer for molecular medicine. J Nucl Med, 1971. 12(6): p. 368-369.
20. Monahan, W.G., R.S. Tilbury, and J.S. Laughlin, Uptake of ¹³N-Labeled Ammonia. Journal of Nuclear Medicine, 1972. 13(4): p. 274-277.
21. Ruben, S., W.Z. Hassid, and M.D. Kamen, RADIOACTIVE NITROGEN IN THE STUDY OF N2 FIXATION BY NON-LEGUMINOUS PLANTS. Science, 1940. 91(2372): p. 578-9.
22. Production of radiochemically pure $^{13}NH_3$ for biomedical studies using the $^{16}O(p,\alpha)^{13}N$ reaction, in 20th Annual SNM Meeting, B.A. Burrows, Editor. 1972, Society of Nuclear Medicine. p. 629-630.
23. Wieland, B., et al., In-target production of [^{13}N] ammonia via proton irradiation of dilute aqueous ethanol and acetic acid mixtures. Int J Rad Appl Instrum A, 1991. 42(11): p. 1095-8.
24. Akhilesh, S.K., et al., Fully automated synthesis of nitrogen-13-NH3 by SHIs HM-18 cyclotron and dedicated module for routine clinical studies: Our institutional experiences. Indian Journal of Nuclear Medicine, 2022. 37(1): p. 50-53.

25. Synowieckia, M., J. Bernarda, and L. Perka, High-yield and straight-forward production of ammonia (^{13}N) using a Siemens Eclipse HP cyclotron, in 2018 Siemens Eclipse Cyclotron Users Meeting Agenda. 2018, Siemens Healthineers: Coimbra, Portugal.
26. Thota, P., et al., A Comparative Study of Pharmacopoeial Quality Standards and Regulations of Radiopharmaceuticals. Indian J Nucl Med, 2021. 36(2): p. 153-162.
27. Organization, W.H., International Atomic Agency (IAEA)/WHO guidelines on good manufacturing practices for radiopharmaceutical products. WHO Drug Information, 2019. 33(3): p. 395-409.
28. Lockwood, A.H., Absorbed doses of radiation after an intravenous injection of N-13 ammonia in man: concise communication. J Nucl Med, 1980. 21(3): p. 276-8.
29. Stabin, M.G., Radiopharmaceuticals for nuclear cardiology: radiation dosimetry, uncertainties, and risk. J Nucl Med, 2008. 49(9): p. 1555-63.
30. Yi, C., et al., Biodistribution and estimation of radiation-absorbed doses in humans for ^{13}N-ammonia PET. Ann Nucl Med, 2015. 29(9): p. 810-5.
31. Yu, X., et al., Improved accuracy of the biodistribution and internal radiation dosimetry of (^{13}) N-ammonia using a total-body PET/CT scanner. Med Phys, 2023. 50(9): p. 5865-5874.
32. Knuuti, J., et al., 2019 ESC Guidelines for the diagnosis and management of chronic coronary syndromes. Eur Heart J, 2020. 41(3): p. 407-477.
33. Agency, I.A.E., Radiation Protection in Newer Medical Imaging Techniques: PET/CT. 2008: Vienna, Austria.
34. Brophey, M.D., et al., Accuracy of (82)Rb PET/CT Myocardial Perfusion Imaging with Regadenoson Stress, Including 3-Year Clinical Outcomes. J Nucl Med Technol, 2017. 45(2): p. 75-81.
35. Dorbala, S. and M.F. Di Carli, Cardiac PET perfusion: prognosis, risk stratification, and clinical management. Semin Nucl Med, 2014. 44(5): p. 344-57.
36. Dorbala, S., et al., Incremental prognostic value of gated Rb-82 positron emission tomography myocardial perfusion imaging over clinical variables and rest LVEF. JACC Cardiovasc Imaging, 2009. 2(7): p. 846-54.
37. Kiko, t., et al., Direct comparisons of left ventricular volume and function by simultaneous cardiac magnetic resonance imaging and gated ^{13}N-ammonia positron emission tomography. Nucl Med Commun, 2020. 41(4): p. 383-388.
38. Maurer, A., et al., Left ventricular function and volumes from gated [^{13}N]-ammonia positron emission tomography myocardial perfusion imaging: A prospective head-to-head comparison against CMR using a hybrid PET/MR device. J Nucl Cadiol, 2023. 30(2): p. 616-625.
39. Slart, R.H.J.A., et al., Comparison of gated PET with MRI for evaluation of left ventricular function in patients with coronary artery disease. J Nucl Med, 2004. 45(2): p. 176-182.
40. Fiechter, M., et al., Diagnostic value of ^{13}N-ammonia myocardial perfusion PET: added value of myocardial flow reserve. J Nucl Med, 2012. 53(8): p. 1230-4.
41. Hajjiri, M.M., et al., Comparison of positron emission tomography measurement of adenosine-stimulated absolute myocardial blood flow versus relative myocardial tracer content for physiological assessment of coronary artery stenosis severity and location. JACC Cardiovasc Imaging, 2009. 2(6): p. 751-758.
42. Morton, G., et al., Quantification of absolute myocardial perfusion in patients with coronary artery disease: comparison between cardiovascular magnetic resonance and positron emission tomography. J Am Coll Cardiol, 2012. 60(16): p. 1546-55.
43. De Spiegeleer, B., et al., Microscale synthesis of nitrogen-13-labeled cisplatin. J Nucl Med, 1986. 27(3): p. 399-403.
44. Kumata, K., et al., One-pot radiosynthesis of [^{13}N] urea and [^{13}N] carbamate using no-carrier-added [^{13}N] NH3. Journal of Labelled Compounds and Radiopharmaceuticals: The Official Journal of the International Isotope Society, 2009. 52(5): p. 166-172.
45. Pieper, J., et al., Initial clinical experience of N13-ammonia myocardial perfusion PET/CT using a compact superconducting production system. Journal of Nuclear Cardiology, 2021. 28(1): p. 295-299.
46. Albano, D., R. Giubbini, and F. Bertagna, (^{13})N-NH(3) PET/CT in oncological disease. Jpn J Radiol, 2019. 37(12): p. 799-807.
47. Gomez-Vallejo, V., et al., Nitrogen-13: historical review and future perspectives. J Labelled Comp Radiopharm, 2014. 57(4): p. 244-54.
48. Pérez-Campaña, C., et al., Biodistribution of different sized nanoparticles assessed by positron emission tomography: a general strategy for direct activation of metal oxide particles. ACS Nano, 2013. 7(4): p. 3498-505.

Acknowledgements

The authors of this chapter acknowledge with gratitude the contributions of R.H.J.A. Slart, S.N. Blok, B. Maas, M. Deuten, R. J. J. Knol, and the departments of Nuclear Medicine and Molecular Imaging at the University Medical Center, Groningen, and the Northwest Clinics, Alkmaar.

9

[^{18}F] FLUOROESTRADIOL [^{18}F]FES – BREAST CANCER

by Tina Buehner
Bital Savir Baruch

Nuclear Medicine and Theranostics Division, College of Medicine, University of Arizona, US

[18F]FLUOROESTRADIOL ([18F]FES) – BREAST CANCER

This chapter will discuss the application of 16α-[18F]fluoro-17β-oestradiol PET ([18F]FES) in PET/CT imaging for breast cancer. Developed in the 1984 at the University of Illinois, ([18F]FES was the first receptor-based PET tracer. [1] In 2020 FES obtained approval from the United States Food and Drug Administration (FDA) under the trade name Cerianna™ [2] for detecting oestrogen receptor-positive (ER+) lesions in recurrent or metastatic breast cancer. Additionally, in Europe, specifically in France, ([18F]FES is currently authorised under the trade name EstroTep™.[3] In June of 2023, The Society of Nuclear Medicine and Molecular Imaging (SNMMI), together with the European Association of Nuclear Medicine (EANM) released their Procedural Standards and Practice Guidelines for Estrogen Receptor Imaging of Patients with Breast Cancer using 16α[18F]Fluoro-17β-Estradiol PET. [4] This chapter will reflect best practices established by those guidelines.

BREAST CANCER

Incidence, Etiology, and Epidemiology

Breast cancer is the most common cancer among women worldwide. In the United States of America (USA), it ranks as the second most frequently diagnosed cancer in women, following skin cancer. According to the American Cancer Society (ACS), in 2023 there will be approximately 297,790 new cases of invasive breast cancer and 55,722 new cases of ductal carcinoma in situ (DCIS).[5] It is estimated that approximately 43,700 women will die of breast cancer by the end of 2023. On average, the risk of developing breast cancer for women in the United States is 1 in 8, and similar figures apply in Europe.[6]

The risk factors associated with the development of breast cancer are influenced by various factors, including age, genetic mutations, reproductive history, family history of breast or ovarian cancer, previous chest radiation therapy, and having dense breasts. [5]

Histopathology

Immunohistopathology or immuno-histochemistry (IHC) involves tissue analysis through biopsy. Breast cancer encompasses several types, with the most common being invasive ductal carcinoma. Lobular carcinoma accounts for about 10–15% of breast cancer cases, and less frequent types such as inflammatory breast cancer, mucinous carcinoma, tubular carcinoma, metaplastic carcinoma, and Paget's disease of the breast make up a small percentage of breast cancers.[5,7]

There are four main molecular subtypes of these breast cancers, including Luminal A and Luminal B, commonly referred to as Hormone Receptor Positive (HR+) breast cancer. Human Epidermal Growth Factor Receptor-2 enriched (HER2+) breast cancer is another molecular subtype where the HER2 protein promotes the growth and division of cancer cells. Lastly, Triple Negative Breast Cancer (TNBC) is a particularly challenging and aggressive type, lacking receptors on the tumour cell surface.[5,7]

Hormone Receptor Positive breast cancer is related to the receptors on the tumour's surface expressing either oestrogen (ER+), progesterone (PR+), or both (ER+/PR+). These receptors on the cell surface can also serve as targets for treatment. Specifically, Estrogen Receptor-Positive (ER+) breast cancer indicates that the tumour cell tests positive for functional oestrogen receptors, while Progesterone Positive (PR+) indicates tumour cells expressing progesterone.5 This chapter will exclusively focus on ER-positive breast cancer, which can be imaged using ([18F]FES PET.

Chemistry & Properties

Oestradiol, a female sex steroidal hormone and a type of oestrogen, plays a crucial role in the development and maintenance of female reproductive health. It is primarily produced by the ovaries in premenopausal women and in adipose (fat) tissue in postmenopausal women. Oestradiol regulates the menstrual cycle, contributes to the development of the breast and uterine lining, and maintains bone density and strength. Additionally, it has a known protective effect on the cardiovascular system, reducing the risk of heart disease in premenopausal women. Oestradiol is available in various medicinal forms and can be taken to alleviate menopausal symptoms. Moreover, it plays a complex and significant role in certain types of breast cancers.[8]

In oestrogen receptor-positive (ER+) breast cancer, oestrogen binds to receptors on the cell surface stimulating the growth and proliferation of cancer cells. These are referred to as oestrogen receptor-positive (ER+) breast cancers. This type of breast cancer is commonly known as hormone-sensitive breast cancer. [5]

([18F]FES binds to ER with very high affinity, and its in vivo uptake by ER-dependent target tissues in animal models was efficient and selective, findings that preceded its use for PET imaging in patients with breast cancer.[1]

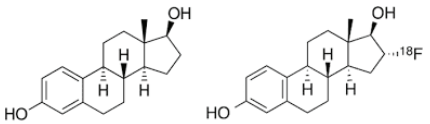

Figure 1. Illustration of the chemical structure of the 17β-oestradiol, as well as its 18F-fluorinated analogue 16α-[18F]fluoro-17β-oestradiol.
GE Package Insert Cerianna™ 2

Labelling / Production

16α-[18F]fluoro-17ß oestradiol is a product of the cyclotron-produced fluorine-18 isotope conjugated onto an oestradiol analogue molecule. Originally developed in the early 1980s, its radiosynthesis involved a two-step method which has been substantially modified since its development. Currently, the commonly used process is referred to as a two-step-one-pot process with simplified synthesis sequences. [9]

Apart from a few large academic institutions with in-house cyclotrons that produce [18F] FES for research, the majority of institutions in the United States obtain unit doses through a local commercial radiopharmacy for clinical use.

Quality Control

There are various quality control measures that need to be successfully conducted prior to ([18F]FES being released for clinical use, including the evaluation of particulates, filter integrity, residual kryptofix, chemical purity, bacterial endotoxins, pH, and sterility. If in-house radiosynthesis is being performed, all release criteria must be met through compliance with established standards, i.e. the United States Pharmacopeia (USP) in the United States and the European Pharmacopoeia (Ph. Eur.) in Europe.[9] As previously mentioned, most imaging centres within the United States obtain unit doses from a commercial radiopharmacy that is required to perform all quality assurance testing prior to the release of commercial doses for clinical use.

Physiological Biodistribution

The normal biodistribution of ([18F]FES includes the liver, biliary system, gallbladder, common bile duct, small bowel, kidneys, ureters, urinary bladder and uterus. Normal variant activity can be seen in the ovaries and pituitary gland. Like other steroidal compounds, ([18F]FES undergoes high extraction and metabolism by the liver, leading to rapid early blood clearance within 10–15 minutes post-injection. The intense uptake observed within the liver poses a limitation for accurately identifying hepatic lesions and is therefore not recommended for evaluating sole intrahepatic lesions.[2-4] Normal physiological ([18F]FES uptake is observed along the vein at the site of ([18F] FES tracer administration, a phenomenon not entirely understood but hypothesised to be associated with the lipophilic nature of the tracer. There is mild uptake within the bone marrow, and minimal to no uptake is seen within the brain parenchyma, making it advantageous for identifying ER-positive cerebral metastases.[2-4]

Focal areas of increased uptake outside of the normal patterns of tracer biodistribution, compared to background uptake in normal tissues, raise concerns about disease localisation which will be discussed later in this chapter in the section

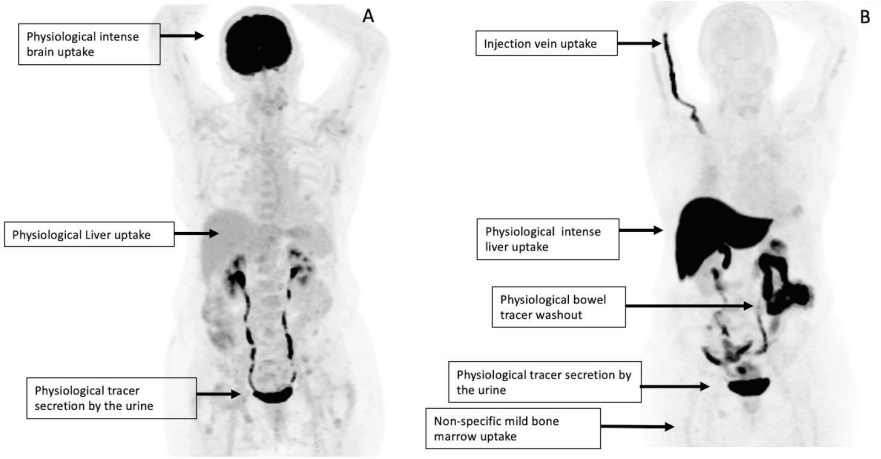

Figure 2. Patient with a history of ER-positive invasive lobular breast cancer. She presented with right breast biopsy-proven ER-positive recurrent disease. The patient underwent an [18F]FDG PET/CT followed by an [18F]FES PET/CT with negative findings for recurrent disease.

on interpretation. Figure 2 illustrates the normal biodistribution of ([18F]FES uptake and excretion, compared to [18F]FDG (FDG)

Figure 2 shows comparison of normal biodistribution between FDG (A) and ([18F] FES (B) in a patient with biopsy-proven ER-positive breast cancer.

PATIENT PREPARATION

Clinical history

All relevant clinical history should be thoroughly reviewed and documented to determine the appropriate patient selection for ([18F]FES PET imaging.[4]

The documented clinical history should include:

» Patient demographics.

» Breast cancer stage and subtype, as well as biopsy pathology/IHC of ER-positive tumour expression.

» Current and previous endocrine therapies that may interfere with ([18F]FES binding and the date of the last treatment.

» Patient pregnancy and lactation status. Pregnancy status should be documented in accordance with institutional policies for women of childbearing potential. If patient is breastfeeding, she should be advised not to breastfeed for 4 hours after administration 2, and to be mindful of radiation exposure due to close proximity

when feeding the baby (e.g., bottle) during that period.

» Menopausal status or date of the last menstrual period should be documented; however, studies looking at endogenous oestrogen levels do not affect ([18F]FES binding to ER-positive lesions. Additionally, oral contraceptives are found to produce oestradiol levels similar to that of endogenous levels and are unlikely to affect ([18F]FES binding but may be documented as part of institutional policy.

» Recent staging/restaging imaging studies.

Diet

[18F]Flouroestradiol is a receptor-targeted radiopharmaceutical, and therefore patients undergoing imaging do not need to fast or abstain from exercise prior to imaging, as required for ([18F]FDG PET scans. Nonetheless, they should be encouraged to hydrate well before their appointment.[2-4]

Contraindications/drug interactions

There are no known contraindications for use; however, patients should be properly screened for drug interactions before imaging. Two classes of drugs used as systemic endocrine therapies in ER-positive breast cancer interfere with ([18F]FES binding to the cell. These drugs are known as SERMs (Selective Estrogen Receptor Modulators) and SERDs (Selective Estrogen Receptor Down-regulators). SERMs directly block oestrogen receptors and are recommended to be discontinued for at least 8 weeks before imaging, with Tamoxifen being a commonly prescribed SERM in the USA.2-4 Conversely, SERDs degrade oestrogen receptors, making it difficult for ([18F]FES to bind to the receptor. Fulvestrant is the most prescribed SERD in the United States, and due to its long effective half-life of 40 days, it is recommended to be discontinued for 28 weeks before imaging.[2-4]

There has been a recent emergence of novel oral SERDs in the treatment paradigm for ER-positive breast cancer. Recently the FDA approved the first oral SERD, namely elacestrant for ER-positive, HER2-negative breast cancer, with more expected to come. Oral SERDs have a shorter half-life and therefore shorter washout periods, typically measured in days. Further research is needed to determine the exact washout period for these novel ER-blocking oestradiol analogues, and decisions should be made on an individual basis considering the effective half-life of the pharmaceutical. Despite the mentioned drug interaction, patients' clinical management should not be delayed for ([18F]FES PET imaging.[4]

Other types of hormonal therapies, such as aromatase inhibitors (AI), block the transition of androgens into oestrogens but do not interfere with ([18F]FES uptake and binding. In this case, no cessation of usage is required before imaging. Additionally, other drugs commonly given in combination with ER-targeted therapies, such as CDK4/6 and mTOR inhibitors, do not interfere with ([18F]FES binding to ER-positive lesions. [2-4] It is worth noting that the oestrogen concentration of ([18F]FES is less than 5 micromoles and has not been found to have any physiological effect in humans.[2-4]

Dosage and Administration

The recommended [18F]FES activity is typically 222 MBq with a range of 111 MBq to 280 MBq. [2-4] It should be administered intravenously via an indwelling angiocatheter of at least 20 gauge, preferably on the contralateral side to the known breast cancer. The [18F]FES injection should be administered over 1 to 2 minutes and flushed well with at least 10cc of normal saline.

IMAGING

Clinical indications for ([18F]FES PET imaging include the detection of ER-positive lesions in patients with known or suspected recurrent or metastatic breast cancer. This may involve lesions that are challenging to biopsy or biopsy results that are inconclusive.[2-3] According to the SNMMI/EANM guidelines, ([18F]FES PET imaging may also be used to guide therapy after the progression of metastatic disease or after the initial presentation of metastatic disease.[4]

The recommended image acquisition time is from 20 to 80 minutes post-injection [2-4], with an optimal imaging time of 60 minutes, which aligns well with most departmental imaging schedules. Patients should be instructed to empty their bladder before imaging. They are then positioned supine with arms above the head in a headrest or holder, if possible. While standard whole-body images of [18F] FDG PET scans are commonly acquired from "eyes to thighs", ([18F]FES PET imaging should incorporate vertex to thighs due to the low background uptake of ([18F]FES within the brain parenchyma, allowing the potential identification of cerebral metastases.[4]

A multimodal PET system, such as Positron Emission Tomography (PET) imaging combined with a Computed Tomography (CT) (PET/CT) or PET combined with Magnetic Resonance Imaging (MRI) (PET/MRI), can be used for imaging acquisition. PET/CT scan may be performed as a low-dose CT scan for attenuation correction or as part of a diagnostic examination with or without the use of oral and intravenous (I.V.) contrast. Although less commonly used in clinical practice, PET/MR may be employed for image acquisition. PET and CT or PET and MRI acquisition parameters are specific to each system and should be customised accordingly to optimise image quality. Similarly, imaging reconstruction parameters will vary by system and interpreting physician preference.[4]

Regardless of the system combination used for the acquisition of ([18F]FES PET imaging, it is important to note that ([18F]FES will not identify all breast cancer lesions, but rather detect lesions that are ER-positive.

Therefore, additional anatomical imaging such as CT or molecular imaging with [18F] FDG PET should be performed in addition to ([18F]FES PET to evaluate the full extent of the disease.[4]

RESULTS & INTERPRETATION

Nuclear Medicine Technologists should document the following to assist interpreting physicians with reporting:

- Radiopharmaceutical dose (assayed dose less the syringe residual after administration)
- Date and time of administration
- Radiopharmaceutical batch or lot number
- Route and site of administration
- Patient's current body weight and height.

As discussed in the section on physiological biodistribution, ([18F]FES is primarily metabolised and excreted by the liver, with a lesser extent of excretion through the urinary system. Therefore, tracer washout within the hepatobiliary and renal collecting systems often reflects intense uptake. The uterus is also frequently visible on ([18F]FES imaging. Normal variant uptake can be observed within the ovaries and pituitary gland.

Interpretation of ([18F]FES uptakes depends on the ER density and function within the tumours as well as within physiological tissue, including the liver, ovaries, and uterus.[2-4] Interpretation is, therefore, primarily a qualitative assessment of uptake in suspected lesions compared to background uptake within normal tissues (Figure 3). ([18F]FES metabolisation by the liver serves as a limitation to the evaluation of hepatic lesions; however, evaluation of extrahepatic lesions can be determined as follows:

- Lesion uptake greater than that of normal background low-uptake tissue and blood pool are considered to be ER-positive lesions, indicating that the lesion is expressing ER.
- Lesion uptake less than that of normal tissue and vascular background of blood pool are typically considered to be ER-negative, indicating the absence of ER expression on the tumour.[2-4]
- Several studies have been done in the USA and in Europe investigating quantitative analysis of ([18F]FES uptake, including positivity thresholds to differentiate positive vs. negative lesions. Currently, qualitative visual analysis is the most preferred method of ([18F]FES image interpretation. Table 1 provides a summary of common causes of false negatives and positives in ([18F]FES imaging.

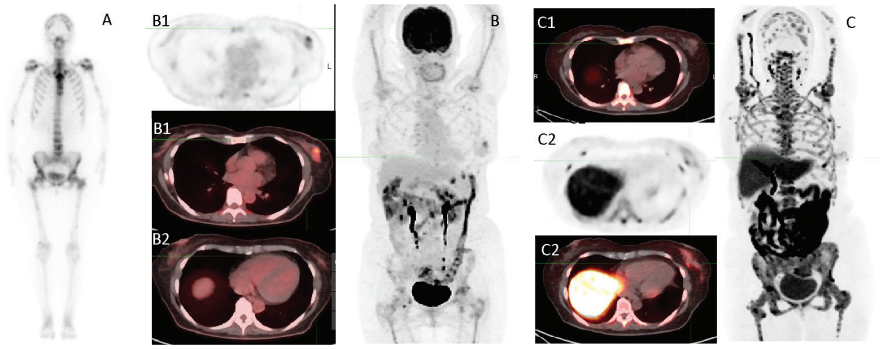

Figure 3. A patient presented with newly diagnosed metastatic low-ER-expression left-breast-invasive ductal carcinoma (IDC) ER+ 1%, PR+ 1%, ki67 30%, HER2-negative. An iliac bone biopsy demonstrated high ER expression (ER+ 80%, PR-negative, Her 2-positive, Ki67 20%). (A) 99mTc-MDP bone scan was significant for diffuse metastatic disease with mild uptake. (B) [18F]FDG PET CT was obtained with abnormal uptake in the left breast IDC (B1). No significant uptake was noted in the bones. (C) - [18F] FES-PET/CT obtained 2 weeks later demonstrated no uptake in the biopsied breast lesion (C1) with suspicious uptake in a different breast lesion (C2) and diffuse bone uptake (C) consistent with known iliac biopsy. Patient started endocrine therapy.

False Negatives	False Positives
ER-blocking/degrading medications without appropriate washout periods: SERMs (8 weeks) and SERDs (28 weeks)2,4	Benign neoplasms expressing ER receptors (e.g. leiomyomas, meningiomas)2,4
ER-expressing lesions that can be obscured by high background uptake (e.g. hepatic lesions)2,4	Benign neoplasms expressing ER receptors (e.g. leiomyomas, meningiomas)2,4
Intense tracer washout within small intestine may obscure peritoneal carcinomatosis 4	Other malignant neoplasm expressing ER receptors (e.g. ovarian cancer and endometrial cancer)2,4
Sub-centimetre lesions and lymph nodes may be difficult to detect due to the scanner resolution and partial volume effect 4	Pulmonary fibrosis, especially post radiation therapy 2,4,11
	Diffuse uptake without correlative abnormality (although some highly intense and diffuse uptake in marrow may indicate marrow-based spread) 4

Table 1: False Findings Quick Reference Chart courtesy of University of Arizona, Tucson, AZ, USA.

DOSIMETRY

The estimated effective dose of [18F] FES administration in female patients was 0.022mSv/MBq, and the organ with the highest dose was the liver (0.13mGy/MBq).[10]

REFERENCES

1. Katzenellenbogen JA. The quest for improving the management of breast cancer by functional imaging: The discovery and development of 16Œ±-[18F]fluoroestradiol (FES), a PET radiotracer for the estrogen receptor, a historical review. Nucl Med Biol. 2021 Jan;92:24-37. https://doi.org/10.1016/j.nucmedbio.2020.02.007. Epub 2020 Feb 22. PMID: 32229068; PMCID: PMC7442693.
2. GE Healthcare. CeriannaTM (fluoroestradiol F18) Injection. Available from: https://www.gehealthcare.com/products/nuclear-imaging-agents/cerianna.
3. EstroTep (Fluoroestradiol 18F). Available from: https://www.gehealthcare.com/products/nuclear-imaging-agents/cerianna.
4. Mankoff D, et al. SNMMI Procedure Standard/EANM Practice Guideline for Estrogen Receptor Imaging of Patients with Breast Cancer Using 16Œ±-[18F] Fluoro-17Œ≤-Estradiol PET.
5. American Cancer Society. Key Statistics for Breast Cancer. Available from: https://www.cancer.org/cancer/types/breast-cancer/about/how-common-is-breast-cancer.html#:~:text=It%20is%20about%2030%25%20(or,(DCIS)%20will%20be%20diagnosed.
6. European Commission. Cancer statistics - specific cancers. Available from: https://ec.europa.eu/eurostat/statistics-explained/index.php?title=Cancer_statistics_-_specific_cancers&oldid=578153#Breast_cancer.
7. Mohammed, AA. The clinical behavior of different molecular subtypes of breast cancer. Cancer Treatement and Research Communications. Volume 29, 2021, 100469. Available from: https://www.sciencedirect.com/science/article/pii/S2468294221001659.
8. Farkas S, Szabó A, Hegyi AE, Török B, Fazekas CL, Ernszt D, Kovács T, Zelena D. Estradiol and Estrogen-like Alternative Therapies in Use: The Importance of the Selective and Non-Classical Actions. Biomedicines. 2022 Apr 6;10(4):861. https://doi.org/10.3390/biomedicines10040861. PMID: 35453610; PMCID: PMC9029610.
9. Wang M, Glick-Wilson BE, Zheng QH. Fully automated radiosynthesis and quality control of estrogen receptor targeting radiopharmaceutical 16Œ±-[18F]fluoroestradiol ([18F]FES) for human breast cancer imaging. Appl Radiat Isot. 2020 Jun;160:109109. https://doi.org/10.1016/j.apradiso.2020.109109. Epub 2020 Mar 3. PMID: 32174461.9.
10. Mankoff DA, Peterson LM, Tewson TJ, Link JM, Gralow JR, Graham MM, Krohn KA. [18F] fluoroestradiol radiation dosimetry in human PET studies. J Nucl Med. 2001 Apr;42(4):679-84. PMID: 11337559.
11. Mahalik, Aparna MBBS; Chaudhary, Beena BRT; Kumar, Rakesh PhD; Tripathi, Madhavi MD; Bal, Chandrasekhar MD. 18F-FES Uptake in Radiation Pneumonitis. Clinical Nuclear Medicine 48(10):p e468-e469, October 2023. https://doi.org/10.1097/RLU.0000000000004788

TG24 - https://doi.org/10.52717/PESK2100

Publisher:
European Association of Nuclear Medicine
Schmalzhofgasse 26, 1060 Vienna, Austria
Phone: +43 1 890 44 27 | +43 1 890 44 27-9
Email: office@eanm.org | URL: www.eanm.org

Main Editor:
Luísa Roldão Pereira

Co-Editors:
Paolo Turco
Christopher Bruneby

English Language Editing:
Angela Parker

Project Management:
Sophie Karsai, EANM Executive Office
Henar Alonso-Marcos, EANM Executive Office

Layout & Design:
Katerina Maslova, EANM Executive Office

Content:
No responsibility is taken for the correctness of this information.
Information as per date of printing December 2024.